Nanoscale

REVIEW

View Article Online
View Journal | View Issue

Cite this: *Nanoscale*, 2023, **15**, 2997

Biomolecules incorporated in halide perovskite nanocrystals: synthesis, optical properties, and applications†

Masoud Aminzare, ‡[a] Jennifer Jiang, ‡[a] Gabrielle A. Mandl, ‡[b] Sara Mahshid, [c] John A. Capobianco [b] and Noémie-Manuelle Dorval Courchesne *[a]

Halide perovskite nanocrystals (HPNCs) have emerged at the forefront of nanomaterials research over the past two decades. The physicochemical and optoelectronic properties of these inorganic semiconductor nanoparticles can be modulated through the introduction of various ligands. The use of biomolecules as ligands has been demonstrated to improve the stability, luminescence, conductivity and biocompatibility of HPNCs. The rapid advancement of this field relies on a strong understanding of how the structure and properties of biomolecules influences their interactions with HPNCs, as well as their potential to extend applications of HPNCs towards biological applications. This review addresses the role of several classes of biomolecules (amino acids, proteins, carbohydrates, nucleotides, *etc.*) that have shown promise for improving the performance of HPNCs and their potential applications. Specifically, we have reviewed the recent advances on incorporating biomolecules with HP nanomaterials on the formation, physicochemical properties, and stability of HP compounds. We have also shed light on the potential for using HPs in biological and environmental applications by compiling some recent of proof-of-concept demonstrations. Overall, this review aims to guide the field towards incorporating biomolecules into the next-generation of high-performance HPNCs for biological and environmental applications.

Received 7th October 2022,
Accepted 10th January 2023

DOI: 10.1039/d2nr05565a

rsc.li/nanoscale

1. Introduction

Over the past two decades there has been a world-wide increase in the use of optoelectronic technologies in nearly every aspect of life. From display technologies to telecommunications and solar cells, the modern world relies on the rapid development of optoelectronic devices. These devices rely on the development of materials which can convert photons to electrical energy, or *vice versa*. Semiconducting materials have paved the way for the success of optoelectronic technologies. In particular, semiconducting nanoparticles have garnered particular attention. For example, quantum dot light emitting diodes (QLEDs) based on CdSe and InP have risen to the forefront of display technologies; however, their price, elemental rarity, and toxicity render them sub-optimal for continued widespread use. There is therefore a need to develop alternative high-performance materials for optoelectronic applications that consist of earth-abundant elements.[1] Fortunately, halide perovskites (HPs) have recently emerged as attractive candidates for developing low cost, earth abundant, and highly efficient photovoltaic (PV) materials.[2–7] HPs have the general chemical formula of ABX_3, where "A" and "B" are monovalent and divalent cations, respectively, and "X" is a monovalent halide ion coordinated to both "A" and "B". The "A" cation is usually methylamine (MA^+), or Cs^+ and the "B" cation is most commonly Pb^{2+} or Sn^{2+}. Nanocrystalline HPs are a promising class of nanomaterials with remarkable optical and electronic properties, allowing them to emerge not only as strong candidates for PVs,[8] but also for many other state-of-the-art applications such as light emitting devices (LEDs),[9] photodetectors,[10] and lasers.[11] HPNCs are also commonly referred to as quantum dots, owing to their quantum confinement effects. For the sake of brevity, we will refer to all halide perovskite nanomaterials herein as halide perovskite nanocrystals (HPNCs) or nanocrystals (NCs). Discussed herein, there are a myriad of advantages and drawbacks of HPNCs, which can be addressed through the introduction of

[a]*Department of Chemical Engineering, McGill University, 3610 University Street, Wong Building, Room 4180, Montréal, QC, H3A 0C5, Canada. E-mail: noemie.dorvalcourchesne@mcgill.ca*
[b]*Department of Chemistry and Biochemistry and Centre for NanoScience Research, 7141 Rue Sherbrooke Ouest, Concordia University, Montreal, QC, H4B 1R6, Canada*
[c]*Department of Bioengineering, McGill University, 817 Sherbrooke Street West, Macdonald Engineering Building, Room 355, Montréal, QC, H3A 0C3, Canada*

†Electronic supplementary information (ESI) available: The chemical structures of the used ligands in this review paper. See DOI: https://doi.org/10.1039/d2nr05565a

‡These authors contributed equally to this work.

biomolecules either at the surface or within the crystal structure of these materials.

The optoelectronic properties of HPNCs can be varied by modulating their composition, size, dimensionality and synthesis methods.[12–14] The ability to modulate the optical properties of HPNCs stems from their tunable bandgap, owing to the strong quantum confinement effects exhibited in these materials.[15,16] Recent studies have shown that HPNCs can exhibit photoluminescence quantum yields (PLQY) approaching 100% efficiency.[17,18] In addition to their impressive efficiencies, HPNCs can be synthesized *via* low-cost, facile methods relative to other types of semiconductor and PV materials, making them highly attractive alternatives to traditional compounds.[19] With regard to their electronic properties, high-performance HPNCs should exhibit conductivity that is tolerant to the presence of defects, allow for a good degree of charge separation and carrier mobility with minimal recombination within the perovskite layer, and long carrier diffusion lengths. With respect to optical properties, HPNCs should exhibit efficient radiative recombination (high PLQY), tunable spectral excitations and emissions, narrow full-width at half maximum (FWHM) of emission bands, nanosecond photoluminescence (PL) lifetimes, and minimal photobleaching or photoblinking.

Despite their impressive optoelectronic properties, HPs exhibit markedly-reduced physicochemical stability relative to other state-of-the-art luminescent materials.[20,21] They are sensitive to high temperatures, broadband illumination, moisture, and oxygen. This instability is due to the ionic nature of the material, and the low energy of formation of the HPs crystal structure. This is consequently accompanied by a propensity to form defects which allow moisture and air to further penetrate the crystal and degrade.[22–24] Ion migration due to the electron vacancies of halides at the perovskite surface and at grain boundaries, as well as ion clusters, caused by an excess of anions or cations in the perovskite solution, are also believed to facilitate material degradation.[25–28] Such defects are also known to have deleterious effects on the optical properties of the HPs, for instance serving as non-radiative recombination centers and dramatically decreasing the optoelectronic performance of HPs. Successful defect control not only reduces non-radiative recombination centers to improve the materials performance, but also increases the stability and thereby lifetime of the charge carriers.[24,29,30] Although the superior optoelectronic properties of HPNCs make them attractive for industrial use, several challenges remain that impede their mass production and application. Of practical importance, it is currently not possible to produce HPNCs at an industrial scale while maintaining the high performance obtained using small-scale synthesis techniques. Additionally, HPNCs lack long-term stability, and Pb^{2+}-containing compositions are inherently toxic. Consequently, there is an urgent need to develop strategies to mitigate these concerns, such as making physicochemical modifications to existing high-performance lead-based HPNC materials, or through the development of novel materials or techniques that facilitate their commercial usage for a variety of applications.[31–38]

One of the most successful routes to generating high-quality HPNCs with minimal defects is through the use of ligand-mediated synthesis strategies. Ligands are organic molecules which aid in nucleation and growth of the crystal lattice, and also act to passivate the HPNC surface.[39,40] Ligands with a wide range of properties have been used, including cationic, anionic, and zwitterionic species with varying charges.[41] In order to obtain well-passivated, highly-crystalline HPNCs with strong luminescence and good stability, it is of paramount importance to select an appropriate ligand for the nucleation and growth process. The size, charge, polarity, polarizability, shape, orientation, and types of potential inter-ligand interactions are all parameters that determine the usefulness of a ligand.[41,42] The ligand-assisted reprecipitation technique (LARP) and hot injection methods are two of the most commonly used synthesis techniques. The LARP process is conducted by mixing a precursor solution consisting of (1) a polar solvent, (2) perovskite precursors and (3) organic ligands, with a nonpolar solvent at room temperature. The difference in solubility of perovskite precursors in polar and nonpolar solvents induces rapid nucleation and growth of the HPNCs, which is mediated by the ligands. The synthesis route also impacts the shape, size, morphology and crystallinity of NCs during the synthesis.[39,43] Conventional organic ligands used during the production of HPNCs include oleic acid (OA), oleyamine (OAm), octadecene, octylamine, and (3-aminopropyl)triethoxysilane (APTES), among others. These molecules are hydrophobic, with long hydrocarbon tails that aid in surface passivation by preventing the dissolution and re-growth of the crystals.[44] Despite their wide-use, OA and other

Noémie-Manuelle Dorval Courchesne

Noémie-Manuelle Dorval Courchesne is an Assistant Professor of Chemical Engineering at McGill University and a Canada Research Chair in Biologically-Derived Materials. Previously, she obtained her PhD in Chemical Engineering from MIT and completed at postdoc at the Wyss Institute for Biologically Inspired Engineering at Harvard. Her diverse and multidisciplinary research group works at the interface of materials, biological and chemical engineering to tackle sustainability and health challenges. Prof. Dorval Courchesne has received several recent honors and awards, including the 2020 Christopher Pierre Award for Research Excellence (Early Career) at McGill, the title of "Emerging Leader in Chemical Engineering" from the Canadian Society for Chemical Engineering in 2020, a new Canada Research Chair in 2021, and a Johnson & Johnson WiSTEM2D award in 2022.

similar organic ligands have several drawbacks. First, the insulating nature of the long hydrocarbon chain of these molecules makes charge injection extremely difficult, therefore inhibiting the application of HPNCs in conductive devices.[44] Second, these ligands do not provide complete protection against environmental stressors, such as humidity and oxygen, as they do not continuously cover the HNPC surface. In addition, the hydrophobicity of OA and similar ligands makes them unsuitable for use in fully aqueous synthesis routes, which are much more environmentally-friendly than conventional synthesis methods which use large amounts of non-polar solvents. Another challenge of achieving fully-aqueous synthesis, besides the lack of suitable ligands, is the moisture sensitivity of HP compounds. Particularly, the high degree of interaction between water molecules and HPs results in the rapid conversion of HPs to their metal halide salt precursors, thereby degrading the HP crystal. At this time, a complete understanding of the interactions hindering the formation of HPNCs in fully aqueous media are not sufficiently understood, thus they are difficult to control.[45] Recently, the successful synthesis of HPNCs in aqueous media by proper adjustment of solubility equilibrium was reported.[46] $MAPbX_3$ (X = Br or Cl/Br) NCs were synthesized directly in acidic aqueous solution (pH = 0–5) *via* the reaction between a lead halide complex and methylamine. The rapid degradation of $MAPbBr_3$ powders synthesized in DMF in contact with pure water or CH_3NH_2 solution was observed, while the HPNCs maintained stability in the presence of lead halide complexes $[PbBr_6]^{4-}$ at low pH in water. The fully aqueous synthesis route relies on solubility equilibria of the reactants, which prevents decomposition of HPNCs in water by maintaining the proper ionic balance at the halide-rich surface of HPNCs through the presence of excess $[PbBr_6]^{4-}$ complexes and H^+ and $CH_3NH_3^+$ cations.[46]

While the use of a monofunctional capping ligand such as OA or OAm has proven crucial to the generation of high-performance HPNCs, studies have proven a synergistic effect exists when functional groups of both electron-donating and accepting nature, such as amines and carboxylates, are introduced to passivate the HPNC surface.[47–51] Additionally, previous approaches aimed at neutralizing point defects using ligands with electron donating and withdrawing properties have been promising.[52] Thus, ligands which possess both amine and carboxylate moieties may provide greater benefits than monodentate ligands, or two separate ligands.

Biomolecules are naturally occurring molecules with sophisticated chemical structures and well-preserved biological functions, which are defined as substances produced by cells in living organisms. The four major types of biomolecules are carbohydrates, lipids, nucleic acids, and peptides. These biomolecules are essential for life and each can be found in monomeric or polymeric forms. Interestingly, many types of biomolecules including amino acids (AAs), peptides, DNA, *etc.* often possess both amino and carboxylate functional groups, making them ideal candidates for use as HPNC passivating agents. They are greener alternatives to organic ligands, since they are biodegradable and have minimal toxicity. Molecular self-assembly using biological macromolecules has been shown as a promising alternative in bottom-up fabrication routes to nucleate, bind and organize novel nanostructured materials at low costs and a wider range of morphologies.[53–56]

In light of the rapid development of HPs and the importance of ligands in the synthesis of HPNCs, starting around 2015, biomolecules, specifically AAs, were introduced as ligands in the synthesis of HPNCs.[57,58] AAs are zwitterionic molecules which possess both amine and carboxylate groups, making them favorable candidates for HPNC synthesis as discussed in section 2.1. Later, other types of biomolecules were also explored as ligands, owing to the success of AAs for this purpose.[59,60] Biomolecules are not only able to act as passivating agents, they can also functionalize the NC surface and provide it with additional properties; for example they can improve the self-assembly, control the shape or size, or tune the optical properties of NCs.[61–63] In addition, biomolecules have been directly incorporated into the crystal structure of HPs to improve a variety of properties.[64,65] While OA is technically a biomolecule (a fatty acid), it still suffers from the same drawbacks previously mentioned with long-chain, hydrophobic ligands. As such, it is clear that not all biomolecules are inherently better-suited than synthetic molecules for use in HPNCs development.

In this review, we will detail the recent advances in HPNCs research involving the incorporation of biomolecules, both on fundamental and applied levels and their impacts on HPNC properties. This nascent field aims to develop biohybrid HP nanomaterials with improved performance and stability and to incorporate these novel materials into applications for biological and environmental purposes. Biomolecules have been used as either a stand-alone ligand or additional ligand in a cocktail of precursors during the synthesis of HPNCs. We will discuss the effects of biomolecules on the physicochemical and optoelectronic properties of HPNCs, as well as their role in HPNC synthesis. The impacts of biomolecules on the applications of HPNCs in biologically-relevant fields will also be discussed.

2. Biomolecules as ligands

As previously mentioned, carboxyl and amino functional groups can be used as ligands during the synthesis of HPNCs to improve stability, optical properties, and other unique features (Table 1 and Fig. S1†).[66–68] AAs are biomolecules which, by definition, contain both carboxylates and amines. The identity of each AA comes from the structure of its side chain, which also governs the degree to which different AAs may modulate HPNC synthesis and properties.

Unless otherwise stated herein, it has been established that the carboxylate in AAs act as a Lewis acid, coordinating to metal sites or cationic defects, donating electron density into the nanocrystal and the amino group can act as a Lewis base, coordinating to halides or anionic defects and remove electron density from the lattice. Lastly, the properties of functional groups present in the side chains will act in a similar manner

Table 1 Summary of the incorporated biomolecules with HPNCs and the corresponding synthesis conditions as well as optoelectronic properties

HP	Ligand	Size (nm)	E_g (eV)	PLQY (%)	Lifetime (ns)	Stability	Synthesis method	Synthesis solvent	Ref.
Amino acids									
$MAPbBr_3$	Cys	5–20	N/A	2.4–53.7	85.6–642	>60 h	LARP	DMF, Tol	61
$CsPbBr_3$	Cys	N/A	N/A	N/A	N/A	N/A	LARP	DMF, ODE, OA, Tol	62
$CsPbBr_3$	Cys	2.1	N/A	≤60	N/A	N/A	Hot-injection	OA, ODE, OAm	69
$MAPbBr_3$	Arg	6.9 ± 0.4	1.7	92 ± 7	N/A	7 d	LARP	DMF, HEA, Tol	77
$MAPbBr_3$	Arg	5.3 ± 0.6	1.9	72 ± 20	N/A	N/A	LARP	DMF, OLA, Tol	77
$MAPbBr_3$	Arg	5.3 ± 0.9	1.8	71 ± 17	N/A	N/A	LARP	DMF, ADA, Tol	77
$MAPbBr_3$	Arg	6.4 ± 0.3	1.9	7 ± 2	N/A	N/A	LARP	DMF, HEA, $CHCl_3$	77
$MAPbBr_3$	Arg	8.6 ± 0.3	2.3	33 ± 14	N/A	N/A	LARP	DMF, OAm, $CHCl_3$	77
$MAPbBr_3$	Arg	3.3 ± 0.2	2	4 ± 1	N/A	N/A	LARP	DMF, ADA, $CHCl_3$	77
$MAPbBr_3$	Arg-tBoc	5.7 ± 0.3	2.2	94 + 5	N/A	N/A	LARP	HEA, Tol	77
$CsPbX_3/Cs_4PbX_6$ (X = Cl or Br)	Lys	200	N/A	N/A	20.2	N/A	SS – grinding	N/A	76
$CsPbX_3/Cs_4PbX_6$ (X = Cl or Br)	Lys	50	N/A	N/A	8.64	N/A	SS – knocking	N/A	76
$CsPbX_3/Cs_4PbX_6$ (X = Cl or Br)	Lys	5–8	N/A	N/A	9.02	>100 h	SS – stirring	N/A	76
$MAPbBr_3$	Lys	9.3 ± 0.9	2	76 ± 19	N/A	7 d	LARP	DMF, HEA, Tol	77
$MAPbBr_3$	Lys	7.9 ± 1.2	2	75 ± 19	N/A	N/A	LARP	DMF, OAm, Tol	77
$MAPbBr_3$	Lys	3.9 ± 0.3	2.1	71 ± 28	N/A	N/A	LARP	DMF, ADA, Tol	77
$MAPbBr_3$	Lys	5.5 ± 0.3	2.1	5 ± 2	N/A	N/A	LARP	DMF, HEA, $CHCl_3$	77
$MAPbBr_3$	Lys	5 ± 0.3	2.2	19 ± 9	N/A	N/A	LARP	DMF, OAm, $CHCl_3$	77
$MAPbBr_3$	Lys	6.8 ± 1	2.1	6 ± 1	N/A	N/A	LARP	DMF, ADA, $CHCl_3$	77
$MAPbBr_3$	Lys-tBoc	4.4 ± 0.3	2.4	57 ± 10	N/A	N/A	LARP	HEA, Tol	77
$MAPbBr_3$	Lys-tBoc	<10	2.38–2.52	57–75	N/A	N/A	LARP	DMF, Hex, Tol, H_2O	78
$MAPbBr_3$	Phe	N/A	2.41	N/A	N/A	N/A	SS – grinding	N/A	63
$MAPbBr_3$	Phe	10.2 ± 1.7	N/A	78	N/A	98%, 2 h, Tol, AC	LARP	DMF, OA, APTES, Tol	79
$MAPbBr_3$	Phe	N/A	N/A	87	N/A	98%, 2 h, IPA, AC	LARP	DMF, MPA, APTES, Tol	79
$MAPbBr_3$	Phe	N/A	N/A	56	N/A	n/a	LARP	DMF, APTES, Tol	79
$MAPbBr_3$	Phe	12–35	N/A	N/A	1 to 32	N/A	Aqueous precipitation	H_2O	46
$MAPbBr_{2.8}Cl_{0.2}$	Phe	12–18	N/A	N/A	12 to 40	N/A	Aqueous precipitation	H_2O	46
$MAPbBr_{2.4}Cl_{0.6}$	Phe	12–18	N/A	N/A	3 to 13	N/A	Aqueous precipitation	H_2O	46
$MAPbBr_{1.8}Cl_{1.2}$	Phe	12–18	N/A	N/A	2 to 9	N/A	Aqueous precipitation	H_2O	46
$CsPbX_3$ (X = Cl, Br, I)	Phe	N/A	N/A	N/A	N/A	6 months, AC	LARP	DMF, Tol	80
$CsPbX_3$ (X = Cl, Br, I)	Phe	12–16	N/A	N/A	N/A	6 months, AC	SS	N/A	80
$CsPbI_3$	Phe	10	N/A	65–93	60–85	15 d, AC	Hot-injection	OAm, OA	81
$CsPbBr_3$	Phe	5.6	N/A	N/A	N/A	N/A	LARP	DMF, ODE, OA, Tol	62
$CsPbBr_3$	Trp	2.2–5.2	2.44–2.6	33–94	N/A	40–60% 48 h C.I./65–95%, 7 d, AC	LARP	DMF, ODE, OA, Tol	62
$CsPbX_3$ (X = Cl, Br, I)	Trp	12–16	varies	N/A	N/A	6 months, AC	SS	N/A	80
$CsPbX_3$ (X = Cl, Br, I)	Tyr	12–16	varies	N/A	N/A	6 months, AC	SS	N/A	80
$CsPb(BrI)_3$ $Cs_4Pb(BrI)_6$	Asp	25	N/A	N/A	N/A	24.7%, 52 h	Hot-injection	OA, ODE, OAm	82
$MAPbBr_3$	Asp	N/A	N/A	N/A	N/A	N/A	LARP	DMF, OA, APTES, Tol	79
$CsPbBr_3$	Glu	N/A	N/A	N/A	N/A	N/A	Hot-injection + ligand exchange	OA, OAm, ODE, Tol	83
$CsPbBr_3$	Glu-tBoc	14	N/A	~100	22.5	10%, 60 d AC/95% 24 h C.I.	Ligand exchange	Tol	84
$MAPbBr_3$	Asn	N/A	N/A	N/A	N/A	N/A	LARP	DMF, OA, APTES, Tol	79
$MAPbI_3$–2D RP	His	Micron	N/A	N/A	N/A	N/A	Recrystallization	HI, IPA	85
$CsPbBr_3/Cs_4PbBr_6$	His	N/A	N/A	N/A	N/A	N/A	SS – stirring	N/A	76
$CsPbBr_3$	His	N/A	N/A	N/A	N/A	N/A	LARP	DMF, ODE, OA, Tol	62
$CsPbBr_3$	Ala	N/A	N/A	N/A	N/A	2 h, ethanol	LARP	DMF, tol	61
MaPbBr3	Ala	N/A	2.42	N/A	N/A	N/A	SS grinding	N/A	63
$MAPbBr_3$	Gly	N/A	2.44	N/A	N/A	N/A	SS grinding	N/A	63
$CsPbBr_3$	Gly	7	2.36	N/A	11.84	95%, 120 h, AC	Hot-injection	OA, OAm, ODE, EA, ACN	86
$CsPbBr_3$	Leu	N/A	N/A	N/A	N/A	N/A	LARP	DMF, ODE, OA, Tol	62
$MAPbBr_3$	Leu	3.5	2.39	N/A	N/A	6 months (AC)	SS grinding	N/A	63
$CsPbBr_3$	α-ABA	10–16	2.73	52.5	11.614	7 d (AC)	Ligand exchange	Tol	87
CsPbI3	PEA	11.5	N/A	82.6	72.4	N/A	Hot injection + ligand exchange	OA, OAm, ODE, MeOAc	88

Table 1 *(Contd.)*

HP	Ligand	Size (nm)	E_g (eV)	PLQY (%)	Lifetime (ns)	Stability	Synthesis method	Synthesis solvent	Ref.
$CsPbI_3$	PEA	16–18	N/A	95	31–58	N/A	Hot-injection + ligand exchange	OA, OAm, ODE	89
$CsPbBr_3$	PEA	6–14	N/A	93	5.44–11.03	N/A	Hot-injection + ligand exchange	OA, OAm, ODE	89
$CsPbI_3$	PIDP	12.2	1.8	70–87	36.3–38.8	N/A	Hot-injection	ODE, OA, OAm, Tol	90
$CsPbI_3$	PEAI	12–14	N/A	81.7	N/A	N/A	Hot-injection	ODE, OA	91
$CsPbI_3$	CF_3-PEAI	10.8–13.7	1.77–1.81	92	51.4–61.6	>60 d (AC)	Hot-injection	ODE, OA	91
$CsPbBr_3$	Lys-TFA	N/A	N/A	N/A	N/A	2 h, H_2O	Precipitation	DMF, HBr, OAm	92
Peptides									
$MAPbBr_3$	Simulated (6,8,12-AA)	3.9	N/A	N/A	N/A	N/A	LARP	DMF, Tol	59
$MAPbBr_3$	Simulated (6,8,12-AA)		N/A	N/A	N/A	N/A	LARP	DMF, Tol	59
$MAPbBr_3$	Simulated (6,8,12-AA)	8.6	N/A	N/A	N/A	N/A	LARP	DMF, Tol	59
$MAPbBr_3$	Cyclo (RGDFK)	6–10	2.73	52.5	11.614	7 d, AC	Ligand exchange	Tol	93
$CsSnCl_3$	Bone gelatin	38	N/A	3.13	7.11	95%, 55 h, H_2O, AC	Hot-injection + coating treatment	OA, OAm, ODE, glycerol	94
$CsSnCl_3$	Skin gelatin	7	N/A	N/A	8.84	80%, 48 h H_2O, AC	Hot-injection + coating treatment	OA, OAm, ODE, glycerol	95
Proteins									
$MAPbBr_3$	Casein	N/A	2.32	50 ± 5	34.49	N/A	Aqueous Precipitation	H_2O	96
$MAPbBr_3$	BSA	7 ± 2	2.31	43 ± 4	26.15	>90%, 80 d AC, 48 h CI	Aqueous precipitation	H_2O	96
$MAPbBr_3$	Hemoglobin	N/A	2.31	20 ± 5	26.07	N/A	Aqueous precipitation	H_2O	96
$MAPbBr_3$	Lysozyme	N/A	2.3	10 ± 4	15.82	N/A	Aqueous precipitation	H_2O	96
$MAPbBr_3$	Trypsin	N/A	2.3	<9	7.03	N/A	Aqueous precipitation	H_2O	96
$MAPbBr_3$	Pepsin	N/A	2.28	<3	3.65	N/A	Aqueous precipitation	H_2O	96
$MAPbCl_3$	BSA	N/A	3.12	9 ± 4	2.55	N/A	Aqueous Precipitation	H_2O	96
$MAPbI_3$	BSA	N/A	1.52	26 ± 3	41.68	N/A	Aqueous Precipitation	H_2O	96
$CsPbBr_3$	M13 bacteriophage	13 ± 2.69	N/A	59–82	7.63	80%, 25 d, AC	LARP	butylamine, OA, DMF, Tol	97
Carbohydrates									
$CsPbBr_3$	SH-β-CD	8 ± 1	N/A	50–90	1.22–3.06	N/A	Hot injection	ODE, OLA, OA, Tol	98
$MAPbBr_3$	β-CD	4.3	N/A	90	t_1 = 9.73 t_2 = 74.23	55%, 120 h, C.I.	LARP	Hex, DMF, Tol	99
$CsPbBr_3$	α-CD	11.5	N/A	85	48.6	65 %, 300 min, AC	LARP	DCM, DMF	100
$CsPbBr_3$	β-CD	13.2	N/A	80	61.9	N/A	LARP	Tol, DMF	100
$CsPbBr_3$	α-CD	14.1	N/A	70	N/A	N/A	LARP	Tol, DMF	100
$CsPbBr_3$	6A-β-CD	1–2	N/A	75	t_1 = 9.6 ps t_2 = 1.5 ns	N/A	LARP	ODE, OA, Tol	101
$CsPbBr_3$	SBE-β-CD	20	N/A	N/A	N/A	100%, 3 h, H_2O	Sonication	OA, OAm, Hex, mineral oil	102
$CsPbBr_3$	BCP	10–20	N/A	>70	5.29–19.6	N/A	Host–guest self assembly	DMSO, DMF	103
Nucleotides									
$FAPbI_3/G_2PbI_4$	Guanine	N/A	1.51	N/A	N/A	5 weeks, AC	SS – grinding	γ-Butyrolactone	104
$CsPbCl_{1.4}Br_{1.6}$	UID-caffeine	6.6	N/A	35.7	5.67	43.2%, 1 h, 90 °C, 70%RH	Hot injection	OA, OAm, ODE, hexane	105
$CsPbCl_{1.4}Br_{1.6}$	UID-caffeine	6.6	N/A	35.7	5.67	43.2%, 1 h, 90 °C, 70%RH	Hot injection	OA, OAm, ODE, hexane	105
$CsPbCl_{1.4}Br_{1.6}$	UID-caffeine	6.6	N/A	35.7	5.67	43.2%, 1 h, 90 °C, 70%RH	Hot injection	OA, OAm, ODE, hexane	105
$CsPbBr_3$	Uracil-caffeine	7.4	N/A	91.4	10.55	39.2%, 1 h, 90 °C, 70%RH	Hot injection	OA, OAm, ODE, hexane	105
$CsPbBr_3$	UID-4-ANMP	7.8	N/A	68.1	7.41	20.7%, 1 h, 90 °C, 70%RH	Hot injection	OA, OAm, ODE, hexane	105
$CsPbBr_3$	UID-6-ADMU	7.8	N/A	80.2	9.57	30.7%, 1 h, 90 °C, 70%RH	Hot injection	OA, OAm, ODE, hexane	105
$CsPbBrI_3$	UID-caffeine	8.7	N/A	95.6	76.23	28.5%, 1 h, 90 °C, 70%RH	Hot injection	OA, OAm, ODE, hexane	105
$CsPbBrI_3$	UID-4-ANMP	8.6	N/A	76.4	51.92	10.3%, 1 h, 90 °C, 70%RH	Hot injection	OA, OAm, ODE, hexane	105
$CsPbBrI_3$	UID-6-ADMU	8.9	N/A	87	64.63	18.2%, 1 h, 90 °C, 70%RH	Hot injection	OA, OAm, ODE, hexane	105
Phospholipids									
$CsPbX_3$ (X = Cl, Br, I)	DOPC, DOPE, DSPE-mPEG, OA	50	N/A	N/A	N/A	37 d in H_2O	LARP + thin film hydration	DMF, OA, OcAm, Hex, $CHCl_3$	106
$CsPbBr_3$	DOPC	70.3 ± 8.2[a]	N/A	28.3	N/A	65.4% 14 d in H_2O	LARP + thin film hydration	OA, OAm, $CHCl_3$	107
$CsPbBr_3$	DOPC/DOTAP	79.1 ± 7.3[a]	N/A	23.7	N/A	54.8% 14 d in H_2O	LARP + thin film hydration	OA, OAm, $CHCl_3$	107
$CsPbBr_3$	DOPC/DOPG	73.2 ± 8.3[a]	N/A	18.2	N/A	68.4% 14 d in H_2O	LARP + thin film hydration	OA, OAm, $CHCl_3$	107
$CsPbBr_3$	Soy lecithin	6–10	N/A	70–90	N/A	N/A	Hot injection	ODE, Tol	108
$CsPbBr_3$	Carnauba wax	7 ± 1.71	N/A	68–70	5.7	91%, 1 d, H_2O/83% 3 months, AC	Hot injection	OA, OAm, Tol	109
Vitamins									
$CsPbCl_{1.5}Br_{1.5}$	Ascorbic acid	7.5 ± 1.51	N/A	21.5	2.17	<50%, 42 d, AC	Hot injection + ligand exchange	OA, OAm, ODE, Hex	110
$CsPbClBr_2$	Ascorbic acid	8.20 ± 0.8	N/A	51	4.72	>60%, 42 d, AC	Hot injection + ligand exchange	OA, OAm, ODE, Hex	110

Table 1 *(Contd.)*

HP	Ligand	Size (nm)	E_g (eV)	PLQY (%)	Lifetime (ns)	Stability	Synthesis method	Synthesis solvent	Ref.
$CsPbBr_3$	Ascorbic acid	8.64 ± 0.55	N/A	99	5.7	72%, 42 d, AC	Hot injection + ligand exchange	OA, OAm, ODE, Hex	110
$CsPbBr_2I$	Ascorbic acid	9.46 ± 0.47	N/A	98	8.09	>60%, 42 d, AC	Hot injection + ligand exchange	OA, OAm, ODE, Hex	110
$CsPbBr_{1.25}I_{1.75}$	Ascorbic acid	9.44 ± 1.23	N/A	96	33.15	>60%, 42 d, AC	Hot injection + ligand exchange	OA, OAm, ODE, Hex	110
$CsPbBrI_2$	Ascorbic acid	11.63 ± 0.60	N/A	95	46.78	69%, 42 d, AC	Hot injection + ligand exchange	OA, OAm, ODE, Hex	110
$CsPbI_3$	Ascorbic acid	10.51 ± 0.50	N/A	95	49.99	<50%, 42 d, AC	Hot injection + ligand exchange	OA, OAm, ODE, Hex	110
Other biomolecules									
$MAPbBr_3$	Succinic acid	10–15	N/A	34	48.44	66%, 1 h, H_2O, AC	LARP	OAm, DMF, $CHCl_3$	111
$CsPbBr_3$	Succinic acid	8.9 ± 0.5	N/A	N/A	N/A	100%, 28 d, H_2O, AC	Hot injection + ligand & phase transfer	OA, OAm, ODE, Tol + PBS/H_2O	112
$CsPbBr_3$	Benzoic acid	7.94 ± 0.4	N/A	97 ± 2	8.09	65%, 1 year, AC	Hot injection + ligand exchange	OA, OAm, ODE, Hex	113
$CsPbBr_3$	4-Bromo-butyric acid	10	N/A	86.4	46.18	79%, 72 h, H_2O, AC	Recrystallization	DMA, OAm, OA, water	114

[a] Hydrodynamic diameter, N/A: not reported. Abbreviations: 6,8,12-AA: 6,8,12-aminododecanoic acid, 6A-β-CD: (6-amino-6-deoxy)-β-cyclodextrin, α-ABA: α-amino butyric acid, AC: ambient conditions, ADA, BCP: polysaccharide-based maltoheptaose-*block*-polyisoprene-*block*-maltoheptaose triblock copolymer, BSA: bovine serum albumin, CD: cyclodextrin, CI: continuous irradiation, cyclo(RGDFK): cyclo(arginine, glycine, aspartic acid, phenylalanine, lysine), DOPA: 1,2-dioleoyl-*sn*-*glycero*-3-phosphate DOPC: 1,2-dioleoyl-*sn*-*glycero*-3-phosphocholine DOTAP: 1,2-dioleoyl-3-trimethylammonium-propane DOPG: 1,2-dioleoyl-*sn*-*glycero*-3-phospho-(1'-*rac*-glycerol) DSPE-mPEG: 1,2-distearoyl-*sn*-glycero-3-phosphoethanolamine-methoxyl poly(ethylene glycol) HEA: hexanoic acid, Hex: hexanes, LARP: ligand assisted re-precipitation, MeOAC: methyl acetate, MPA, OA: oleic acid OcAm: octylamine, OAm: oleylamine, ODE: octadecene, PEA: phenylethylamine, PEAI: iodo-phenylethylamine, PIDP: *p*-iodo-D-Phenylalanine, RP: Ruddlesden–Popper, SBE-β-CD: sulfobutylether-β-cyclodextrin, SH-β-CD: mercapto-β-cyclodextrin, Tfa-Lys: *N*-6-trifluoroacetyl-L-lysine, Tol: toluene, UID: uracil imide derivative; PBS: phosphate buffered saline; DMA: dimethylacetamide.

to carboxylates and amines depending on the electron donating and withdrawing nature of the functional group. AAs that possess side chains with terminal functional groups are of particular interest for HPNCs, largely due to their greater differences in hydrophobicity, polarity, and length relative to AAs with unfunctionalized alkyl side chains. It is therefore logical to assume that bifunctional or trifunctional ligands possessing two or more of these functional groups could be useful ligands during the synthesis of HPNCs.

AAs can be divided into two classes, proteinogenic AAs which are genetically-encoded for protein synthesis, and non-proteinogenic AAs that are not encoded for protein assembly.

Derivatives of AAs discussed in section 2.1.9 are those which are related to common AAs but have structural and/or physicochemical modifications.

2.1. Proteinogenic amino acids as surface ligands

2.1.1. Cysteine. Sulfur-containing ligands such as thiocyanate and thiourea have been used to enhance the optical properties of HPNCs *via* effective passivation of their surface traps and defects.[69–72] Cysteine (Cys) is a sulfur-containing AA with a hydrophobic, neutral, polar sulfhydryl terminal group (–SH). Generally, the lone pairs on sulfur have been shown to coordinate with Pb^{2+} and cationic vacancies in all reports of HPNCs synthesized with Cys.[61,62,69] The strong coordination of S and Pb^{2+} have allowed for the possibility to modulate the morphology of HPNCs during synthesis, and the ability of Cys to form disulfide bonds has enabled the generation of complex structures, as discussed below.

In terms of optical performance, the use of Cys has resulted in varying outcomes that we believe can be attributed to differences in the A site cation in the perovskite. Zhao *et al.* observed no improvements in the performance of Cys-$CsPbBr_3$, relative to OA-capped $CsPbBr_3$.[62] Wang *et al.*[61] demonstrated that altering the concentration of Cys during the synthesis of Cys-$MAPbBr_3$ altered the PLQY, PL intensity and lifetime of $MAPbBr_3$, but report a maximum PLQY of 53.7% for Cys-$MAPbBr_3$, which is lower than what is reported for traditional OA-capped $MAPbBr_3$, around 83%.[73] The conflicting results seem to suggest that relative to using OA as a ligand, Cys either causes no change in optical properties (in case of $CsPbBr_3$), or reduces the performance (in the case of $MAPbBr_3$). Alone, these results suggest Cys may not be worth pursuing for advancing HPNC based technologies. However, the trifunctional nature of Cys enabled the formation of HPNC superstructures, which were used to generate high-performance LEDs (Fig. 1a). Self-assembly of the supercrystal structure was facilitated by the formation of disulfide bonds between Cys molecules on different nanocrystals. Since Cys is the only AA possessing a sulfhydryl group, this type of self-assembly is unique to this AA, as shown by the lack of supercystal formation when Ala was used as a control in the same study.[61]

Additionally, Li *et al.* demonstrated the preparation of ultrathin $CsPbBr_3$ nanowires (NWs) through a post-synthesis treatment of $CsPbBr_3$ nanocubes with aqueous solutions of sulfur-containing Cys, thiourea and thioacetamide (Fig. 1b).[69] As

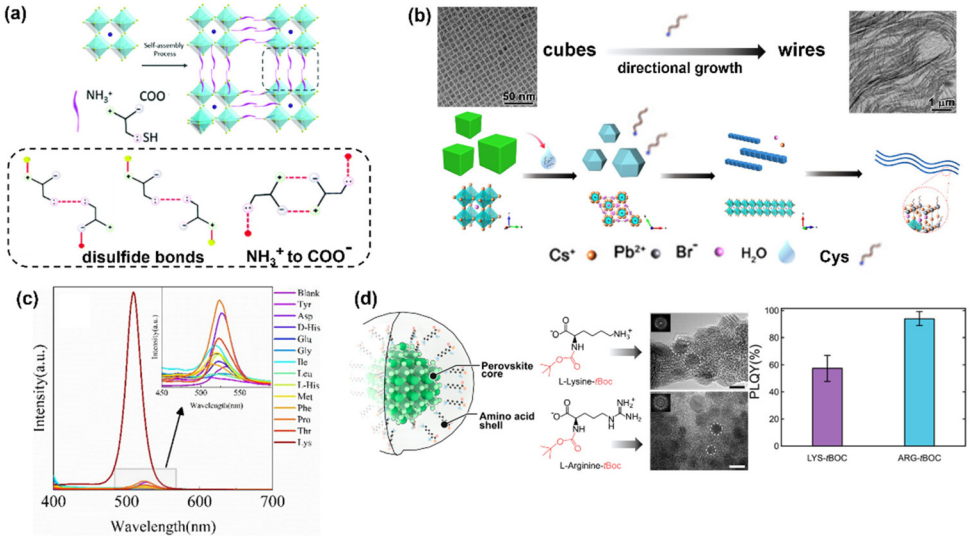

Fig. 1 Specific examples of AA-HPNCs using AAs with an overall positive charge. (a) Schematic representation of the self-assembly mechanism of $MAPbBr_3$ supercrystals using trifunctional Cys.[61] (b) Schematic of the transformation of $CsPbBr_3$ from nanocubes to ultrathin NWs *via* ligand mediated exfoliation in the presence of thiourea, Cys, or thioacetamide solutions and corresponding TEM images.[69] (c) PL emission intensity of HPNCs using different AAs.[76] (d) Schematic illustration of $MAPbBr_3$ NCs capped by Lys-tBoc and Arg-tBoc with their corresponding TEM images and PLQYs.[77] All figures were re-produced and/or modified with permission from the listed references. Panels 1b and d adapted with permission from ref. 69 and 77 Copyright 2019 American Chemical Society.

expected, the sulfur lone pair was shown to coordinate with Pb^{2+} to form relatively stable Pb^{2+}–ligand complexes. These complexes then underwent a two-step conversion to NWs, through a process similar to what is known as a ligand-mediated exfoliation.[74,75] As such, the presence of the sulfhydryl group in Cys is a unique property of this AA that can enable modulation of the morphology of HPNCs.

2.1.2. Lysine and arginine. Lysine (Lys) is a polar, hydrophilic, and basic AA with a side chain composed of a 4-carbon alkyl chain with a terminal amine that is positively-charged at physiological pH. Arginine (Arg) is similar to Lys, except it has a 3-carbon chain with a guanidinium group at the distal end of the side chain, instead of a primary amine; it is also positively-charged at physiological pH. The additional terminal N-containing groups in these AAs provides a unique opportunity to passivate additional anionic defects or increase the number of coordinated halides at the HPNC surface.

Lys has been shown to improve the properties of HPNCs when acting as a surface ligand,[76–78] and when directly incorporated into the crystal structure.[65] Solid-phase mechanochemical synthesis of cesium lead bromide HPNCs (Cs_4PbBr_6 and $CsPbBr_3$) was performed using Lys as a capping ligand.[76] HPNCs synthesized using Lys exhibited much higher PL intensity than NCs with no AA capping ligand, or those synthesized with other AAs (Asp, Glu, Gly, His, Ile, Leu, Met, Phe, Pro, Thr, Tyr), shown in Fig. 1c. Interestingly, Lys was the only AA studied in this series with an additional primary terminal amine. It is unclear whether the presence of the additional amine is the major contributor of the effect, though we postulate this the case. It would be interesting to see the results of Arg, Asn and Gln, also possessing a terminal amine on the side chain, compared to Lys. Different structures and stoichiometries of Cs_xPbBr_y (Cs_4PbBr_6 and $CsPbBr_3$) were formed using the different AAs, and it was found that a larger percentage of $CsPbBr_3$ was obtained when Lys was used, compared to the other AAs. However, in the absence of Lys, no Cs_4PbBr_6 was observed. The authors use X-ray photoelectron spectroscopy (XPS) to confirm the interaction of the terminal $-NH_3$ group with Br^- on the HPNC surface, and postulate the added interaction made possible by the side group on Lys directs the outcome of the composition.

Given that Lys contains two primary amines (one at the alpha position and one on the terminal end of the side chain), and Arg has 3 primary amines (one alpha, two on the side chain), there are two and three opportunities for bonding to HPNCs through an amine group in Lys and Arg, respectively. Prochazkova and colleagues investigated the potential for differences in the $MAPbBr_3$ HPNC synthesis using LARP with both AAs, and the different amines within each one.[77] To achieve this, they used a tBoc protecting group on the alpha amines of Arg and Lys in order to restrict coordination to the terminal amine(s) in the side chains with Br^- during the HPNC synthesis (Fig. 1d). HPNCs prepared with tBoc-modified Lys and Arg had smaller sizes relative to their unmodified AA counterparts. The change in size was attributed to improved nucleation when only the terminal amine is available for coordination to the HPNC precursors. Typically, unmodified AAs are known to self-assemble, which can hinder the nucleation rate of HPNCs and consequently result in increased sizes. With respect to their optical properties, Arg-HPNCs exhibited higher PLQYs than their Lys counterparts in all cases (Fig. 1d). Since, in both cases, the alpha-amine was protected, the major

changes in luminescence stem from the number of terminal primary amines on the side chains as well as the differences in chain length. This suggests that the presence of more amines acts to improve passivation of defects and/or remove more electron density from the lattice, resulting in improved optical performance. The tBoc-Lys HPNCs were chosen for subsequent analysis regarding the effect of water on the optical properties of HPNCs.[78] The authors proposed that due to the strongly hygroscopic nature of tBoc-Lys, hydrogen bonds formed between water and Lys could induce more efficient formation of HPNCs. Small amounts of water resulted in an increase in PLQY, and a decrease in FWHM of tBoc-Lys HPNCs relative to the same nanoparticles synthesized in an anhydrous conditions. However, the perovskites were still unstable when treated with high volumes of water, suggesting that there is a limit to how much water can improve the properties of HPNCs in the presence of tBoc-Lys.

In summary, the presence of the terminal amines in the side chains of Arg and Lys present an additional opportunity to coordinate to the halides on the HPNC surface through a second (or third) amine. The increased coordination to anionic sites due to the increased number of amine groups in these AAs generally seems to improve the luminescence properties (PLQY, emission wavelength and FWHM) of the nanoparticles.

2.1.3. Phenylalanine. Along with Tyrosine (Tyr) and Tryptophan (Trp), Phenylalanine (Phe) is one of the three aromatic AAs containing phenyl groups. Phe is the most basic aromatic AA, with a single unmodified phenyl ring as a side chain. Several studies have found that Phe improves the optical properties and physical stability of HPNCs when used as a ligand. Although its side chain is an unfunctionalized hydrocarbon, the nature of the phenyl ring means Phe has the ability to interact with HPNCs *via* its π system.[113,115] Additionally, the bulky and hydrophobic nature of the benzyl ring can protect the HPNC surface from interaction with water, thus improving the stability of the HPNCs.[62,79–81,116]

Geng *et al.* demonstrated that Phe could be used to improve the PLQY of $MAPbBr_3$ by nearly 40% in the first fully-aqueous synthesis of HPNCs.[46] The authors conclude that the three necessary components of a successful aqueous synthesis of HPNCs is the presence of a lead halide complex, an acidic pH below 5, and the presence of an amine-containing ligand. Interestingly, the reasoning for the use of Phe as the amine-containing ligand in particular was not discussed. It is presently unclear whether other AAs would perform as well in this synthesis method. Furthermore, it was demonstrated that an increase in Phe concentration enhanced the stability of the HPNCs under continuous light irradiation and prolonged storage. Presumably, the hydrophobic nature of Phe, along with the presence of the π system, plays a role in protecting the HPNC crystals from the environment and thus improves the stability.[46]

Phe-capped $MAPbBr_3$ was found to yield a higher PL intensity than HPNCs synthesized with Gly, Ala, and Leu.[63] The attribute the improvement in PLQY to the presence of the phenyl ring, in agreement with other researchers who also demonstrate that the phenyl ring can coordinate to Pb^{2+} through π-mediated Lewis base interactions.[113,115] The HPNCs in this study were synthesized mechanochemically, and Phe-HPNCs showed improved PL with both increased grinding time and Phe concentration up to a threshold, shown in Fig. 2a. This was attributed to increased interactions between the π system of Phe and Pb^{2+} as the grinding time is prolonged.

Multiple additional studies using Phe in HPNC synthesis have demonstrated improved optical properties and stability, attributing the result to the hydrophobic bulky nature of the phenyl ring in the side chain.[62,79–81,116] In all cases, the authors conclude Phe is able to provide more efficient passivation of the HPNC surface relative to traditional ligands used in LARP and hot injection syntheses. Another study compared the performance of Phe relative to other AAs, namely asparagine (Asn) and aspartic acid (Asp). Phe-$MAPbBr_3$ exhibited greater PL intensity and smaller FWHM (Fig. 2b), attributed to improved passivation in the presence of the bulky, hydrophobic phenyl ring.[116]

An in-depth comparison of the performance of $CsPbX_3$ (X = Cl, Br, I) synthesized with the aromatic AAs (Phe, Tyr and Trp) was performed to evaluate the effects of ligand hydrophobicity.[80] The order of HPNC performance was Phe > Trp > Tyr > bare HP. This was in agreement with the expected effects of hydrophobicity, as Phe is the most hydrophobic and Tyr is the least hydrophobic of the three AAs. To further demonstrate this, the contact angles of $CsPbBr_3$ NCs with each AA coating and bare NCs were evaluated. The bare HPNCs and Phe-HPNCs had contact angles of 10.0° and 119° respectively (Fig. 2c). Since larger contact angles indicate decreased physical contact with the environment, this conclusively demonstrates that increased hydrophobicity of the capping ligands directly influenced the degree to which HPNCs interact with their environment.

Shi *et al.* investigated the use of Phe on the optoelectronic properties of $CsPbI_3$ HPNCs, and modelled the effects of Phe on defect density.[81] Phe-capped HPNCs exhibited greater PLQY and stability relative to uncapped HPNCs (Fig. 2d). Density functional theory (DFT) calculations were used to confirm that Phe reduces defect density when on the HPNC surface. Phe had a higher adsorption energy (3.9 eV) than OA (2.3 eV) and OLA (2.5 eV), and a higher vacancy formation energy (3.5 eV) relative to OA (1.6 eV) and OLA (1.4 eV) (Fig. 2e). Combined, these results suggest it is more difficult to form trapping states in the presence of Phe. This also corresponds to an increase in HPNC stability, as it requires more energy to form a defect when Phe is present. Solar cell performance and external quantum efficiency (EQE) of red LED devices based on Phe-$CsPbI_3$ NCs were 14.62% and 10.21%, a significant improvement relative to their pristine counterparts at 13.59% and 3.71% for performance and EQE, respectively (Fig. 2f).[81]

In summary, the aromatic, hydrophobic, bulky properties of Phe have been found to improve HPNC properties on mul-

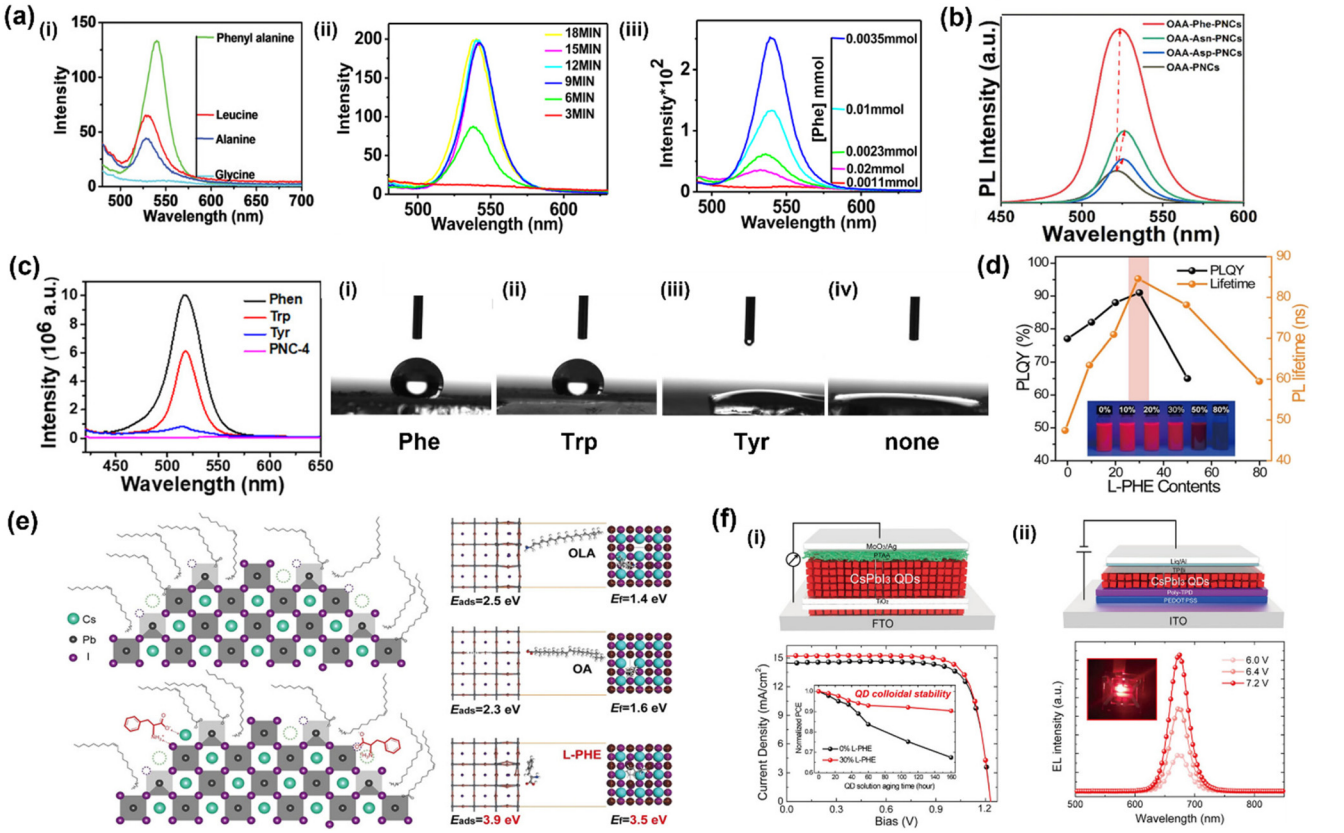

Fig. 2 Highlighted examples of HPNCs synthesized using Phe. (a) PL emission spectra of HPNCs synthesized with Phe, Leu, Ala and Gly *via* a mechanochemical approach. Emission spectra of Phe-HPNCs synthesized under different grinding times and Phe concentrations.[63] (b) PL emission spectra of Phe-, Asn-, and Asp-capped $MAPbBr_3$ HPNCs synthesized *via* hot injection.[79] (c) PL emission of $CsPbBr_3$ NCs mechanochemically synthesized without aromatic amino acids (PNC-4), Phe, Trp, and Tyr as capping agents. The contact angles of $CsPbBr_3$ NCs with (i) Phe, (ii) Trp, (iii) Tyr, and (iv) without ligand.[80] (d) PLQY and PL lifetime of $CsPbI_3$ NCs prepared with different Phe concentrations.[81] (e) Graphical depiction of the surface of $CsPbI_3$ NCs with and without Phe molecules and their corresponding adsorption energy (E_{ads}) and vacancy formation energy (E_f) after the adsorption of OA, OLA, and Phe capping agents on the optimized HPNC surfaces.[81] (f) (i) Structure of the solar cell device constructed based on Phe-$CsPbI_3$ NCs and its *J*–*V* curve and device PCE as a function of storage time. (ii) Photograph of the red LED constructed based on Phe-$CsPbI_3$ NCs and its EL emission at various driving voltages.[81] All figures were re-produced and/or modified with permission from the listed references. Panels 2c and d adapted with permission from ref. 79 and 80 Copyright 2021, 2022 American Chemical Society.

tiple occasions, using different HPNC compositions and synthetic routes. The variety of reports that demonstrate improvements using Phe indicate that the use of this ligand may be regarded as a general strategy for improving HPNC performance.

2.1.4. Tryptophan and tyrosine. Tryptophan (Trp) is an AA which possesses a neutral, nonpolar, aromatic indole as the side chain. Notably, it has been demonstrated that the indole group in Trp can be used to modulate the morphology of $CsPbBr_3$ HPNCs. Zhao *et al.* reported 2D growth of $CsPbBr_3$ by altering the Trp concentration in a modified LARP synthesis (Fig. 3a).[62] Five AAs were examined in this study (Cys, His, Leu, Phe, Trp), and Trp was the only AA to form $CsPbBr_3$ in the desired 2D platelet morphology. While it is not the only AA studied that possesses an aromatic ring, or a ring possessing a heteroatom, it is the only one with a bicyclic system. Reduced growth kinetics were observed in the presence of Trp, concurrent with the production of a 2D morphology. The authors hypothesized that the indole nitrogen in the side chain of Trp could interact with the surface Pb^{2+} ions, reducing the growth rate and encouraging anisotropic growth. However, His was also studied (which possesses an aromatic ring containing a nitrogen) and did not yield 2D HPNCs. The major difference between His and Trp is their monocyclic and bicyclic ring systems, respectively. This comparison was not mentioned, but should be considered for further investigation. Finally, as detailed in Table 1, an increase in PLQY was observed with an increase in the Trp : Pb ratio, along with a gradual red shift of the PL (attributed to the quantum confinement effect), and prolonged physicochemical stability.

Tyrosine (Tyr) is the least hydrophobic of the AAs that contain an aromatic side chain. It has a neutral aromatic phenoxy group at the terminal position of the side chain. As explained in the previous section, Ghosh *et al.* compared the effects of Trp, Tyr and Phe on the mechanochemical synthesis of $CsPbBr_3$, and concluded Tyr exhibited the lowest degree of

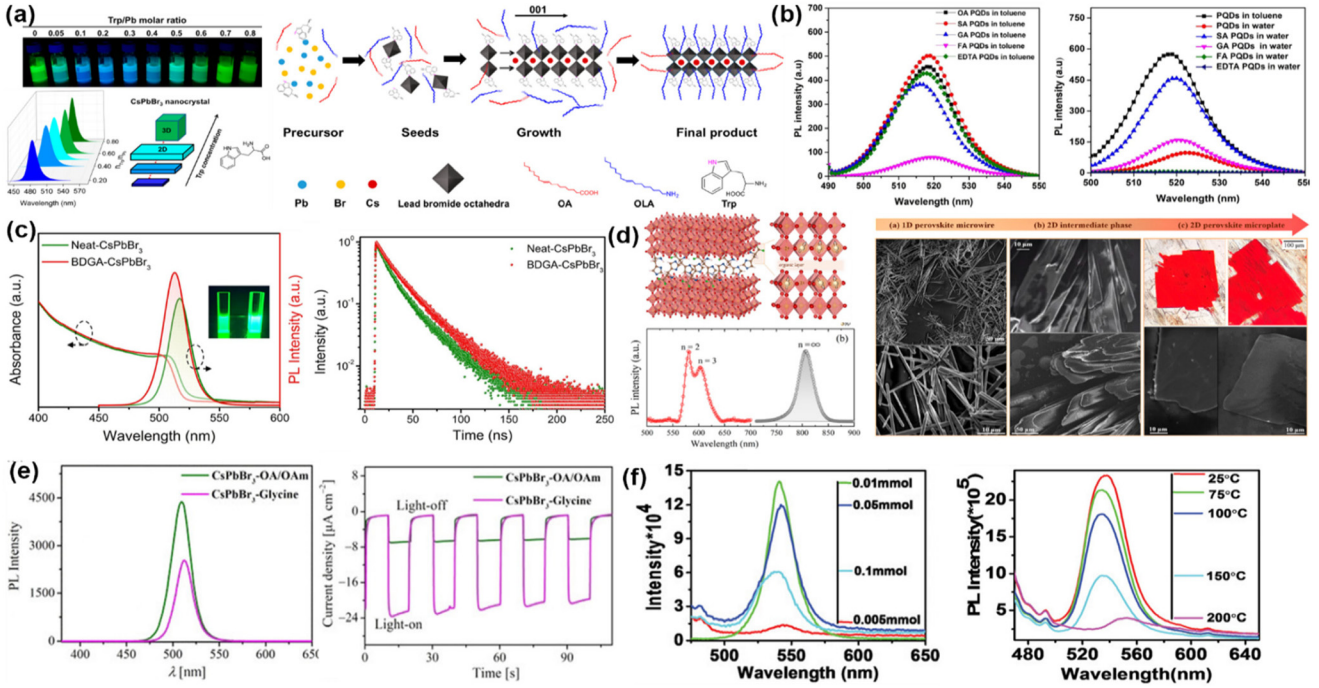

Fig. 3 (a) Photographs and corresponding spectra of PL emission of Trp-$CsPbBr_3$under UV light as a function of Trp concentration. Schematic illustration of the formation of 2D platelets using Trp.[62] (b) PL spectra of $CsPbBr_3$ HPNCs with OA, folic acid (FA), ethylenediamine tetra-acetic acid (EDTA), succinic acid (SA) and glutamic acid (GA) in toluene and water.[83] (c) PL and UV–vis spectra and PL decay under 365 nm excitation of the neat- and BDGA-$CsPbBr_3$ NCs.[84] (d) Crystal structure of 2D RP perovskites as the result of insertion of His spacer and the respective steady-state PL spectra of bulk and 2D RP $MAPbI_3$ phases. SEM and optical images of the samples prepared with different concentration of histidine from low to high histidine concentration regimes.[85] (e) PL spectra of $CsPbBr_3$-Gly NCs dispersed in *n*-hexane in comparison with $CsPbBr_3$-OA/OAm NCs. The photocurrent density of $CsPbBr_3$-Gly NCs is noticeably larger than that of $CsPbBr_3$-OA/OAm NCs. Accordingly, Gly-functionalized $CsPbBr_3$ NCs revealed five times higher conversion yield for the visible light photocatalysis reduction of CO2 than that of control sample.[86] (f) The impact of Leu concentration on the PL emission as well as the temperature-dependent PL spectra of mechanochemically synthesized $MAPbBr_3$ HPNCs.[63] Reproduced and/or modified with permission from the listed references. Panels 3a and d adapted with permission from ref. 62 and 85 Copyright 2018, 2022 American Chemical Society.

enhancement.[80] This was attributed to the lowest hydrophobicity relative to the other two AAs, as confirmed by their contact angles (Fig. 2d). To our knowledge, no other studies evaluate the performance of Tyr relative to other AAs, thus it is difficult to draw conclusions on how this AA may further affect the properties of HPNCs.

2.1.5. Glutamic acid, aspartic acid, and asparagine. Glutamic acid (Glu) and aspartic acid (Asp) are anionic AAs which possess a terminal carboxylate on their side groups; they differ by a single carbon on their alkyl chains. Of note, they are the only AAs that possess multiple carboxylates. Thus, both exhibit higher electron donating capabilities than most AAs. Asparagine (Asn) is an analogue of Asp, as it has a terminal amide instead of a terminal carboxylate.

Interestingly, both Glu and Asp were found to have deleterious effects on HPNC performance.[79,83] Glu was investigated[83] for replacing OA/OAm in the synthesis of $CsPbBr_3$ while Asp was investigated with $MAPbBr_3$ HPNCs.[79] Despite having multiple carboxylate groups, Glu was found to have a lower binding energy than OA to the HPNC surface, which explains the decrease in performance as a lower degree of passivation would be expected with reduced binding energy.[83] Interestingly, when compared with Asp-$MAPbBr_3$, Asn-coated analogues were found to exhibit greater luminescence. This suggests that the presence of additional amines is more beneficial than the presence of additional carboxylate groups. This is corroborated by the results obtained for Arg and Lys-coated HPNCs, as previously mentioned (Fig. 1d).[77]

In contrast, Zhang *et al.* reported PLQYs of $CsPbBr_3$ approaching unity when treated with tBoc-D-Glu (BDGA) post-synthesis (Fig. 3b).[84] They report dramatically improved colloidal stability, high thermal resistance, structural stability, and photostability upon continuous illumination relative to as-synthesized HPNCs (see Table 1). However, the HPNCs were produced using 4,4-aminobis(cyanoaminovaleric acid) (CA) and OAm, and the authors previously report CA-capped HPNCs to have significantly improved long-term optical properties relative to OA-capped HPNCs.[117] In BDGA, the tBoc group protects the amine, thus the only mode of interaction with the NC surface is *via* the available carboxylate groups. It is unclear why such large improvements in optical performance would occur when the amine is protected, but would be interesting to investigate further. The BDGA-$CsPbBr_3$ NCs were applied to produce white light-emitting diodes (WLEDs) with a

high luminous efficacy of 93.5 lm W^{-1} and a wide color gamut about 95% of the value established in the International Telecommunication Union recommendation BT.2020 (Rec.2020) for ultra-high definition displays.[84]

Interestingly, Fang *et al.* used the bicarboxylic nature of Asp to form a core@shell structure of $CsPb(BrI)_3$@Asp-$Cs_4Pb(BrI)_6$.[82] $CsPbX_3$@$Cs_4Pb(BrI)_6$ core@shell NCs could not be formed using other AAs. Asp was the only AA studied that possesses two carboxyl groups, thus the formation of the core@shell material must be attributed to this property of the AA. The core@shell HPNCs exhibited significantly improved ultraviolet, water, and thermal stabilities in comparison with $CsPb(BrI)_3$, owing to the protection of the HPNC core from the environment.

The use of unmodified bicarboxylate-containing AAs does not appear to be promising as a strategy for improving the optical properties of core-only HPNCs, as evidenced by the studies on Asp and Glu-coated HPNCs.[83,84] However, the use of bicarboxylate-containing AAs enabled the successful synthesis of core@shell HPNC materials, which do exhibit improved stability.[82] More studies need to be performed to elucidate the reasons why additional electron donating groups would be deleterious for luminescence and additional electron withdrawing groups are beneficial for HPNC luminescence. Presumably since both act to passivate defects on HPNC surfaces, it is unexpected that one type of passivation is more effective than the other. Interestingly, the results reported for Asp and Glu-coated HPNCs are opposite of what is reported for gelatin and bacteriophages, as discussed in sections 2.2.1 and 2.3.

2.1.6. Histidine. Histidine (His) is a hydrophilic amino acid with an alkyl side chain having a terminal imidazole group, which is partially protonated at physiological pH. It is known as one of the strongest metal coordinating ligands among AAs.[85,118]

Although using His to synthesize $CsPbBr_3$ had minimal impact on their optical properties,[62] it was successfully used to grow 2D layered structures based on $MAPbI_3$ Ruddlesden–Popper (RP) perovskites with n = 2 and 3 (Fig. 3c).[85] The layered nature of RP perovskites relies on the use of a bifunctional spacer molecule, as discussed in section 3. The amount of His determined the number of layers, and notably this is the first instance reported of the imidazole from His successfully coordinating to Pb^{2+} in a HP. The authors demonstrate that His acts as a spacer *via* coordination of the alpha amine in His to I^- in the $[PbI_6]^{4-}$ octahedra in one layer, while the imidazole and carboxyl groups coordinate to metal centers on the other layer. The coordination of His with the lead ions was also observed to locally generate Pb^{3+} instead of Pb^{2+} at the interface, which induced magnetic properties in the material.[85]

Given there are not many reports of using His to modulate HPNC synthesis, it is difficult to draw conclusions about its usefulness. However, the strong metal-coordinating properties of His have been shown to facilitate the production of HPs with magnetic properties. To our knowledge, this is not a common occurrence and thus the use of His for generating magnetic materials may be worthwhile for in-depth exploration.

2.1.7. Alanine, glycine, and leucine. Glycine (Gly), alanine (Ala), leucine (Leu) are the simplest AAs. Gly and Ala have a single hydrogen atom and a methyl group as their side chains, respectively. Leu has a slightly longer alkyl chain than Ala, also with no functional groups. Sharma *et al.*[63] demonstrated that $CsPbBr_3$ synthesized with Gly exhibited almost no luminescence, while PL intensity improved with increasing side chain length and/or the addition of a functional group when using other AAs. This suggests the presence of a side chain, however short, is necessary to obtain HPNC luminescence. The use of Ala gave markedly increased PL intensity relative to Gly, despite the side chain being a methyl group (Fig. 2b), though overall there was relatively insignificant improvement in optical performance using Ala.

Studies on different compositions of HPNCs ($MAPbBr_3$ and $CsPbBr_3$) using different synthetic techniques (mechanochemical and LARP, respectively) have both demonstrated a lack of effect of Ala on improving the optical properties HPNCs.[61,63] The agreement in results, despite the very different synthesis conditions, strengthens the likelihood that Ala is generally not promising for improving optical properties of HPNCs. This indicates that although amine and carboxylic acid functional groups of AAs are vital to passivate HPNCs,[66,68] the side chain, however simple, also plays a role in the formation of stable, luminescent HPNCs.

Although Gly is thus far not effective at improving the optical properties of HPNCs, it has been demonstrated that it can be used to increase the photocatalytic efficiency of $CsPbBr_3$ HPNCs. Xu *et al.* applied a simple ligand-exchange technique as a post-synthesis treatment to replace conventional OA and OAm ligands with Gly, endowing the $CsPbBr_3$ HPNCs with a five times higher CO_2-to-CO conversion efficiency relative to their untreated counterparts (Fig. 3d).[86] This was attributed to the increased charge separation of photogenerated carriers due to a reduction in steric hindrance when using the short-chain Gly molecules.[86] Despite these promising results, further investigation is vital to conclusively establish the role of AAs in the photocatalytic performance of HPNCs, and the properties that govern their role in modulating the photocatalytic efficiency.

Leu has a slightly longer alkyl side chain than Ala, thus it has increased hydrophobicity but no functional groups. The addition of Leu in a LARP synthesis of $CsPbBr_3$ was not found to affect the PL wavelength or intensity of the HPNCs, regardless of the concentration used, nor did it improve the PL of Cs_4PbBr_6 and $CsPbBr_3$ HPNCs when synthesized *via* a mechanochemical stirring approach (Fig. 1c).[62,76] In contrast, $MAPbBr_3$ synthesized *via* mechanochemical grinding using Leu as a ligand resulted in improved optical properties relative to the same HPNCs synthesized using Ala and Gly (Fig. 2b), but no comparison was made to HPNCs synthesized with traditional ligands such as OA.[63] They further established that there was an optimal Leu concentration required to obtain the

highest PL intensity, and further increasing concentrations of Leu were found to be deleterious (Fig. 3e-i). This suggests an excess of Leu relative to the inorganic components hinders the PL process, potentially due to the insulating effect hydrophobic molecules tend to have on HPNCs, as previously mentioned. While the authors did not perform a direct comparison of the stability of Leu-$MAPbBr_3$ *versus* conventional OA- and OAm-$MAPbBr_3$, the reported stabilities of the Leu-HPNCs are markedly improved relative to literature reports of OA and OAm-$MAPbBr_3$ (see Table 1). Whereas OA and OLA-$MAPbBr_3$ are generally reported to be stable in ambient, dark conditions for days, and decompose at temperatures above 70 °C, Leu-$MAPbBr_3$ HPNCs were found to exhibit long-term storage stability and high temperature and moisture resistance (Fig. 3e-ii).[116,119,120] These results build on the observation that hydrophobic ligands maintain the stability of NCs by protecting the HPNCs from water, and indicates that Leu might be superior at improving the stability of HPNCs than OA and OAm.

Though more research is needed to demonstrate the universality of the observations presented above, the results of these studies suggest that while the carboxylate and amine functionalities of AAs improve the synthesis of HPNCs, with respect to optical properties, the presence of an alkyl-based AA side chain is essential for obtaining any degree of luminescence. Interestingly, despite the reduced optical performance of HPNCs made using Gly, a marked improvement in CO_2-to-CO conversion was demonstrated. Thus, AAs which have been written-off as impractical for improving optical properties may still be beneficial for improving other properties of HPNCs; this should be investigated in more detail.

2.1.8. Non-proteinogenic amino acids and their derivatives. As previously mentioned, non-proteinogenic AAs are not used in protein assembly, but they still possess the desired amine and carboxylate functionalities useful for HPNC synthesis. Furthermore, many of the non-proteinogenic AAs and AA derivatives have similar structures to the essential AAs, and thus can expand the scope of their use in HPNC synthesis.

A ligand exchange method was used to synthesize α-ABA-$CsPbBr_3$ NCs by ligand exchange with OA and OLA.[87] α-amino butyric acid (α-ABA) is a non-proteinogenic AA with a side chain that is one carbon longer than the alanine side chain. The addition of α-ABA resulted in increased fluorescence and a larger bandgap, despite a decrease in particle size of HPNCs after ligand exchange. They also showed better stability in toluene over seven days compared to the as-synthesized HPNCs. It was proposed that the α-ABA was able to better passivate the NC surface and improve electron transport, thus reducing non-radiative recombination relative to OA and OAm. While long chain organic ligands such as OA and OLA are known to increase the stability of HPNCs, they are also known to hinder efficient charge transport, thus the short chains of α-ABA are advantageous in this respect. The authors in this study were able to produce a single composition HPNC with tandem band gaps, by encapsulating the pristine HPNCs and the α-ABA-HPNCs with TiO_2. The encapsulation brought together two NCs with different ligands, showing no loss in individuality since there was no loss in PL intensity or changes in the optical properties of either NC, as PL spectra showed distinct peaks for the two different types of NCs. This further demonstrates that α-ABA was able to effectively passivate the surface anionic defects of HPNCs and minimize ion exchange.

In addition, several derivatives of Phe have been studied, including phenylethylamine (PEA) and *p*-iodo-D-Phe.[88–91] Derivatives of Phe appear to produce a similar degree of success to Phe itself, with multiple improvements to HPNCs demonstrated through the use of these derivative molecules. Phenylethylamine (PEA) has been used on multiple occasions to produce $CsPbX_3$ ($X = Br^-, I^-$) HPNCs with remarkably high PLQY.[88,89] PEA is a derivative of Phe with a terminal primary amine on one end, and a phenyl ring at the opposite end. While PEA does not possess a carboxylate group, it is able to coordinate with the HPNC surface through π interactions with the phenyl ring, and through electrostatic coordination between the amine and the halide ion on the NC surface, as demonstrated by XPS.[79] Two reports utilized a partial ligand exchange technique to introduce PEA to the HPNC surface while keeping OA and OAm partially intact on the surface.[88,89] By reducing the amount of OA and OAm, the insulating effects of these ligands were reduced, allowing for increased charge transport. Addition of PEA simultaneously acted to passivate the HPNC surface and improve the PLQY and stability. Li *et al.* reported a PLQY of 95% and 93% for PEA-treated $CsPbBr_3$ and $CsPbI_3$, respectively (Fig. 4a), while Zhang *et al.* reported a PLQY of 82.6% for PEA-treated $CsPbI_3$.[88,89] Both works attribute the improvements to efficient neutralization of surface defects and improved surface passivation, thereby suppressing deleterious non-radiative recombination pathways. The improved surface passivation was proven by measuring contact angles, showing PEA-treated $CsPbI_3$ was more hydrophobic with a contact angle of 88°, while the untreated control had a contact angle of 66°.[79] This is in agreement with what was observed for Phe, Tyr and Trp-coated HPNCs, where higher contact angles were associated with better passivation and stability, as previously discussed (Fig. 2d).[80]

External quantum efficiencies (EQE) of 14.18% and 14.08% were reported for PEA-treated $CsPbI_3$ HPNCs and PEA-treated $CsPbBr_3$ HPNCs when incorporated into thin film solar cells[79] and LED devices,[80] respectively (Fig. 4a and b). It should be noted that these HPNC thin films were generated using discrete nanoparticles, unlike the HP thin films discussed in section 3. Interestingly, these achievements may imply that the presence of the carboxylates in AAs may not contribute significantly to improved PLQY when aromatic groups are present, as the major difference between Phe and PEA is the presence of the carboxylate moiety, and both are found to improve the PLQY of $CsPbX_3$ HPNCs. Given that both carboxylates and aromatic rings are able to coordinate to metal centers and act to reduce electron density at the HPNC surface, it is unsurprising that they may have interchangeable roles.

Halogenated derivatives of Phe have also been demonstrated to passivate the surface of $CsPbI_3$ HPNCs upon post-synthesis ligand exchange. Tang *et al.* used PIDP to replace OA

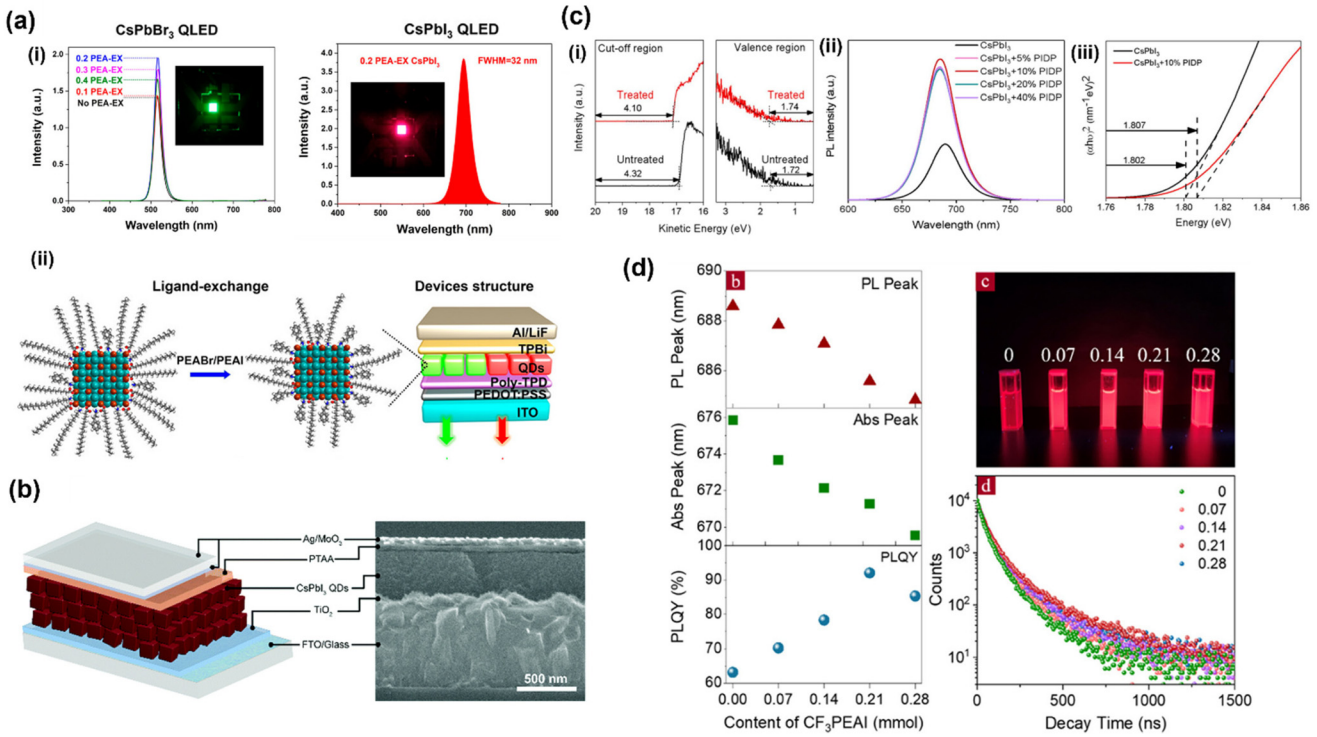

Fig. 4 Selected examples of halogenated AA-HPNC studies. (a) Schematic of the ligand exchange to partially replace OA with PEABr/PEAI for the fabrication of high-performance $CsPbBr_3$ and $CsPbI_3$ QLEDs and the corresponding photographs and emission spectra of the QLEDs.[89] (b) PL lifetimes of $CsPbI_3$ HPNCs at different PEA concentrations together with the diagram and SEM image of the corresponding fabricated solar cells.[88] (c) (i) PL spectra of $CsPbI_3$ NCs as a function of PIDP : PbI_2 ratio under 405 nm light. (ii) Impact of treatment time on PLQY of the pristine and the PIDP-treated CsPbI NCs. (iii) UPS spectra and Tauc plots of pristine and PIDP-treated $CsPbI_3$ NCs.[90] (d) The effect of different amounts of CF_3PEAI on the optical properties $CsPbI_3$ NCs.[91] Reproduced and/or modified with permissions from the listed references. Panel 4a and d adapted with permission from ref. 89 and 91 Copyright 2018, 2022 American Chemical Society.

and OAm on the surface of $CsPbI_3$ HPNCs.[90] The PIDP-treated HPNCs exhibited improved PL intensity, PLQY, lifetime and charge injection capabilities relative to their untreated counterparts with identical size and bandgaps (Fig. 4c). The improvement in optical properties was attributed to the ability of PIDP to passivate the surface *via* the same mechanisms as Phe, but with the added role of the terminal iodine to fill the halogen vacancies on the HPNC surface, thereby reducing the number of surface trap states and minimizing nonradiative recombination pathways, as confirmed by XPS. Finally, the authors also fabricated a highly efficient red-emission LED device with an EQE of 12.4%, more than double that of pristine NCs at 5.8%. Another halogenated Phe derivative, 4-trifluorophenethylammonium iodide (CF_3PEAI), was shown to assist the formation of $CsPbI_3$ HPNCs by effectively filling the I^- vacancy on the HPNC surface, as well as partially replacing OAm ligands.[91] The performance of CF_3PEAI was compared to unhalogenated PEAI and OAm ligands, and it was found that the presence of the terminal fluorides substantially increased the overall polarity of the ligand, which subsequently reduced the defect density on the HPNC surface by reducing the electron density of the nanocrystal. A quantifiable decrease in defect density was demonstrated, along with an increase in PLQY relative to OAm-$CsPbI_3$. The reduced defect density also enhanced the thermal stability of the HPNCs and improved their long-term storage in ambient conditions. As observed with other AAs, the enhancements were dependent on the concentration of CF_3PEAI capping agent (Fig. 4d). The red LEDs based on CF_3PEAI-$CsPbI_3$ HPNCs were found to produce a 4.6-fold improvement in maximal luminance relative to OAm-$CsPbI_3$. A maximum EQE of 12.5%, was obtained for the CF_3PEAI-NCs, while the EQE of the LEDs based on PEAI- and OAm-$CsPbI_3$ NCs were 9.92% and 5.46%, respectively.[91] A similar report using a fluorinated analogue of Lys (Tfa-Lys) demonstrated improved optical properties, presumably for similar reasons.[92]

Overall, the introduction of halogenated aromatic AA derivatives appears to be an attractive strategy to neutralize surface defects resulting from halogen vacancies, as well as remove excess electron density in the nanocrystal host. This should be investigated further with other halogens, HPNC compositions, and other AA derivatives.

2.1.9. Incorporating amino acids into the crystal structure of halide perovskites. Biomolecules like AAs are not only useful ligands for improving the properties of perovskites by surface passivation, but they can also directly be incorporated into the crystal lattice structure of HPs. Their incorporation can either occur much in the same way that methylammonium

has been used as the "A" cation in the ABX_3 structure to form conventional HPNCs, or they can be used to generate 2D perovskite layered structures with the general formula of A_2BX_4.

In this regard, a huge number of new HP compositions have been formed using biomolecules including but not limited to alanine,[64,121,122] 3-aminobutyric acid,[123] 4-aminobutyric acid (GABA),[124,125] 5-aminovaleric acid and its derivatives,[122,126–128] cysteine,[129] glycine,[130] histidine,[129] leucine,[122] lysine,[65,131] ornithine,[131] phenylethylamine,[126,132–137] proline,[138] and taurine.[129] While a few of the examples listed above represent novel ABX_3 HPNCs, the vast majority represent novel 2D perovskite layered structures. The A^+ cation in the 2D layered structure creates an organic bilayer and divides the perovskite sheets, which generates a novel and extensive class of HPs by varying the organic cation's structure.[129,132] Therefore, the addition of such molecules into the HP structure is of considerable importance due to their intrinsic organic (insulating) and inorganic (semiconducting) structures. HP thin films are discussed in section 3. This new class of HPs often possesses increased stability and remarkable optoelectronic properties on account of their structural and compositional flexibility, which enables new functionalities in optoelectronic and magnetic HP materials.

2.1.10. General trends and outlook on the future use of amino acids in halide perovskite nanocrystals. It has been observed that functional groups, especially those on the side chain of AAs, act to either modulate the synthesis or the optoelectronic properties of HPNCs. While both carboxyl and amine groups play a role in the synthesis dynamics, amine groups seems to be investigated more thoroughly and their presence may have a more prominent effect on modulating the morphology and optoelectronic properties of the HPNCs. In addition, trifunctional AAs possessing additional functional groups on their side chains make it possible to generate more complex structures such as RP perovskites and supercrystals.

The presence of a side chain on AAs generally improves luminescence – it has a definite influence on the luminescence properties over and above what is induced by the presence of the carboxyl and amine groups. Additional amines can coordinate to halides and reduce electron density, seemingly resulting in improved luminescence. In contrast, additional carboxylates seem to be deleterious to the luminescence despite their coordination to metal sites, owing to their electron donating properties. Aromatic groups can also coordinate to metals *via* their π systems and increase electron densities, having a positive effect similar to what is generated with carboxylates. There is also a positive correlation between increased hydrophobicity of the aromatic group and stability and luminescence of the HPNC.

Shorter, linear molecules are seen to improve the conductivity of HPNC, while longer and more hydrophobic molecules have insulating effects. However, molecules that are more bulky or hydrophobic were able to shield HPNCs from environmental stressors such as humidity. These trade-offs should be considered in each specific application.

2.2. Peptides

Peptides are short chains of two or more AAs connected *via* peptide bonds. Similar to AAs, peptides are interesting candidates because they also possess terminal carboxyl and amino groups. What separates peptides from individual AAs is the possibility for incorporating an unlimited combination of functional groups into a peptide chain through the choice of AAs and their side chains, instead of using multiple individual ligands. Furthermore, peptides have a much-reduced ratio of free amines and carboxylates relative to AAs, as these groups are used to form the peptide bonds that generate the peptide structure.

Luo *et al.*[59] simulated the effect of using short peptides by using 6-, 8-, and 12-aminododecanoic acid (6-, 8,- and 12-AA), in the synthesis of both $MAPbBr_3$ and $CsPbBr_3$ HPNCs *via* LARP. These molecules have alkyl chains of various lengths, with amine and carboxyl groups on either end, thus representing the terminal ends of a peptide chain but without the complex functional groups or peptide bonds in the middle. 12-AA-HPNCs exhibited the strongest PL intensity, demonstrating adequate protection from the surrounding environment in a similar manner to OA. This study found that increasing the 12-AA concentration beyond a threshold caused a decrease in HPNC size, with a rapid loss in PL intensity when the ligand concentration passed 0.15 mM, suggesting an increase in defect density as the particles became smaller. Thus, there is an optimal concentration of ligands needed to generate high quality HPNCs, which is in accordance with the results obtained using AAs.[63]

Prochazkova *et al.* synthesized $MAPbBr_3$ HPNCs with a commercial cyclic peptide cyclo(RGDFK), composed of 5 proteinogenic AAs: Arg, Asp, Gly, Lys, and Phe, as shown in Fig. 5a.[93] Computational analysis was used to determine whether cyclo (RGDFK) coordinates to the HPNCs *via* its free guanidyl group on Asp or through its free primary amine on Arg, but coordination *via* the terminal carboxylate and phenyl group on Phe was not considered, nor was coordination *via* the central peptide ring through the N atoms. Given the original OA-mediated synthesis relies on coordination of the carboxylate to mediate the nucleation and growth of the NCs, it is peculiar that coordination *via* the carboxylate was not considered. Regardless, bonding through the primary amine was found to result in a minimized Gibbs free energy, thus the authors conclude this is the most likely scenario. This is consistent with another study which used chains of nucleic acids where the primary amine group is also the most favorable group in binding to the surface of HPNCs.[60] The PLQY of cyclo (RGDFK)-$MAPbBr_3$ was reported to be 20%, is significantly lower than most HPNC reports using ligands possessing amino and carboxyl groups. The reduced PLQY was attributed to charge transfer between the peptides and the HPNCs, causing additional non-radiative quenching pathways. Additionally, the absorption spectrum of cyclo(RGDFK) also overlaps with the emissions of $MAPbBr_3$[139] thus it can re-absorb some of the light emitted by the HPNCs and cause

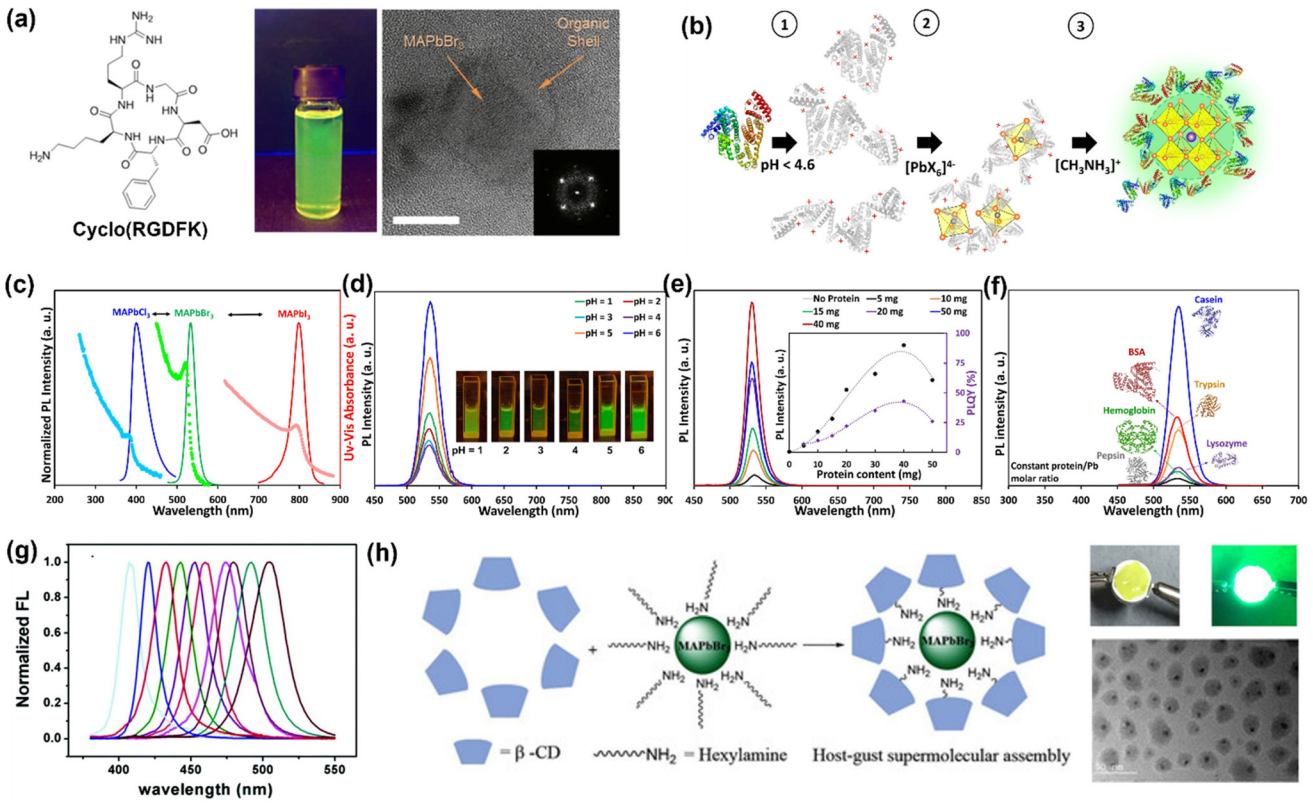

Fig. 5 Selected examples of HPNCs synthesized with macromolecules. (a) TEM of cyclo(RGDFK)-HPNCs, photograph of PL from cyclo(RGDFK)-HPNCs and chemical structure of the cyclo(RGDFK) cyclic peptide.[93] (b) Schematic of the aqueous synthesis mechanism of $MAPbBr_3$ NCs using BSA protein as the surface capping agent. (c) UV-vis absorption and PL emission of BSA-encapsulated $MAPbCl_3$, $MAPbBr_3$, and $MAPbI_3$ NCs.[96] (d) PL emission (λ_{ex} = 405 nm) of BSA-HPNCs as a function of protein concentration. The inset exhibits the PL peak intensities along with PLQY variations with the amount of BSA protein.[96] (e) Impact of pH of the synthesis solution on PL emission of BSA-HPNCs. The inset photos show the emission of colloidal NCs under UV illumination at different pH.[96] (f) The impact of casein, BSA, hemoglobin, trypsin, lysozyme, and pepsin proteins on the PL spectra of HPNCs synthesized with constant protein molar ratio.[96] (g) PL emission spectra of the encapsulated $CsPbBr_3$ NCs as a function of SH-β-CD concentration.[98] (h) TEM image and schematic of $MAPbBr_3$/β-CD NCs achieved through host–guest interactions between β-CD and hexylamine, photograph of LED fabricated using these HPNCs.[99] Reproduced and/or modified with permission from the listed references.

reduced PLQY; this was not discussed by the authors but we postulate this to be a contributing factor.[140]

2.2.1. Gelatin. Gelatin is a hydrolyzed form of collagen, and can be regarded as a variant of a peptide. As such, it contains both carboxyl and amino groups, along with other functional groups depending on the source of the gelatin. Gelatin extracted from animal skin[95] and bone[94] have been applied post-synthesis to $CsSnX_3$ ($X = Cl^-, Br^-, I^-$) HPNCs with successful results. In both cases, surface defect passivation was achieved along with suppression of oxidation of Sn^{2+} to Sn^{4+}. These water-soluble, natural polymeric materials were found to coordinate to the HPNC surface *via* amino-Sn, carboxylate-Sn, and halogen-ammonium hydrogen-bonding interactions. The bone-derived gelatin-HPNCs exhibited slightly better water stability (95% retention of the PL intensity after 55 h) and larger crystal size than the skin gelatin-HPNCs (80% retention of the PL intensity after 48 h in water). The authors attribute the increased stability of the bone gelatin-HPNCs relative to the skin-gelatin HPNCs to be due to a substantially higher proportion of carboxylate groups in bone gelatin, which they postulate allows for a higher degree of coordination to the surface metal cations. This is in contrast to what was observed with a higher proportion of carboxylates when Asp and Glu were used as ligands in HPNC synthesis. The hydrophilic, polymeric nature of gelatin along with the variable carboxylate : amine ratio depending on the source of the material may allow for future tunable ratios of these functional groups that provide even greater surface passivation and aqueous stability. However, there appears to be limited understanding of the degree to which each type of functional group contributes to improving the HPNC properties, as discussed in section 2.1.

2.3. Proteins

Proteins exhibit a much higher degree of chemical, conformational and functional diversity than AAs and peptides. The complex nature of these macromolecules makes it possible to rationally design protein–inorganic material interactions and direct the synthesis of complex hierarchical structures which are not easily attainable by traditional techniques. Various new nanostructures generated through protein–inorganic material

interactions have been synthesized using the templating properties of proteins.[141–145] Thus far, the interaction between proteins and HPNCs has not been extensively explored, nor has the impact of proteins on the stability and optoelectronic properties of HPNCs in an aqueous environment. Inspired by the advancements made using AA-HPNCs, our research group has used proteins for the first time, to the best of our knowledge, to mediate and protect $MAPbX_3$ ($X = Cl^-$, Br^-, and I^-) NCs in a fully aqueous environment (Fig. 5b).[96] We experimented with different proteins during the synthesis process, including casein, BSA, hemoglobin, trypsin, lysozyme, and pepsin, to demonstrate the versatility of our approach. Overall, casein-passivated HPNCs showed the highest PL intensity (Fig. 5d and e) and PLQY, as well as the longest PL lifetime among the other protein-capped HPNCs, which indicates that casein is the most effective and efficient at passivation of surface defects and traps. BSA- and casein-HPNCs are stabilized in fully aqueous environment for about 3 months, with only a 10% reduction in PL intensity. This is a dramatic improvement from most systems reported thus far, as most systems are reported to be stable in ambient conditions (*i.e.* in powder form) for only weeks. The protein-HPNCs are optically active from pH 1 to 6, and their optoelectronic properties are contingent on pH and protein concentration, with the optimal luminescence observed at pH = 6 and protein content of 40 mg in the case of BSA (Fig. 5f and g). These features are very important and in high demand for biological applications. In this regard, we believe that several characteristics of the protein molecules can directly impact the quality of the NCs, including but not limited to the 3D structure, AA sequence and composition, size, degree of hydrophobicity and isoelectric point.[96] Given the complex nature of proteins and the inter-related nature of these parameters, further studies are needed to elucidate the precise roles of each of the above-mentioned parameters on the optoelectronic properties of HPNCs.

Complex biological agents like viruses also can be roughly thought of as an amalgamation of macromolecules, and therefore may be interesting for passivating a HP surface. The M13 bacteriophage has pVIII proteins on its surface and has been studied for the purpose of growing a stable one-dimensional cubic-shaped $CsPbBr_3$ NC network.[97] The M13 bacteriophage possesses Ala, Lys, Asp, and Glu AAs on its surface. Asp and Glu were found to coordinate to Pb^{2+} and increase electron density at the surface metal cation sites, thereby lowing the energy of the valence band. The authors report suppressed degradation of the HPNCs, which they attribute to the change in valence band energy. They propose the change in valence band energy makes it more difficult to oxidize the HPNCs and induce their decomposition, which is an interesting avenue for modulating stability and should be investigated in more depth. Computational and experimental analyses proved that adding the bacteriophage had a critical impact on the lattice constant and band energies of the HPNCs, leading to improved optical properties in all respects compared with the pristine sample (Table 1). It was further demonstrated that it was possible to induce genetic modifications in the bacteriophages to bear more negative charges (*i.e.*, increased surface charge density) at the terminus of the p8 protein. This was found to assist in improved growth and binding of NCs as well as greater quantum confinement effects, thus improving PLQY up to 82%.[97]

In summary, proteins and protein-containing agents are highly promising for improving HPNC properties, especially with respect to stability in aqueous environments. The virtually unlimited variations in protein structures can allow for precise tuning of properties that are optimal for the HPNCs being investigated. Future studies taking advantage of proteins as ligands are promising and can potentially also provide the ability to sense analytes or deliver drugs conjugated to the protein structure. It will be interesting to see the avenues taken using these biomolecules as ligands.

2.4. Carbohydrates

Carbohydrates are macromolecules composed of saccharide molecules, which are commonly five or six-membered rings with the empirical formula $C_m(H_2O)_n$. When two or more of these simple macrocycles are bonded together *via* glycosidic linkages, they are referred to as disaccharides, oligosaccharides or polysaccharides. Cyclodextrins (CDs) are cyclic oligosaccharides composed of glucose subunits joined together *via* α-1,4-glycosidic bonds. The number of glucose units in the ring gives rise to CDs of different sizes, where the inner cavity of the macromolecule is hydrophobic and the externally-facing rims are hydrophilic due to the presence of multiple hydroxyl groups. The 3D, toroidal shape of cyclodextrins makes them ideal candidates for use in host–guest systems, they can accommodate a variety of different hydrophobic guest molecules in their cavity. β-Cyclodextrin (β-CD) is the most popular CD, consisting of seven glucose subunits. The hydroxyl groups on the rims of CDs can be modified with a range of different functionalities, imparting CDs with different properties.

Several modified CDs have been used to encapsulate or coat the surface of HPNCs, taking advantage of the hydrophilic and hydrophobic regions of these biomolecules.[98–102] This has been achieved either by host–guest interaction of CDs with alkyl ligands on the surface of as-synthesized HPNCs, or by using CDs as ligands themselves.

Mercapto-β-cyclodextrin (SH-β-CD) was used in the first demonstration of PL emission modulation of HPNCs exclusively through supramolecular interactions.[98] To achieve the supramolecular interaction, OA and OAm-capped $CsPbBr_3$ HPNCs capped with OA and OAm simply dispersed in solutions of different concentrations of SH-β-CD. The alkyl chains of OA and OAm on the HPNC surface were included in the hydrophobic cavity of SH-β-CD *via* host–guest interactions, resulting in blue-shifted PL emissions that spanned over half of the visible spectral region depending on the concentration of SH-β-CD (Fig. 5h). Increasing concentrations of SH-β-CD resulted in more substantial blue-shifts, as well as a decrease in HPNC size as evidenced by TEM. The reason for the decrease in NC size upon introduction of the CDs remains unclear. Interestingly, the use of unmodified β-CD did not

induce a shift in PL emission, and neither did the introduction of sulfhydrl groups in the absence of CDs, thus indicating both components were crucial for obtaining the change in optical properties. The prominent role of the sulfhydryl group of SH-B-CD in modulating the optical properties of $CsPbBr_3$ is somewhat surprising, given that HPNCs synthesized with Cys exhibited either no change in PL, or reduced PLQY.[61,62] This suggests a synergistic effect between the sulfhydryl group and CD host–guest interaction with the HPNCs that results in desirable outcomes on the PL properties, and should be investigated in more detail.

Unmodified β-CD was subsequently shown to improve the optical properties of $MAPbBr_3$ when hexylamine was used as the capping agent.[99] The obtained β-CD-hex-HPNCs exhibited a high PLQY of about 90% and high stability in the presence of water, heat, and UV light.[99] The formed core/shell NCs were been used as a phosphor to produce LEDs with good color purity (Fig. 5h). The improvement in optical properties may be attributed to the bulky nature of the CD, which could prevent water from interacting with the HPNC surface. Sulfobutylether-β-CDs have also been used to stabilize $CsPbBr_3$ NCs using the host–guest interaction strategy.[102] The CD-coated HPNCs demonstrated improved stability in aqueous media, but no change in optical properties relative to OA/OAm-coated $CsPbBr_3$.

In summary, the three studies above demonstrated different outcomes of CDs on HPNCs of the same composition. Taken together, type of CD, its functionalization, and the effect of pre- or post-synthesis incorporation of CDs should certainly be investigated further, as it is unclear to what extent each of these variables has on the optical properties. Regardless, host–guest interactions between the alkyl chains on HPNC ligands and CD cavities appear to a viable route to improve the stability of HPNCs, but their role in modulating optical properties remains unclear.

Instead of utilizing host–guest interactions to passivate the surface of HPNCs with CDs, Guo *et al.* synthesized $CsPbBr_3$ NCs solely with α- and β-CDs as a ligand.[100] XPS and FTIR analyses confirmed strong coordination of the electron lone pairs on oxygen in the hydroxyl groups of CDs with the metal cations in the HPNCs, generating surface-passivated HPNCs solely using CD molecules. The HPNCs passivated with α-CD exhibited higher PL intensity relative to β-CD-HPNCs, attribute to be due to the smaller size of α-CD, which leads to increased coverage of the HPNC surface and therefore better passivation. α-CD-$CsPbBr_3$ NCs exhibited similar optical properties to the same NCs coated with OA/OAm, but vastly improved stability (Table 1). Thus, directly capping HPNCs with CDs appears to provide efficient passivation and represents an attractive route to producing highly stable HPs.[100] Of interest, the colloidal stability of the α-CD-HPNCs in water was not demonstrated, despite the demonstrated long-term stability of the NCs in humid environments. Future studies should certainly aim to investigate the stability of these materials in aqueous solutions, given that the hydrophilic nature of the outer rim of CDs should result in colloidal dispersibility in water.

Beyond acting as surface passivating agents, CDs have also been used as templates to modulate the size of HPNCs during synthesis.[101] Ultrasmall $CsPbBr_3$ NCs (1–2 nm) with bright and wide blue emissions and PLQY of 72.4% were synthesized using (6-amino-6-deoxy)-β-cyclodextrin (6A-β-CD) to restrict the growth of HPNCs to the width of the CD cavity.[101] There were no variations on the size and morphology of NCs when the concentration of 6A-β-CD was altered; this suggests the growth of the NPs is restricted to the intrinsic size of the cavity, confirming that 6A-β-CD is acting as a template. Templated NC growth through host–guest chemistry represents a unique and highly attractive route to obtaining ultrasmall, highly uniform NCs. It would be interesting to examine if the size of NCs could be modulated through the use of larger or smaller CDs, as well as the potential for obtaining different NC morphologies through templated synthesis using other host molecules like pillarenes, for example.[146]

2.5. Nucleotides

Consisting of a five-carbon sugar, a phosphate group, and a nitrogenous base, nucleotides are the building blocks of DNA and RNA. There are five nucleotides which encode DNA and RNA: adenine (A), thymine (T), cytosine (C), and (G) encode DNA, and A, C, G, plus uracil (U) encodes for RNA. Along with phospholipids (discussed in section 2.6), they are the only class of biomolecules discussed which contain a phosphate group, which is more electron-donating than a carboxylate. Furthermore, nucleotides are able to bond to one another through supramolecular interactions, and their intermolecular interactions are more specific than amino acids or proteins, thus they have great potential for use in HPNC-mediated biosensing applications.

Thymine-based peptide nucleic acids (PNAs) have been used as a surface ligand for stabilizing $MAPbBr_3$ HPNCs synthesized *via* LARP.[60] PNAs are different from oligonucleotides, as the nucleotide subunits are joined together by a pseudopeptide backbone. Monomeric T-PNA (M-T-PNA) and trimeric T-PNA (T-T-PNA) were added *in situ* during LARP with hexylamine acting as a capping agent to form $MAPbBr_3$ HPNCs. FTIR and DFT calculations were used to determine the PNAs were coordinating to Pb^{2+} *via* the primary amines in the peptide backbone, not through the nitrogenous base of the nucleotide. The optical properties of the HPNCs containing either both types of T-PNAs exhibited extremely low PLQYs (below 5%) as colloidal dispersions in chloroform and toluene. Interestingly, M-T-PNA HPNCs showed slightly higher PLQY than the T-T-PNA HPNCs, despite their similar size, which suggests longer nucleotide chains may be deleterious for the optical properties of HPNCs. Charge-transfer is a well-established phenomenon in PNAs, as such one can postulate that increased chain length would cause a greater charge-transfer effect and therefore be deleterious for optical performance.

To our knowledge, this is the only example of nucleotide-mediated HPNC synthesis. Unfortunately, the PLQYs obtained in this report suggest that nucleotides may not be a viable route to producing high-performance HPNCs. However, HP

thin films have been synthesized using guanine and thymine, both demonstrating improved properties, as discussed in section 3.2. Moreover, the unique ability of nucleotides to pair with one another with high specificity presents an attractive route to achieving biosensing with a high degree of sensitivity and specificity. We believe additional studies are needed, especially with other nucleotides, other backbones, different nucleotide combinations, chain lengths and HPNC compositions to determine the true value of nucleotides in the future of HPNC development.

2.6. Lipids

2.6.1. Phospholipids. Phospholipids are a particularly interesting class of biomolecules because of their amphiphilic nature. This is due to the presence of hydrophilic phosphate head-groups and hydrophobic hydrocarbon tails. Phospholipids are perhaps best known for their role in forming cell membranes. The propensity for phospholipids to self-assemble into tightly-packed layers makes them highly attractive for use as ligands, as this should allow for a high degree of defect passivation and protection from the external environment. Furthermore, phospholipids are also known to interact with proteins and other complex biomolecules through non-covalent interactions, thus providing the opportunity to incorporate additional functionality to the HPNC surface.[147,148]

Phospholipids interact with the HPNC surface *via* their phosphate head groups, similar to the coordination mechanism of OA. But the amphiphilic nature of these molecules makes it possible to generate bilayers through intercalation of the lipid tails with the alkyl chains on as-synthesized OA-HPNCs. Thus, its possible to also have phosphate groups pointing toward the external environment. In 2019, Yang *et al.* reported the first example of phospholipid-coated $CsPbX_3$ (X = Cl^-, Br^-, I^-), using DOPC, DOPE and with DSPE-mPEG.[147] The OA coating was retained on the HPNC surface to facilitate the hydrophilic tails of the lipids interacting with the OA alkyl chains, and the phosphate head groups were pointing toward the aqueous environment generating a micelle-like structure. This strategy strongly passivates the HPNC surface, as the hydrophobicity of the alkyl chains prevent water from interacting with the crystal surface, while the hydrophilic head groups impart the HPNCs with colloidal stability in aqueous media. Li *et al.* further explored how the structural properties of the phosphate head group affect the properties of HPNCs.[148] Phospholipid-coated $CsPbBr_3$ composed of DOPC, DOTAP and DOPG were synthesized, each having the same hydrophobic tail but different head groups; with DOPC, DOTAP and DOPG having neutral (zwitterionic), positive and negatively-charged head groups, respectively.[148] Twelve combinations of these lipids were explored and evaluated for their optical properties and stability in aqueous media. A red-shift in PL maximum was observed from 514 to 529 nm, concurrent with a change in zeta potential from positive to negative when DOTAP was replaced with DOPG. The authors attribute this red-shift to a change in NP size, though they do not discuss why the size change would occur. With respect to stability, a higher content of DOPC resulted in improved retention of PL intensity over the course of two weeks, suggesting the bifunctional nature of this head group provides the greatest degree of passivation, in line with what has been demonstrated using AAs. The much-improved physicochemical stability of HPNCs encapsulated with phospholipids, combined with the opportunity for functionalization with other biomolecules, makes these biomolecules a particularly promising option for the use of HPNCs in biological applications. Both of the phospholipid–HPNC systems reported above were successfully applied for biologically-relevant applications, as discussed in section 4.

2.6.2. Complex lipid mixtures. Soy lecithin (SL) is a popular natural emulsifier in the food industry and is composed of a mixture of phospholipids and triglycerides. There are a variety of phospholipids in SL with varying degrees of saturation and alkyl chain length. However, all phospholipids in the mixture contain zwitterionic head groups, which makes SL attractive bifunctional ligands for use in HPNC synthesis, similar to what was reported when using DOPC.[108] Krieg *et al.* demonstrated the use of SL as a passivating agent for the synthesis of $CsPbX_3$ (X = Cl^-, Br^-), and investigated the effects of the surface coating on colloidal stability.[108] As expected, the physical and optical properties of the SL-HPNCs were not vastly different than what is obtained in a conventional synthesis using OA and ODE, given the similarity in alkyl chain lengths. The SL-capped HPNCs exhibited extremely high colloidal stability, allowing for the generation of ultra-concentrated and ultra-dilute colloids ranging from a few ng mL^{-1} to >400 mg mL^{-1}. The generation of colloids with such unique properties was attributed to the polydispersity of the hydrophobic tails of the different phospholipids in the SL mixture, allowing for tight packing and therefore a high grafting density on the surface of the HPNCs. The effects of packing density on colloidal saturation were determined experimental and theoretically, showing the interdigitization of the lipid chains was essential for generating the observed colloidal stability, which was observed for over 1 month without sedimentation or changes in optical properties. The ultraconcentrated colloids were applied as ink for one-step deposition of thick, smooth, optically clear films by spin coating, and the ultradilute colloids were proposed for single-dot spectroscopy with single-photon emission. While the SL-HPNCs demonstrated here exhibit a high degree of hydrophobicity and are therefore unsuitable for dispersion in aqueous media, we postulate the same principles of polydisperse ligand mixtures could be utilized to generate hydrophilic coatings which generate a high packing density and could be applied for biological applications. The proposed single-dot spectroscopic techniques may be potentially useful in bioimaging in the future.

Carnauba wax (CW) is a complex mixture of long-chain hydrocarbons, hydroxy acids, alcohols and esters derived from the leaves of palm plants. Similar to the report from Karabel Ocal *et al.* using soy lecithin, CW has been used to passivate the surface of HPNCs by taking advantage of the long-chained molecules present in CW that are reminiscent of OA and

ODE.[109] Interestingly, the properties of CW enabled the successful use of CW instead of ODE in a hot injection synthesis of HPNCs. The CW-HPNCs exhibited greatly improved thermal, water, and air stabilities, which one may postulate could be due to a similar polydispersity employed from multi-length SL ligands.[109] The fabricated CW-HPNCs composites were then used as ready-to-use printable–writable solid inks (*via* a pen-on-paper printing approach) as well as malleable play doughs to create 2D and 3D photoluminescent architectures, respectively, due to the promising thermal and mechanical properties of the CW.[109]

Collectively, naturally-derived complex mixtures of lipid and lipid-like molecules appear to provide a high degree of surface passivation and improved optoelectronic properties relative to what can be achieved with OA and OAm. Presumably the complex nature of the ligand cocktail allows for a greater degree of packing, assembly and surface coverage, resulting in HPNCs which are still hydrophobic but exhibit markedly improved colloidal stability and resistance to humidity.

2.7. Vitamins

While vitamins are not technically biomolecules, they are essential for biological function. In particular, ascorbic acid (vitamin C) has been used on multiple occasions to mediate the growth of several different HPNC compositions.[110,149,150] Ascorbic acid has 4 terminal hydroxyl groups which can coordinate to the B site cations such as Pb^{2+} and Sn^{2+}, and a 5-membered ring which can also chelate metal cations. Notably, ascorbic acid has been investigated for use in mitigating lead toxicity, as discussed in section 5, and thus is a particularly attractive option for use in HPNCs when bioapplications are under consideration. Vitamin C has shown effective surface passivation of a variety of HPNCs (*i.e.*, $CsPbX_3$ X = Cl^-, Br^-, I^-), resulting in improved PL intensity, lifetime, and PLQYs up to 95%. In the aforementioned study, vitamin C was introduced to the HPNC surface *via* a post-synthesis ligand exchange, demonstrating that this molecule is beneficial for HPNC properties regardless of the initial ligands utilized. Additionally, AscA-treated HPNCs exhibited stability in ambient conditions and under continuous illumination for 55 days and 5 days, respectively. The improved stability and PL properties were attributed to the reductive nature of AscA, as well as the strong coordination between Pb^{2+} in the HPNCs and O^{2-} in AscA. The authors postulate that the improvements are due to the presence of the strongly-bonding AscA that hinders the lability of the remaining OA and OAm ligands, thus improving surface passivation. Similarly, when AscA was used in the synthesis of $CsSnI_3$ and $MA_{0.5}FA_{0.5}Pb_{1-x}Sn_xI_3$ HPs, a higher degree of crystallinity and improved stability and semiconducting properties were observed and attributed to the reductive nature of AscA as well as its efficient binding to lead and tin.[149,150]

2.8. Other biomolecules as surface ligands

Succinic acid (SA) is a biomolecule involved in the synthesis of ATP, thus it has metabolic relevance. It has been used in HPNC synthesis owing to its bifunctional nature, having two terminal carboxylates. $MAPbBr_3$ and $CsPbBr_3$ HPNCs have been treated post-synthesis with SA.[111,112] The terminal carboxylate groups were found to coordinate to Pb^{2+} on adjacent HPNCs and facilitate the growth of larger NCs, indicating SA can be used to modulate HPNC size. Furthermore, SA-HPNCs were found to be stable in aqueous media, despite the propensity for both carboxylates to coordinate to Pb^{2+} ions. It is unclear how both carboxylates were prevented from coordinating to the HPNC surface, as presumably one carboxylate must be free in solution to impart the NCs with aqueous dispersability. Benzoic acid (BA), primarily generated in plants, has similarly been applied in a post-synthetic treatment of $CsPbBr_3$ HPNCs.[113] Of note, it is a monofunctional biomolecule, with a single carboxylate group, in contrast to the multi-functional biomolecules discussed throughout this review. The BA-HPNCs exhibited a near-unity PLQY and long-term stability of 65% retention of the initial PL intensity upon 1 year of storage in ambient conditions. This improvement in stability and PLQY was attributed to benzoic acid coordinating to Pb^{2+} *via* the carboxylate and the π system, and donating electron density into the lattice to passivate the surface, in a manner consistent with what is observed for Phe-HPNCs,[62,63] which has a similar structure.

Besides the aforementioned biomolecules, other bio-inspired and naturally derived species have also been utilized to mediate, template or encapsulate HPNC components such as poly(lactic-*co*-glycolic acid) (PLGA),[151] folic acid,[83] butyric acid[114] and uracil derivatives[105] which have been summarized in Table 1.

3. Perovskite thin films

3.1. Amino acids in halide perovskite thin films

One of the most intriguing applications of halide perovskites is perhaps as an active layer in thin film optoelectronic devices, such as LEDs and solar cells (PSCs). Not only do HPs have high electron/hole mobilities and strong light-absorption coefficients, which suit optoelectronic device applications, but their material properties also ease the fabrication process. The physical properties of HPs allow for the fabrication of HP films *via* low temperature deposition methods.[152] This presents an opportunity for using biomolecules to manipulate the film formation and properties, since biomolecules often denature and lose their functionality at high temperatures.[153] HP thin films can be categorized into two main groups: polycrystalline films made of 3D HPNCs, and films made of 2D or quasi-2D HPNCs that consist of a layered architecture. The degree of crystallinity greatly impacts the conductivity of the film, and therefore its performance. The overwhelming objective in the development of HP thin films for optoelectronic devices is to generate highly uniform films with minimal defects. The appropriate biomolecules for use in improving the performance of thin-film devices largely depends on their application. In applications relying on optical properties of HPs such as LEDs,

maximizing the EQE and minimizing nonradiative recombination is the primary focus, whereas photovoltaics and other related devices rely on maximizing charge transport efficiency across interfaces and thus recombination is undesired.

With respect to photovoltaics, one of the major hurdles in maximizing conversion efficiency is preventing radiative and nonradiative recombination at the interfaces between the transport layers and the perovskite, as well as minimizing charge diffusion in the active layer. With respect to minimizing charge diffusion in the active layer, it is imperative that HP thin films exhibit a high degree of crystallinity with minimal voids in the film. In the case of polycrystalline films, it is desirable to have larger crystalline grains and smooth grain boundaries, as these boundaries can hinder charge transport and act as recombination sites. All of these considerations can be addressed through careful defect control, and biomolecules are particularly well-suited to modulate this. The zwitterionic nature of AAs has made them highly successful for passivating anionic and cationic defects during the synthesis of HPNCs, as previously described. AAs are the most frequently studied biomolecules for improving the quality and performance of HP thin films, owing to their possession of multiple functional groups and exhibition of a wide range of lengths, hydrophobicity, and charges. Improvements in HP thin film formation using biomolecules have been particularly well-demonstrated with AAs, as the carboxylate of the AA can coordinate to the metals in the electron transport layer (most commonly Ti^{4+} or Sn^{4+}) and the amine can coordinate to the halide ions in the perovskite, thereby anchoring the two materials together.[58,154–156]

Nearly all of the studies on HP thin film-based solar cells treated with AAs report improved PCE relative to the untreated systems, demonstrating the generality of this strategy towards improving HP-based PVs.[58,154–168] Moreover, there is strong consensus that the improvements in PCE are due to reduced resistance at the perovskite/substrate interface causing improved charge transport across the layer boundaries. The improved charge transport at the interfaces is attributed to defect passivation of cationic and anionic vacancies by the AA carboxylate and amine groups, along with the generation of more uniform films with less voids. In the case of polycrystalline films, general features observed include increased grain size, narrower grain size distributions, smoother grain boundaries and preferred orientation of the grains, ultimately resulting in higher-quality films than what can be produced in the absence of AAs.[155–157,159,160,167]

The greatest percent improvements in PCE relative to a pristine control were reported for $MAPbI_3$ HP films treated with lysine,[155] glycine,[58] cysteine[159] and alanine[154,162] anchored to a TiO_2 substrate. Interestingly, these represent the AAs with the shortest side chains, and none of these AAs have charged side-chain functionalities. Given that long-chain ligands are known to have insulating properties, it is unsurprising that short-chain AAs give rise to the greatest improvements in PCE. This was demonstrated to be the case when Shih *et al.* used glycine to treat TiO_2/$MAPbI_3$ solar cells, and improved the power conversion efficiency (PCE) from 8.35% to 12.02% for untreated and treated solar cells, respectively.[58] Treatment with Gly resulted in a more uniform crystalline film, reduced voids, a narrower grain size distribution and preferred orientation, all of which are improvements over the untreated controls. These results are in agreement with a previously discussed report which found Gly-treated HPNCs exhibited poor luminescence, but good photocatalytic efficiency and charge separation.[86] With respect to unmodified AAs, L-lysine-$CsPbBr_3$ films exhibited the greatest improvement in PCE, with a 61.23% enhancement after the addition of the biomolecule (9.69% *vs.* 6.01% for treated and untreated, respectively).[155] Interestingly, the greatest absolute PCEs were reported for HP thin films were those treated with modified AAs and their derivatives. HP solar cells treated with Fmoc-5-AVA (20.64%), d-*t*Bu-Phe (20.4%), and 4-amino-2-hydroxybutyric acid (20.31%) exhibited the highest reported PCEs using mixed cation-mixed anion perovskites composed of $Cs_xMA_yFA_zPb_rBr_sI_t$.[157,166,167] It is likely that none of these systems represented the greatest absolute percent improvements because the base untreated solar cells already had relatively efficient PCEs around 18%. However, given that these are 3 independent reports, it does indicate that HPs treated with bulky AAs are generally able to further improve pre-optimized solar cell compositions by improving the passivation of the HP film and improving charge transport.

Beyond these generalized conclusions, there were a few results demonstrated to be specific to certain structural features of AAs. Specifically, when the efficiencies of Pro- and Gly-treated $MAPbI_3$-solar cells were compared, a marked improvement in PCE was observed for Pro-treated HPs relative to Gly (19.6% *vs.* 18.5%, respectively). The authors attribute this to the additional coordination site provided by the amine in the 5-membered ring in Pro, resulting in improved crystal growth and larger grain sizes.[156] Another group reported an increase in PCE when HP films were treated with AAs having increased electron donating capability. $Cs_{0.05}FA_{0.81}MA_{0.14}PbI_{2.55}Br_{0.45}$ HPs treated with PEA, Val, Phe and *p*-*t*-Butyl-Phe, were all demonstrated to improve PCE relative to untreated controls, but *p*-*t*-Butyl-Phe treated HP solar cells had a markedly higher PCE (20.4%) than the HP solar cells treated with Phe, PEA and Val (19, 19.2 and 19.3% respectively).[157] The improved PCE was attributed to increased electron density in the phenyl ring due to the presence of the *t*-Butyl group, causing improved passivation of grain boundaries. In this series, the presence of aliphatic groups appeared to have a positive effect, as the HP solar cells treated with Phe (which has an aromatic ring) resulted in the least improvement in PCE. Broadly, the results obtained in these two studies may suggest there is an optimal degree of hydrophobicity (and therefore alkyl chain length and bulkiness) that improves HP film formation without being deleterious for the conductivity of the solar cell.

Interestingly, a study by Jia *et al.* showed that treating the surface of HPs with AAs (β-Ala, D-Ala, and Lys) did not enhance performance as much as a traditional $Pb(NO_3)_2$ treatment; however, a Gly treatment did improve the PL intensity and PCE of thin films relative to the traditional treatment.[162] Similarly,

a study which deposited D-valine, β-alanine, or L-glutamic acid on the TiO_2 layer demonstrated a reduction in initial efficiency, but improved long-term retention of efficiency in glovebox storage under illumination at room temperature.[163] The authors proposed that the improved stability occurs due to the AAs protecting the surface of the $MAPbI_3$ layer from exposure to radicals generated under UV irradiation, thus reducing degradation of the film.[131]

The role of molecular rigidity has also been explored in the synthesis of HP films. Rigid 4-aminobenzoic acid (PABA) and flexible γ-aminobutyric acid (GABA) were investigated as linkers to improve HP attachment onto the mesoporous TiO_2 layer.[164] Both AA-linked perovskite films showed better crystallinity, improved film flatness, more uniform and greater attachment to TiO_2, as well as an increase in PCE, and enhanced short-circuit current density. However, the rigid PABA-linked HP films outperformed the flexible GABA-treated HPs in all of the above-mentioned categories. It was postulated that the rigidity of the benzene ring afforded a better degree of grain alignment within the polycrystalline HP film, providing reduced defects and improved conductivity. The results of Yun *et al.* corroborate these results.[124] They observe a modest improvement in PCE (17.4% *vs.* 16.4%) and moisture stability using PABA in $MAPbBrI_3$ HP films and attributed the improvement to the role of the π-system of benzene improving the crosslinking efficiency between interfaces and generating a more uniform alignment of HP grains. This corresponds to our conclusion in section 2.1.3 with regards to amino acids possessing functional groups with benzene rings.

5-AVA has been particularly effective at enhancing PCE efficiency of HP films due to its ability to substitute directly into the A cation site of HPs. Mei *et al.* first incorporated 5-AVA in the synthesis of mixed cation HP thin films in 2014, forming $(5\text{-AVA})_x(MA)_{1-x}PbI_3$.[165] The role of 5-AVA cations was to template the formation of perovskite crystals onto the mesoporous oxide substrate, inducing preferential growth in the normal direction. Remarkably, the cell achieved a certified PCE of 12.8% and was stable for >1000 hours in ambient air under full sunlight. The improved stability and PCE were attributed to a reduction in defects, a reduced number of voids, and improved charge mobility. Subsequently, the incorporation of 5-AVA into 2D Ruddlesden–Popper (RP) HPs were investigated in detail regarding the change in perovskite composition with increasing 5-AVA concentration.[128] Low-dimensional $5\text{-AVA}_2MA_{n-1}Pb_nBr_{3n+1}$ (n = 1, 2, 3) layered HPs were generated, and it was observed that the stability of these compounds decreased rapidly with increasing layer thickness. The Tauc plot gives an optical band gap of 3.78 eV, with a significant exciton peak, demonstrating the promising optoelectronic properties of RP-type perovskites. The use of 5-AVA for generating highly-uniform 2D HP films was further demonstrated by Zhang *et al.*[169] and Wang *et al.*,[170] where the number of layers could be tuned through modulating the 5-AVA concentration, and improved grain size and a high degree of film smoothness were observed. Given the complex architecture afforded by layered HPs, hybrid 2D/3D HP films were theoretically explored to observe the changes in band edge alignment when the top layer of $MAPbI_3$ films were replaced with AVA-RP-HPs.[171] The simulations demonstrated RP-HP terminated with 5-AVA layers were able to promote the formation of confined dipoles and generate more favorable interface alignment relative to MA-terminated HPs, which should translate to increased charge transport efficiency at the HP-substrate interface.

3.2. Macromolecules and other biomolecules in thin films

Pigment molecules have also been used to improve solar cell efficiency, owing to their ability to absorb light. Melanin, a complex polymer derived from the AA Tyr, is found in the skin of mammals. It absorbs sunlight and transforms the light energy into heat, protecting skin cells from UV rays. $MAPbI_3$ thin films were coated with melanin, and the resultant thermoelectric device increased 7000% in output power compared to the blank device under illumination.[172] It showed a solar-thermal quantum yield of 99.56% and solar-thermal conversion efficiency of over 80% under (one-sun illumination AM 1.5), which surpassed the typical carbon materials (70%). Another pigment, bacteriochlorin, which is a derivative of chlorophyll, was determined to be effective hole-transporting material in $MAPbI_3$ thin films through a similar mechanism.[173]

Macromolecules have also been used to enhance PSC performance. Bacteriorhodopsins, a type of light-sensitive protein, were integrated between the TiO_2 and $MAPbI_3$ perovskite layer, acting as a photosensitizer for photon absorption and charge carrier transfer.[174] The additional layer of bacteriorhodopsin was shown to facilitate electron transfer and significantly reduce the interfacial charge recombination, which led to improved PCE. As previously mentioned in section 2.3, bacteriophages can be thought of as complex macromolecules owing to the proteins on their surface. Denatured M13 bacteriophage-based solar cells demonstrated increased grain size, reduced trap-sites, and increased PCE, compared to the reference $MAPbI_3$ PSCs.[175] The PCEs increased with an increase in M13 solution temperature, which the authors attributed to the denaturation of the M13 resulting in better passivation of the perovskite. Despite the complex nature of these "ligands", the basic premise of using multi-functional agents to passivate the HP surface remains a generally successful strategy. These results are in agreement with what was previously demonstrated using M13 bacteriophages to generate $CsPbBr_3$ NC networks.[97]

Whereas AAs have been successfully utilized at the interface of the HP active layer and the electron transport layer, nucleotides have been investigated for use as a hole transport layer. In a study by Yusoff *et al.*, DNA–hexadecyl trimethyl ammonium chloride was incorporated into $MAPbI_3$ PSCs as a hole-transport and electron blocking layer.[176] The hole-transport allows holes to travel to the active area of the PSC to radiatively recombine with electrons; the electron blocking layer prevents the flow of electrons in the incorrect direction, thus optimizing device efficiency. DNA has previously been shown to exhibit hole transport.[177] The device exhibited reductions in

PL intensity and decay times, which indicates that DNA-CTMA can be used to extract and transport holes from the perovskite film. This greatly improved the stability of DNA-CTMA-PSCs compared to the reference device (degradation after 1 day *vs.* 10 days for the DNA and DNA-CTMA PSCs respectively).

The adsorption of nucleotides on $MAPbI_3$ thin films have been studied using computational approaches, and it was found that for HP with PbI terminations, the nucleotides/perovskite interfacial structures were stabilized by the interactions between the under-coordinated Pb^{2+} atoms and the electron-rich nitrogen or oxygen atoms in the nucleotides.[178] On the other hand, cation-terminated perovskite surfaces had larger separation distances and weaker interactions between the adsorbent and adsorbate. Unfortunately, there isn't a large enough difference between the adsorption energy of the different nucleotides, indicating that HP materials present relatively poor selectivity for the nucleotides, making them sub-optimal for DNA screening applications based on this report. In another report using nucleotides, $Cs_{0.175}MA_{0.075}FA_{0.75}PbI_{2.92}Br_{0.08}$ HP films were synthesized using thymine coated onto the HP film to act as an interface between the HP and hole transport layer.[179] The amine group of thymine was found to coordinate to I^- and passivate the surface in a similar fashion to what was observed in the formation of HPNCs discussed in section 2.5.[60] The thymine-treated PV devices exhibited improved charge transport capacity and improved stability relative to untreated devices. Guanine (G)-treated HP thin films also exhibited improved properties, suggesting perhaps that using DNA (which is a chain of nucleotides) induces different effects than discrete nucleic acids.[178] Guanine was also used to generate mixed $G_2FA_{n-1}Pb_nPbI_{3n+1}$ films with PCEs of 16.04%, which was improved over neat $FAPbI_3$ films with PCEs of 8.42%.[104] DFT calculations were used to show guanine mediates charge transport and electron delocalization throughout the HP layer, and that guanine exists in the structure as hydrogen-bonded dimers that coordinate to Pb^{2+} *via* the carbonyl in guanine, allowing for the formation of the HP layers. This is in contrast with what was observed for both thymine-treated HPNCs[60] and HP thin films,[179] which were both found to coordinate through terminal amine groups, not the carbonyl. This suggests that the role of nucleotides in HP synthesis may be highly dependent on the identity of the nucleotide used, despite the common functional groups they share.

Thiamine, also known as vitamin B1, has strong antioxidant properties and has been used in the treatment of lead poisoning (see section 5). Unlike vitamin C, thiamine has two aromatic rings, one six-membered aminopyrimidine ring and one 5-membered thiazolium ring, thus it contains primary, secondary and tertiary amines whereas vitamin C does not. $MA_{0.5}FA_{0.5}PbI_3$ HPs thin films synthesized with thiamine were found to coordinate through the A site cation rather than through the B site, and exhibited improved crystallinity, a reduction in defect states, and improved charge extraction efficiency when incorporated into thin film PVs, with a PCE of 21.40%.[180] The authors also observed increased moisture resistance, which they attribute to the formation of a hydrophobic barrier by outward-facing thiamine molecules. As such, the introduction of thiamine to this HP composition appears to improve the optical properties, suggesting the use of organic antioxidants, such as vitamins, can be beneficial for both HPNC and HP thin film synthesis.

In contrast to photovoltaic/solar cell applications, where any form of charge recombination (radiative or non-radiative) in the perovskite layer is generally undesirable, in LED applications, the goal is to maximize radiative recombination within the perovskite layer. Furthermore, the bandgap energy is highly important as it dictates the output wavelength of the LED. Thus, biomolecules and complimentary ligands that improve PLQY and aid in tuning the emission wavelengths of HPs are of great interest in the development of HP-based LEDs. To date, most red LEDs based on HPs are in the deep red region (650 to 690 nm), and only a few reports are related to metal HP LEDs emitting in the range of 630–640 nm, all with low luminance. Impressively, a fluorinated polymer and L-Arg were used to fabricate $CsPbI_{3-x}Br_x$ thin films to develop pure red perovskite LEDs with an emission maximum centered at 637 nm.[181] Here, the fluorine polymer confines the $CsPbI_{3-x}Br_x$ crystal size while L-Arg acts as a passivation agent, which also increased the crystallinity of perovskites. The LEDs had a PLQY up to 40% with a maximum EQE of 4.5% and a maximum brightness of 3100 cd m^{-2} which are quite impressive for LEDs emitting in the 630–640 nm range. Wang *et al.* also explored the formation of LEDs, and introduced 5-AVA and 8-amino-octanoic acid monolayers between ZnO and $MAPbBr_3$ layers to generate films with higher PL intensity and longer PL lifetime.[182] Film coverage was also improved, due to the hydrogen bonds and electrostatic interactions between the amino groups and the perovskites, which promoted the nucleation of perovskite crystals. This resulted in improved brightness and efficiency, with a maximum of 4890 cd m^{-2} and 0.43% achieved for luminance and EQE, respectively.

Polysaccharide-based block copolymers have been used to provide stability to HPNCs during their transfer from colloidal dispersions to thin film devices.[103] Specifically, maltoheptaose-*block*-polyisoprene-*block*-maltoheptaose triblock copolymers (BCP) were used as a matrix to produce bright and stable $CsPbBr_3$-BCP thin films.[103] Improved film formation was attributed to the coordination of Pb^{2+} ions to the sugar (maltoheptaose) domains. The composite films exhibited improved luminescence relative to bare HPNCs and the authors postulate the improvement is due to Lewis acid–base interactions between the hydroxyl groups in the BCP and ions in the HPNCs that reduced the degree of nonradiative exciton recombination. The composite films exhibited improved tensile properties and were used to generate stretchable phototransistor memory electronics.[103]

Besides solar cells and LEDs, biomolecules have also been used to improve HP transistors. HP transistors fabricated with solution-based methods are cost-efficient, but there is a limit to the number of layers that can be deposited, owing to increasing hydrophobicity after each solution-deposited layer.

Thus, to build on top of the solution-deposited layer, other high-cost methods must be employed, which nullifies the cost-effectiveness of using HPs in transistor manufacturing. To combat this problem, a protein solution with mostly protein ovalbumin, extracted from chicken egg-whites, was used as a hydrophilic coating which allows subsequent solution processing of other layers at the surface of transistors, without altering the electrical properties of the dielectric.[183] In an aqueous environment, proteins in their natural configuration mostly have a hydrophobic core and hydrophilic surfaces. Adsorption of protein on hydrophobic surfaces is predominantly due to hydrophobic interactions between the protein core and the surface. This exposes the protein's hydrophilic surface to the environment, which allows subsequent deposition of the HP layers by increasing the hydrophilicity of the device.

To summarize, while HP films have the same unit cell structure as their NC counterparts, they differ with NCs in that they are a continuous layer of single or polycrystalline material grown on top of a substrate. The intended application of the HP film largely governs its desired properties, where minimal recombination in the perovskite layer is desirable for PV applications, and maximum radiative recombination in the perovskite layer is desired for LED applications. In both cases, the incorporation of biomolecules can significantly increase the efficiency of the HP films, and consequently improve the PCE and EQE of PV and LED devices, respectively. For both applications, the bi- or multi-functional nature of AAs and other complex biomolecules facilitates the anchoring of the HP film to the substrate layer, with all around improved anchoring properties reported for the biomolecules studied. All of the reports also demonstrate improved crystallinity of HP films regardless of the biomolecule or HP studied, with improved passivation of defects, narrowed grain size distributions, increased grain sizes, improved smoothness, and reduced voids in the films.

While this strategy can be generalized to a wide variety of biomolecules, relatively few HP film compositions have been studied (mostly $MAPbI_3$), and few systematic studies on the effects of different properties of biomolecules on HP film synthesis and performance have been reported. Thus, while it is clear that using biomolecules does result in improvement of HP film properties and performance, there is relatively little information on the precise reasons for the improvements in terms of a structure–function relationship. Future studies may aim to pinpoint the precise properties of the ligands that induce the greatest enhancements, allowing for a deeper understanding of the role of biomolecules in HP film production.

4. Biological applications of HPNCs

Biological applications of all luminescent nanoparticles generally require that the materials are water-dispersible, water-stable, appropriately sized, non-toxic, and that their excitation and emission wavelengths are well-suited for their intended application. Some examples of biological applications where HPNCs have been used include sensing, imaging, detection and therapeutics. With respect to *in vitro* and *in vivo* applications, it is of paramount importance that the materials induce minimal toxicity and cellular stress. Given that the surface mediates the interactions between nanoparticles and their environment, the choice of ligand often dictates the success of a nanomaterial for biological applications. The discussion herein will be restricted to examples of HPNCs that have been synthesized or coated with biomolecules and have been demonstrated for biological applications.

HPNCs are particularly attractive materials for biological applications that require strong luminescence, owing to their highly efficient and tunable optical properties. Strong luminescence is typically necessary for luminescence sensing and fluorescence imaging, both of which require high-signal-to-noise ratios. Unfortunately, as previously mentioned, HPNCs are highly unstable in the presence of water, and this is the major hurdle to their success in biomedical applications, as most biomarkers for disease are found in bodily fluids such as blood or urine. Moreover, the highest-performing HPNCs contain lead, thus extreme care must be taken to minimize lead leaching when using these materials in *in vitro* and *in vivo* applications. Both concerns can be addressed through engineering effective surface coatings that prevent direct interaction of the HPNCs with their environment. While it is relatively easy to generate water-dispersible HPNCs through the use of hydrophilic ligands, it is significantly more difficult to achieve prolonged stability, at the time-scale of weeks to months, after the aqueous colloidal suspension is generated. To achieve prolonged stability, the surface of HPNCs must be completely covered such that water cannot interact with the crystal. Complete surface coverage is difficult to achieve with discrete small molecules due to steric hindrance, thus the most successful surface coatings have been polymer or silica-based.[147,184–195] Interestingly, phospholipid-based surface coatings have also been quite successful for generating aqueous dispersions and maintaining PL intensity, despite being small molecules, as previously mentioned in section 2.6.[112,147] For a more in-depth discussion on the use of coatings to generate HPNCs relevant for biological applications, readers are referred to the review of Lian *et al.*[196]

4.1. Biomedical and environmental sensors

Although HPs exhibit high sensitivity to a myriad of environmental stimuli, which is the major hurdle to their practical widespread use, this sensitivity can be harnessed for sensing applications. The potential use of HPs in sensing devices expands the potential scope of application of these materials to fields such as biology and environmental science, which may benefit from advancements in optoelectronic technologies. HPNCs have been successfully used for sensing and detection in the food, medicine, diagnostic, agriculture, water, and environmental industries (Table 2). The mechanisms of HP-based sensors can be generally categorized into photoelectrochemical (PEC), electrochemiluminescence (ECL), and fluo-

Table 2 Summary of the characteristic features of HPNC-based biosensors

Material	Analyte	Sensing range	LOD	Response time	Detection mechanism	Sample tested	Ref.
$CsPbBr_3/SiO_2$–NH_2	Thiamethoxam	14.4–62.4 nM	4.11 nmol L^{-1}	15 min	FRET	Soil, yam	197
$CsPbBr_3$	BSA	0–60 nM	51.47 nM	N/A	FL quenching	N/A	83
$CsPbBr_3$/SBE-β-CD	H_2S	0.5–60.0 μM	0.3 μM	N/A	FL quenching	Zebrafish	102
$CsPbBr_3$/SBE-β-CD	H_2S	0.5–6000 μM	0.19 μM	10 min	Photothermal	Zebrafish	102
$CsPbBr_3$-PL	prostate specific antigen	0.01–80 ng mL^{-1}	0.081 ng mL^{-1}	N/A	FL enhancement	Serum from prostate cancer	198
$CsPbX_3$ (X = Br^-/I^-)	Penicillamine	5–35 nM	1.19 nM	N/A	FL enhancement and shift	Penicillamine tablets	92
$CsPbBr_3$-DNA/MoS_2	*Mycobacterium tuberculosis*	0.2–4.0 nM	51.9 pM	N/A	FRET	PCR products from clinical samples	199
$CsPbBr_3$-PL	Melittin	0.05–150 μM	0.05 μM	20 min	FL, electrochemical	*E. coli* secretions	200
$CsPbBr_3$	H_2S	0–100 μM	0.18 μM	N/A	FL quenching	Rat brain microdialysate	201
$CsPbBr_3$/ mPEG@SiO_2	Glutathione, Hg^{2+}	1–10 μM	0.19 μM	5 min	FL enhancement	Human serum	202
$MAPbBr_3$/PbBr(OH)/ SiO_2-Cit-Eu^{3+}	Tetracycline	0–25 μM	11.15 nM	20 s	FL quenching + FRET	Eggs, fruits, honey, milk, lake water, tap water	203

Abbreviations: N/A: not reported; MIP: molecularly imprinted polymers; CTAB: cetyltrimethylammonium bromide; PMMA: polymethyl methacrylate (PMMA) fiber membrane; DDVP: 2,2-dichlorovinyl dimethyl phosphate; 3-MCPD: 3-chloro-1,2-propanediol (3-MCPD); SEC: *Staphylococcus aureus* enterotoxin-C (SEC); SERS: surface-enhanced Raman scattering; CSF: cerebrospinal fluid (CSF); PEG-PCL: polyethylene glycol-polycaprolactone; FRET: Förster resonance energy transfer; APTES: (3-aminopropyl)triethoxysilane; PL: phospholipid; FL: fluorescenece; Cit: citrate.

rescence (FL) based techniques. Herein, we have summarized the state-of-art of sensing research using biomolecule-based HPs from the perspective of biological and environmental applications (Table 2).

These pioneering works have demonstrated the capability of using biomolecule-functionalized HPs as the active material for low-cost, easy-to-use biosensors with rapid detection, high sensitivity and specificity and low limits of detection at room temperature. Importantly, these studies are all proof-of-concepts, and there is still much to be discovered before HP sensors will attain commercial status.

FL biosensors are the most investigated types of sensors that use HPNCs. These sensors are based on FL quenching and enhancement mechanisms to create "turn on or off" types of biosensors (Fig. 6a and b) or FL wavelength shifts to form visual and colorimetric detectors (Fig. 6c and d).[201–204] FL quenching and enhancement may occur by means of several mechanisms such as structural alteration of HPNCs, charge and energy transfer, FRET, inner filter effect (IFE), photo-induced electron transfer (PET), and complex formation (Table 2). For example, the crystalline structure alteration and degradation of HPNCs has been applied to detect H_2S in rat brain samples (Fig. 6a), living cells, and zebrafish using the changes in FL caused by degradation of the HPNC lattice.[102,201,205,206] In this regard, $CsPbBr_3$@sulfobutylether-β-CD nanocomposites with high water dispersity and stability were employed to develop selective and portable photothermal and FL based sensors to detect H_2S with linear ranges of 0.5–6000 μM and 0.5–60.0 μM, respectively. The practical usage of the developed sensors was successfully evaluated by *ex vivo* detection of H_2S concentrations in various organs of adult zebrafish such as the heart, liver, spleen, and kidneys at room temperature with the concentration of H_2S in all organs found to be approximately 1.0 mmol mg^{-1}.[102] Moreover, Fang *et al.* used the bicarboxylic nature of Asp to form a core@shell structure of $CsPb(BrI)_3$@Asp-$Cs_4Pb(BrI)_6$ and employed it for biosensing.[82] The core@shell HPNC exhibited significantly improved ultraviolet, water, and thermal stabilities in comparison with $CsPb(BrI)_3$, owing to the protection of the HPNC core from the environment. As discussed in section 2.5, despite their extremely low PLQY, PNA-M-$MAPbBr_3$ HPNCs were successfully used to sense adenine with a detection limit of 1.76 ppm.[60] The thymine peptide nucleic acid monomers were able to detect adenine due to the complementarity of the nucleic acids. Moreover, the thymine groups were found to face outward toward the environment, facilitating hydrogen bonding to adenine in solution. It was demonstrated that loading adenine to the colloidal solution of PNA-M-HPNCs results in a PL quenching *via* charge transfer effect between the surface ligand and adenine, which caused a decrease in PL intensity.

Colorimetric sensors are advantageous because they allow for the visual detection of desired compounds. Furthermore, they are inexpensive, as there are no electronic parts involved, easy to operate, and maintenance free. Colorimetric sensors can be made from HPNCs by taking advantage of the high rates of ion exchange in these materials. As mentioned in the introduction, colorimetric changes can occur in HPNCs due to the ionic nature of HPs and the low activation energy for the diffusion of halides. As a result, the emission wavelength shifts (either red or blue shift) as halides are exchanged in the HPNC lattice, generating a change across a wide visible range while a high PL intensity is retained (Fig. 6c and d). This process has been suitable for the sensing of organochlorine

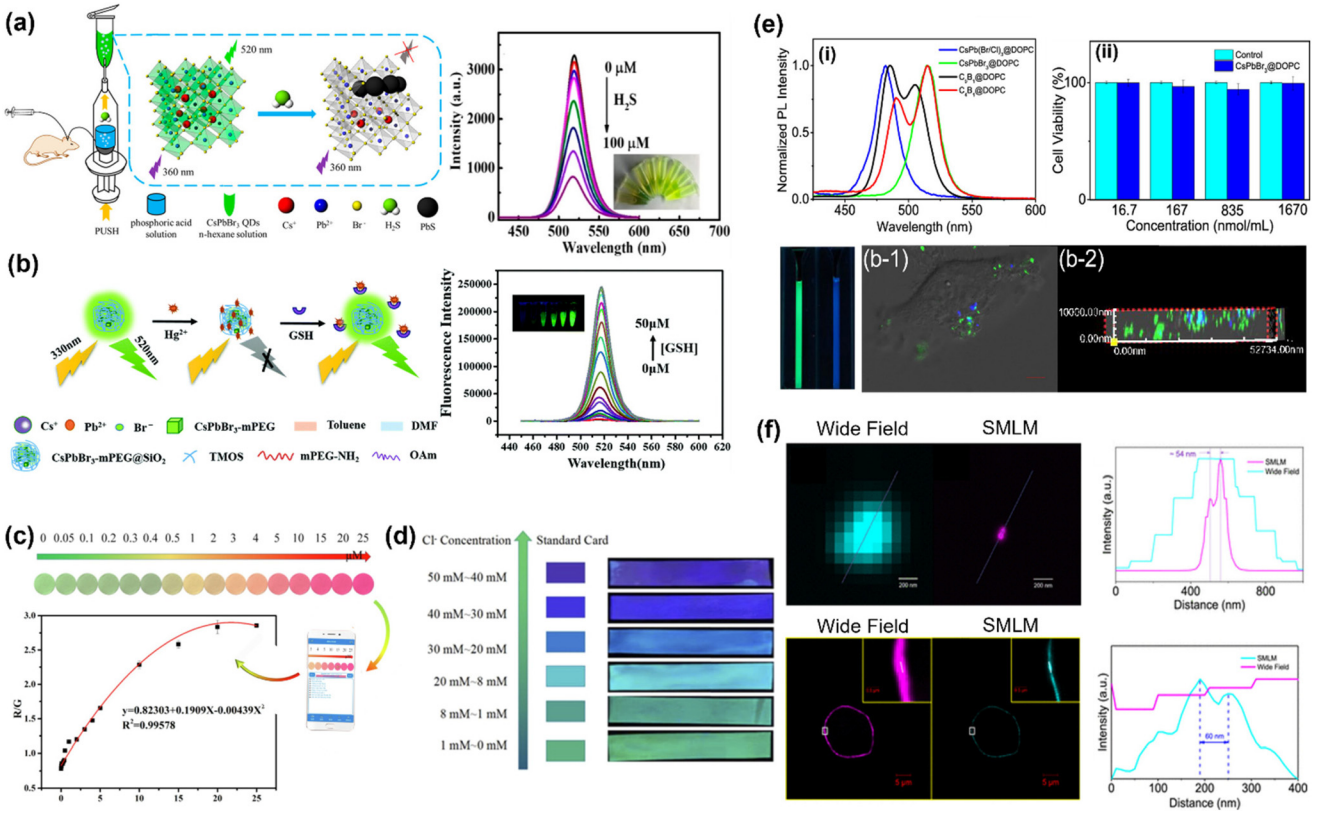

Fig. 6 (a) Schematic illustration of H_2S detection in a rat brain microdialysis sample and FL spectra of $CsPbBr_3$ NCs upon the addition of different concentrations of H_2S in the range of 0–100 μM.[201] (b) "On–off–on" type FL detection of Hg^{2+} and glutathione (GSH) based on $CsPbBr_3$-mPEG@SiO_2 NCs.[202] (c) Fast visual green-red switching sensor for tetracycline detection based on $MAPbBr_3$ NCs with linear response in the range of 0–25 μM, which can be used for detection using a smart phone software.[203] Reproduced and/or modified with permission from the listed references. (d) Colorimetric paper test strips based on $CsPbBr_3$ NCs for the detection of Ciproxan solution in a range from 0 to 50 mM and under UV light (365 nm).[204] (e) PL emissions from $CsPbCl_3$ and $CsPbBr_3$ coated with DOPC/DOTAP and DSPE-mPEG-FA, their corresponding *in vitro* viabilities in HeLa cells, and fluorescence confocal microscopy images showing internalization in HeLa cells and multiplexed luminescence capabilities.[147] (f) Fluorescence microscopy (left) and super-resolution microscopy (right) imaging of nuclear lamina (top) and exosomes (bottom) using CsPb$(Cl_{1-x}Br_x)_3$ HPNCs, and the corresponding FWHM of each signal.[189] Panel 6a adapted with permission from ref. 240 Copyright 2019 American Chemical Society.

pesticides, halomethanes, haloalkanes, chloride in sweat, peroxide number in edible oil, benzoyl peroxide in flour and noodles, among others. For instance, as-prepared Tfa-Lys-$CsPbBr_3$ NCs could undergo an anion exchange process to replace Br^- with I^- and were used as a probe for the detection of penicillamine, a sulfur-containing AA and widely-used drug.[92] Upon the interaction of HPNCs with penicillamine, the PL intensity of the NCs was enhanced and blue-shifted. Consequently, a dual-signal detection sensor could be produced, achieving greater sensitivity by using variations in PL intensity, while also achieving greater accuracy by examining the PL wavelength shift. The developed penicillamine sensor had a linear detection range from 5.0 to 35.0 nM, with a limit of detection of 1.19 nM.

Finally, other bio-related sensors and detecting devices based on HPNCs have been recently developed, including, but not limited to photoelectric heart pulse sensors,[207] artificially-intelligent retina and bionic eyes,[208–212] and artificial synapses.[211,213–230] The wide variety of sensor technologies emerging based on advancements in HPNCs employing biomolecules suggests there is a permanent place in this sector for HPNCs.

4.2. Bioimaging

4.2.1. Photoluminescent halide perovskites in bioimaging applications. HPNCs have been demonstrated as successful candidates for use in *in vitro* imaging and therapeutics, with the number of imaging applications far surpassing the therapeutic demonstrations. When properly passivated, HPNCs are attractive materials for bioimaging because of their strong luminescence, fast lifetimes, and tunable excitation and emissions that can span the near-UV, visible and near-IR regions. Their strong luminescence and short lifetimes allow for high signal-to-noise ratios, which facilitate rapid image acquisition, high contrast and good spatial resolution. Additionally, HPNCs exhibit photoblinking, which can be harnessed for super-resolution imaging through single-molecule localization microscopy (SMLM), enabling imaging of biological structures

at resolutions below the diffraction limit of traditional light microscopy.[190,231] The excitation and emission wavelengths of HPNCs can be easily tuned during their synthesis, allowing for the possibility of multiplexed wavelength imaging using HPNCs with different compositions, as well as with other fluorescent markers.[147,187] At present, there are a handful of proof-of-concept demonstrations of HPNCs used as fluorescent imaging probes in a variety of mammalian cell lines, as well as in *E. coli*, and most of these do not employ biomolecules as ligands or during synthesis.[112,147,184,185,187,188,191,192,194,232–240] Currently, the main focus of these studies is to demonstrate cellular uptake with minimal toxicity from Pb^{2+} leaching and good imaging contrast. Nearly all the reports utilize UV and blue light for excitation, and acquire the images using the green emissions from $CsPbBr_3$ or red emissions from $CsPbI_3$, demonstrating the viability of using HPNCs for basic optical bioimaging.

While there are multiple successful demonstrations of HPNCs as probes for bioimaging, thus far the majority of the HPNC systems remain in the cytosol with no localization at a particular organelle. The incorporation of biomolecules at the surface of HPNCs not only has the potential to improve biocompatibility with respect to cellular uptake, but also for uptake specificity. Molecules which are able to impart HPNCs with targeting capabilities can be functionalized on the HPNC surface, improving their targeting specificity. One example of this utilizes $CsPb(Br/Cl)_3$ HPNCs coated with a DOPC/DOTAP phospholipid micelle that was further coated with a DSPE-mPEG-folic acid (FA) layer used to target cancer cells expressing a folate receptor, such as HeLa.[147] The blue and green emissions from $CsPbCl_3$ and $CsPbBr_3$ respectively, were used for multiplexed imaging of HeLa cells (Fig. 6e). The benefit of using a phospholipid coating (as discussed in section 2.6) is the presence of the lipids imparts improvements to the optical properties of the HPNC and the overall positive charge of the system facilitates relatively rapid cellular uptake (20 minutes incubation was sufficient to obtain a signal). However, the generation of a lipid layer around the $CsPb(Br/Cl)_3$ HPNCs is done *via* a common method which employs hydration of a lipid film in order to create the micelles and induce encapsulation. Thus, the means through which the DOPC/DOTAP lipid layer is created results in an inevitable contact of water with the HPNC surface. The addition of the DSPE-mPEG-FA layer further reduces the interaction of the nanocrystal with an aqueous environment, but does not totally prevent it. Some degree of lead leaching is inevitable, concomitant with an eventual loss of luminescence (in this case, over half of the luminescence signal was lost within 72 hours). The authors further demonstrate that upon injection of zebrafish embryos with the HPNC-lipid-FA nanoparticles, only 78% of embryos hatched 72 hours post-injection, whereas 95–100% of control embryos hatched. While the proof-of-concept is promising, it would certainly be interesting to see this study repeated with lead-free alternatives, with timepoints beyond 72 hours and in mature *in vivo* specimen.

Beyond simple bioimaging, a few reports have taken advantage of surface functionalization with biomolecules such as biotin,[112,189,190] streptavidin,[112] and folate[147] to achieve subcellular labelling of different biological structures. Super-resolution microscopy techniques like SMLM have substantially benefited from the use of HPNCs conjugated to biotin for subcellular structure labelling. Yang *et al.* have taken advantage of the blinking properties of $CsPbX_3$ ($X = Cl^-$, Br^-) HPNCs coated with biotinylated-PEG on two separate occasions, demonstrating impressive advancements in super-resolution imaging using these NCs.[189,190] First, the use of $CsPbBr_3$-PEG-biotin was used to demonstrate that a spatial resolution of 23 nm could be achieved, with the resolution being limited by the size of the NCs.[190] Given that wide-field light-microscopy is limited to resolutions of 200–250 nm, this represents a major advancement in high-resolution microscopy. SMLM imaging of the nuclear lamina was demonstrated with a much higher resolution than what was obtained using wide-field microscopy. The group later demonstrated multiplexed SMLM imaging of exosomes using $CsPb(Cl_{1-x}Br_x)_3$ HPNCs, and were able to distinguish two adjacent exosomes with a sub-10 nm localization precision (Fig. 6f).[189] Since HPNC photoblinking is often regarded as a deleterious phenomenon, it is impressive to see that it can be harnessed to generate major developments in bioimaging. Other super-resolution techniques, such as stimulated emission depletion (STED), have taken advantage of the fast decay times of HPNCs to generate resolutions of 20.6 nm with faster scanning times than what can be achieved using other luminescent nanoparticles, though this has not yet been demonstrated in cells; imaging has thus far only been demonstrated with HPNCs on glass substrates.[241]

While UV and blue light can be used with relative ease to image monolayer cultures as the penetration depth of light in tissues is not an issue, excitation in these regions can cause cellular autofluorescence which is difficult to deconvolute from HPNC luminescence. Additionally, UV light can cause phototoxicity, rendering it sub-optimal for use in live cell imaging, but still viable for applications like fixed cell imaging and exosome imaging.[189,190,193] Exosomes are excreted from cells and harvested for biomarker analysis such as those used in cancer diagnostics. This is done by harvesting exosomes out of cells and then analyzing them *via* microscopy. One such example of HPNCs used for exosome imaging was described using $CsPbBr_3$ coated with a triblock copolymer functionalized with an antibody, anti-CD63.[193] While the particles do exhibit improved luminescence stability relative to un-coated particles, the luminescence signal significantly decreased within 8 days of exposure to water (no study on the stability in biological media was discussed). The anti-CD63 conjugated HPNCs were able to bind to breast cancer-derived exosomes and label them in the extracellular environment. This is interesting for the purposes of following the progression of the exosomes after their release from the cell, as they are implicated in inter-cellular communication and biomolecule trafficking, but are currently difficult to track using existing means. Interestingly, in scenarios where the exosomes are harvested for diagnostic purposes (and not being studied for *in situ* cellular tracking of the exosomes), the leakage of lead within them is less of an issue,

since the exosome is no longer associated with a living specimen and therefore no toxicity concern exists. This work represents not only a facile route to antibody conjugation to HPNCs, but also an alternative usage for HPNC-derived bioimaging that may be more tolerant of the presence of lead.

As previously mentioned, HPNCs are typically excited with UV and blue light, which do not penetrate tissues effectively, and UV can induce cellular damage. With regard to live cell imaging and *in vivo* imaging, there is a serious need to develop materials that can be excited at energies that facilitate deep-tissue imaging, minimize autofluorescence, and induce minimal cellular stress. The use of low-energy excitation light allows for penetration at depths several times what can be achieved using UV and visible light, and it induces minimal photodamage. These considerations are particularly important in diagnostic imaging, where it is essential to preserve the health of the specimen and not introduce abnormalities (or imaging artifacts) that could be falsely diagnosed as disease. Toward this end, there has been significant effort toward developing strategies that take advantage of upconversion, a type of anti-Stokes luminescence.

4.2.2. Upconversion excitation for bioimaging. Upconversion is a luminescence process in which multiple photons of low energy are absorbed by one or more ions, and energy is emitted as a higher-energy photon. This nonlinear, anti-Stokes process is highly attractive because it introduces the possibility to utilize near-infrared (NIR) excitation wavelengths to obtain emissions spanning the UV and visible regions. The upconversion process has been demonstrated for HPNCs through three mechanisms, two-photon absorption (TPA),[237] triplet–triplet annihilation (TTA)[242] and energy-transfer upconversion (ETU).[243] Unfortunately, while TTA-mediated upconversion using HPNCs has seen modest success in photovoltaic applications, there are currently no reports of this phenomenon for bioimaging. Thus, the following discussion will be restricted to upconversion mechanisms as they pertain to bioimaging. The interested reader is directed to the review by Nienhaus *et al.* for an in-depth discussion on TTA-upconversion using HPNCs.[242]

TPA is an attractive route to upconversion because it does not require any modifications to the composition of HPNCs. TPA is facilitated through the use of pulsed lasers that generate extremely high power densities (GW cm^{-2}),[191] allowing for the simultaneous absorption of two low-energy photons to effectively populate an excited state that can be populated through one high-energy photon of equivalent energy. In contrast to TPA, ETU is achieved through incorporation of lanthanide ions into the HPNC lattice, or by inter-particle energy transfer between discrete lanthanide-doped upconverting nanoparticles (LnUCNPs) and HPNCs. In ETU, a sensitizer ion (typically Yb^{3+}) sequentially absorbs multiple NIR photons and transfers energy to an activator ion (typically Er^{3+}, Tm^{3+} and Ho^{3+}), populating the activator excited states from which anti-Stokes emissions are generated. In contrast to TPA, lanthanide-mediated upconversion can be achieved using continuous-wave, low power density lasers (mW cm^{-2}), but requires doping of the HPNC lattice, or the presence of an additional nanocrystal material. Both strategies have their advantages and disadvantages, and each has been demonstrated as a viable route for generating upconversion luminescence using HPNCs. For the sake of brevity, this discussion is restricted to studies of upconversion in HPNCs that have been demonstrated for biological applications.

To our knowledge, all of the current demonstrations of TPA upconversion have been performed using $CsPbBr_3$ HPNCs excited using 800 nm femtosecond pulsed lasers.[191,234,237] In these cases, two 800 nm photons are simultaneously absorbed by an HPNC, generating one 400 nm photon that is efficiently absorbed by $CsPbBr_3$. The green emissions from the nanoparticles are then visualized by microscopy. As previously mentioned, TPA requires highly specialized lasers capable of generating pulses of extremely high power density. Talianov *et al.* studied the effect of power density on the TPA luminescence of $CsPbBr_3$ and $CsPbI_3$ HPNCs, demonstrating green and red emissions were obtainable under power densities of 400 GW cm^{-2}, and did not report studies at power densities lower than 30 GW cm^{-2}.[191] Furthermore, they encapsulated the HPNCs in polylactic acid, a biomolecule derivative, to generate HPNC-microspheres, which were incubated with CT-26 cells and then imaged by microscopy, demonstrating the feasibility of the technique, and also demonstrated non-toxicity *via* histological analysis after injection into a mouse.

Since each study discussed herein on TPA from HPNCs reports extremely different power densities, it is difficult to ascertain the relative efficiencies of each system and more systematic demonstrations at low power densities (mW cm^{-2}) need to be performed. Regardless, these studies demonstrate good proof-of-concepts for TPA upconversion-mediated bioimaging using biomolecule-conjugated HPNCs.

5. Lead toxicity: concerns and strategies

HPNCs have emerged as front-runners among a new generation of luminescent nanomaterials, and will surely continue to play a role in generating new technologies for environmental and biological applications. Their optoelectronic properties are unparalleled with respect to luminescence tunability and efficiency, and their rapid, reliable synthesis techniques facilitate industrial scale production. Unfortunately, their drawbacks are significant, though these issues are being addressed at a rapid pace. The high degree of moisture sensitivity coupled with the presence of Pb^{2+} in the highest-performing compositions ($APbX_3$ where A = Cs^+, MA^+ and X = Cl^-, Br^-, I^-) has brought to light the very real potential for lead toxicity from these nanomaterials. Lead toxicity is not just a concern for biological applications where HPNCs would be intentionally introduced to living specimen, it is a concern for those who are involved in their synthesis at the laboratory and industrial scales, as well as for the environment when waste is generated from their production.[244] It is important that highly

effective means of preventing the leaching of lead ions from HPNCs is achieved prior to their widespread use. Not only is it important from a toxicity perspective, but the performance of HPNCs is also diminished as the materials degrade and release Pb^{2+}.

As mentioned throughout this review, many surface passivation strategies have been investigated and demonstrated to prevent the degradation of HPNCs in air, as well as in organic and aqueous media. Many of the preliminary demonstrations of HPNCs in bioimaging and biosensing applications *in vitro* and *in vivo* perform metabolic activity assays and histologic analyses within 24–72 hours of introducing the HPNCs to the specimen. While these short-term analyses report a lack of toxicity upon introduction of well-passivated HPNCs to a variety of cell lines, there is still evidence to inform upon long-term accumulation of HPNCs in cellular compartments at the *in vitro* scale, or in organs at the *in vivo* scale. Demonstrations of acute non-toxicity in a biological specimen on the scale of hours or days[191] are simply insufficient to claim a lack of ion leaching or long-term consequences, as half-life of lead in certain tissues is such that the introduction of lead into the bloodstream can occur long after the initial exposure.[147,191,193,196]

Interestingly, there are a number of biomolecules that have shown promise in treatment of lead toxicity, which we postulate could be useful for use in HPNC synthesis to mitigate the potential consequences of lead exposure.[245–247] The main consequence of lead exposure is oxidative cellular stress, which occurs when cells are no longer able to efficiently neutralize radicals and other reactive oxygen species. The primary targets of lead toxicity are proteins involved in regulating glutathione redox states, and the enzymes involved in the heme biosynthetic pathway.[248] Dysregulation of both of these avenues ultimately leads to oxidative stress.[245,249] As such, antioxidants have been explored to combat lead toxicity through ion chelation and/or inhibition of radical chain reactions that are damaging to the cell. Some examples of antioxidants investigated for chelating lead are Vitamins B6 (pyridoxine) and B1 (thiamine), vitamin C (ascorbic acid) and vitamin E (alpha-tocopherol), quercetin, choline, ethanolomine, and alpha lipoic acid among others.[245,247] Of these, thiamine[180] and ascorbic acid[110,149,150] have been utilized multiple times for the generation of HPs containing Sn^{2+} and/or Pb^{2+} for the purposes of promoting crystal growth and enhancing their physicochemical and optoelectronic stability, as discussed in sections 2.7 and 3.2. This suggests that the use of antioxidants in the fabrication of HPNCs could serve a dual purpose; to stabilize them and promote growth, but also to mitigate the effects of lead toxicity.

Other strategies have employed biomolecules that aim to aid in regulating glutathione levels or 5-aminolevulinc acid levels. For example, glycine has been shown to be an effective antioxidant and has been demonstrated to increase glutathione levels and decrease lead levels in blood in rats.[246] While glycine-functionalized HPNCs exhibit poor luminescence when used as the sole passivating ligand, the potentially-improved safety of using glycine-coated HPNCs may prompt the development of strategies to incorporate lysine on top of a silica coating, for example. In this manner, the lysine would not interfere with the optical properties of the NCs, but could still act to mitigate lead toxicity.

Finally, the most reliable route to prevent lead toxicity is to simply generate lead-free HPNCs. An ever-increasing number of lead-free HPNCs are being reported as more researchers move towards using these materials in biological applications. While the current compositions of lead-free perovskites exhibit inferior optoelectronic properties relative to their lead-containing counterparts, a variety of defect engineering strategies and compositional tuning will eventually lead to the production of lead-free HPNCs with outstanding properties.[250]

6. Conclusions

Halide perovskite nanoparticles and thin films have emerged as a class of truly impressive luminescent materials, which have been continually improved upon through the development of new and improved synthetic routes. Of importance, biomolecules are particularly attractive for use as ligands with HPNCs, as their properties are often capable of passivating defects in the HPNC lattice. The use of amino acids, peptides, proteins, nucleic acids, cyclodextrins, phospholipids and a variety of other biomolecule derivatives have successfully enabled the production of HPNCs with improved stability, crystallinity and increased optoelectronic performance. Notably, the bi- or multi-functional nature of many biomolecules (especially amino acids) has allowed for the possibility to modulate the luminescence efficiency, emission wavelength, conductivity, and stability of HPNCs through the electron donating and accepting nature of their terminal groups. Moreover, the inherent lack of toxicity of biomolecules makes them excellent candidates for broadening the scope of HPNC applications, such as in biosensing and bioimaging. The use of amino acids as passivating agents has made it possible to generate HPNCs that are stable in ambient conditions for several months, as compared to days for their traditional counterparts. More complex surface functionalizations, like phospholipid micelle-encapsulations of HPNCs, has enabled not only improved stability in ambient conditions, but the ability to generate HPNCs that are dispersible in aqueous solution. Finally, the use of macromolecules such as proteins have enabled robust and reproducible all-aqueous synthesis of HPNCs with good luminescence efficiency and aqueous stability, owing to the effective protection of the HPNC crystal from the environment.

HPNCs are steadily becoming viable nanomaterials for use in biological applications as more and more researchers develop strategies to prevent the degradation of HPNCs and concurrent leakage of lead ions, as well as developing lead-free HPNC alternatives. Several demonstrations of HPNCs as biosensors for a variety of analytes ranging from gaseous agents like NH_3 to antibiotics like penicillamine demonstrate the ver-

satility of sensing capabilities that HPNCs can achieve. Moreover, photoblinking from HPNCs has made it possible to use these materials as fluorescent probes for super-resolution microscopy, generating resolutions that are limited only by the size of the nanoparticles: several hundred nanometers smaller than resolutions that can be achieved in traditional light microscopy. Few nanoparticles thus far have been able to contribute to such advancements in bioimaging in such a major way as HPNCs have. Finally, HPNCs have recently shown their potential as highly efficient scintillating materials with emissions spanning the visible range at impressively low dose rates. HPNC scintillators have emerged as promising candidates for the development of X-ray imaging films that improve upon the traditional film technology in terms of flexibility, cost and resolution.

In conclusion, the use of biomolecules as ligands in the synthesis and applications of HPNCs represent simple, straightforward, safe and abundant means to achieve the production of high-performance HPNCs above and beyond what can be achieved with traditional ligands. The next generation of HPNCs will exhibit high physicochemical stability under a variety of stimuli, exhibit water dispersability and colloidal stability, and will be non-toxic. We believe biomolecular ligands are primed to bring HPNCs to the next level of importance in optoelectronic technologies and look forward to their inevitable success in these fields.

Author contributions

M.A. and N.M.D.C. conceived the topics of the review. M.A., J.J. and G.A.M. synthesized the literature, compiled the figures, wrote, and edited the manuscript and made the TOC graphic. J.A.C., S.M. and N.M.D.C. revised the manuscript and guided the discussion.

Conflicts of interest

There are no conflicts to declare.

Acknowledgements

M. A. gratefully acknowledges support from a Doctoral Research Scholarship from the Fonds de recherche du Québec – Nature et Technologies, and from a McGill Engineering Doctoral Award (MEDA) from the Faculty of Engineering at McGill University. J. J. is grateful for a Natural Sciences and Engineering Research Council of Canada – Summer Undergraduate Research in Engineering (NSERC – SURE) award. G. A. M. is grateful to NSERC for support through the Alexander Graham Bell Canada Graduate Doctoral Scholarship. N.-M. D. C. is grateful for support from the Natural Sciences and Engineering Research Council of Canada (NSERC), the Fonds de Recherche du Québec – Nature et Technologies (FRQNT), the Québec Center for Advanced Materials (QCAM) through the Interinstitutional Collaboration Research program, and the Canada Research Chairs Program. J. A. C. is a Concordia University Research Chair in Nanoscience, and is grateful to FRQNT, NSERC and Concordia University for continued support of his research.

References

1 Q. L. Xu, D. W. Yang, J. Lv, Y. Y. Sun and L. J. Zhang, *Small Methods*, 2018, **2**, 19.
2 M. A. Green, A. Ho-Baillie and H. J. Snaith, *Nat. Photonics*, 2014, **8**, 506–514.
3 A. M. Ganose, C. N. Savory and D. O. Scanlon, *Chem. Commun.*, 2017, **53**, 20–44.
4 W. J. Yin, J. H. Yang, J. Kang, Y. F. Yan and S. H. Wei, *J. Mater. Chem. A*, 2015, **3**, 8926–8942.
5 H. Hu, B. H. Dong and W. Zhang, *J. Mater. Chem. A*, 2017, **5**, 11436–11449.
6 B. Saparov and D. B. Mitzi, *Chem. Rev.*, 2016, **116**, 4558–4596.
7 M. A. Green and A. Ho-Baillie, *ACS Energy Lett.*, 2017, **2**, 822–830.
8 J. Burschka, N. Pellet, S.-J. Moon, R. Humphry-Baker, P. Gao, M. K. Nazeeruddin and M. Grätzel, *Nature*, 2013, **499**, 316–319.
9 Z. K. Tan, R. S. Moghaddam, M. L. Lai, P. Docampo, R. Higler, F. Deschler, M. Price, A. Sadhanala, L. M. Pazos, D. Credgington, F. Hanusch, T. Bein, H. J. Snaith and R. H. Friend, *Nat. Nanotechnol.*, 2014, **9**, 687–692.
10 C. P. Veeramalai, S. Feng, X. Zhang, S. V. N. Pammi, V. Pecunia and C. Li, *Photonics Res.*, 2021, **9**, 968–991.
11 H. Zhu, Y. Fu, F. Meng, X. Wu, Z. Gong, Q. Ding, M. V. Gustafsson, M. T. Trinh, S. Jin and X. Y. Zhu, *Nat. Mater.*, 2015, **14**, 636–642.
12 N. K. Noel, S. D. Stranks, A. Abate, C. Wehrenfennig, S. Guarnera, A. A. Haghighirad, A. Sadhanala, G. E. Eperon, S. K. Pathak, M. B. Johnston, A. Petrozza, L. M. Herz and H. J. Snaith, *Energy Environ. Sci.*, 2014, **7**, 3061–3068.
13 Y. Hassan, Y. Song, R. D. Pensack, A. I. Abdelrahman, Y. Kobayashi, M. A. Winnik and G. D. Scholes, *Adv. Mater.*, 2016, **28**, 566–573.
14 G. Xing, N. Mathews, S. S. Lim, N. Yantara, X. Liu, D. Sabba, M. Gratzel, S. Mhaisalkar and T. C. Sum, *Nat. Mater.*, 2014, **13**, 476–480.
15 P. Tyagi, S. M. Arveson and W. A. Tisdale, *J. Phys. Chem. Lett.*, 2015, **6**, 1911–1916.
16 Y. Hassan, J. H. Park, M. L. Crawford, A. Sadhanala, J. Lee, J. C. Sadighian, E. Mosconi, R. Shivanna, E. Radicchi, M. Jeong, C. Yang, H. Choi, S. H. Park, M. H. Song, F. De Angelis, C. Y. Wong, R. H. Friend, B. R. Lee and H. J. Snaith, *Nature*, 2021, **591**, 72–77.
17 T. Naujoks, R. Jayabalan, C. Kirsch, F. Zu, M. Mandal, J. Wahl, M. Waibel, A. Opitz, N. Koch, D. Andrienko,

M. Scheele and W. Brütting, *ACS Appl. Mater. Interfaces*, 2022, **14**, 28985–28996.
18 A. F. Gualdron-Reyes, S. Masi and I. Mora-Sero, *Trends Chem.*, 2021, **3**, 499–511.
19 C. C. Vidyasagar, B. M. Muñoz Flores and V. M. Jiménez Pérez, *Nanomicro Lett.*, 2018, **10**, 68.
20 G. Grancini, C. Roldan-Carmona, I. Zimmermann, E. Mosconi, X. Lee, D. Martineau, S. Narbey, F. Oswald, F. De Angelis, M. Graetzel and M. K. Nazeeruddin, *Nat. Commun.*, 2017, **8**, 15684.
21 L. Qiu, L. K. Ono and Y. Qi, *Mater. Today Energy*, 2018, **7**, 169–189.
22 D. He, X. Xu, Z. Liang, Y. Niu, Y. Sun, T. Gavin, P. Falaras and L. Hu, *J. Mater. Chem. C*, 2021, **9**, 9584–9591.
23 C. X. Zhang, T. Shen, D. Guo, L. M. Tang, K. Yang and H. X. Deng, *InfoMat*, 2020, **2**, 1034–1056.
24 Y. Chen and H. Zhou, *J. Appl. Phys.*, 2020, **128**, 060903.
25 Y. Yuan, Q. Zhao, Y. Shao, J. Zhou, C. Luo and H. Wang, in *Perovskite Materials and Devices*, 2022, pp. 101–128, DOI: **10.1002/9783527832552.ch4**.
26 E. B. Bi, Z. N. Song, C. W. Li, Z. F. Wu and Y. F. Yan, *Trends Chem.*, 2021, **3**, 575–588.
27 P. P. Teng, S. Reichert, W. D. Xu, S. C. Yang, F. Fu, Y. T. Zou, C. Y. Yin, C. X. Bao, M. Karlsson, X. J. Liu, J. J. Qin, T. Yu, W. Tress, Y. Yang, B. Q. Sun, C. Deibel and F. Gao, *Matter*, 2021, **4**, 3710–3724.
28 D. Zhang, D. Li, Y. Hu, A. Mei and H. Han, *Commun. Mater.*, 2022, **3**, 58.
29 T. J. Smart, H. Takenaka, T. A. Pham, L. Z. Tan, J. Z. Zhang, T. Ogitsu and Y. Ping, *J. Phys. Chem. Lett.*, 2021, **12**, 6299–6304.
30 M. Pratheek, T. Abhinav, S. Bhattacharya, G. K. Chandra and P. Predeep, *Mater. Sci. Energy Technol.*, 2021, **4**, 282–289.
31 M. G. Ju, J. Dai, L. Ma and X. C. Zeng, *J. Am. Chem. Soc.*, 2017, **139**, 8038–8043.
32 F. Giustino and H. J. Snaith, *ACS Energy Lett.*, 2016, **1**, 1233–1240.
33 G. Volonakis, A. A. Haghighirad, H. J. Snaith and F. Giustino, *J. Phys. Chem. Lett.*, 2017, **8**, 3917–3924.
34 X. G. Zhao, J. H. Yang, Y. H. Fu, D. W. Yang, Q. L. Xu, L. P. Yu, S. H. Wei and L. J. Zhang, *J. Am. Chem. Soc.*, 2017, **139**, 2630–2638.
35 G. Volonakis, M. R. Filip, A. A. Haghighirad, N. Sakai, B. Wenger, H. J. Snaith and F. Giustino, *J. Phys. Chem. Lett.*, 2016, **7**, 1254–1259.
36 H. H. Tsai, W. Y. Nie, J. C. Blancon, C. C. S. Toumpos, R. Asadpour, B. Harutyunyan, A. J. Neukirch, R. Verduzco, J. J. Crochet, S. Tretiak, L. Pedesseau, J. Even, M. A. Alam, G. Gupta, J. Lou, P. M. Ajayan, M. J. Bedzyk, M. G. Kanatzidis and A. D. Mohite, *Nature*, 2016, **536**, 312–316.
37 B. Saparov, F. Hong, J. P. Sun, H. S. Duan, W. W. Meng, S. Cameron, I. G. Hill, Y. F. Yan and D. B. Mitzi, *Chem. Mater.*, 2015, **27**, 5622–5632.
38 Z. Z. Li and W. J. Yin, *J. Semicond.*, 2018, **39**, 6.
39 K. Hills-Kimball, H. Yang, T. Cai, J. Wang and O. Chen, *Adv. Sci.*, 2021, **8**, 2100214.
40 Y. Tang, N. Yan, Z. Wang, H. Yuan, Y. Xin and H. Yin, *J. Alloys Compd.*, 2019, **773**, 227–233.
41 J. Z. Zhang, *J. Phys. Chem. Lett.*, 2019, **10**, 5055–5063.
42 M. Kazes, T. Udayabhaskararao, S. Dey and D. Oron, *Acc. Chem. Res.*, 2021, **54**, 1409–1418.
43 S. Sun, D. Yuan, Y. Xu, A. Wang and Z. Deng, *ACS Nano*, 2016, **10**, 3648–3657.
44 B. B. Zhang, S. Yuan, J. P. Ma, Y. Zhou, J. Hou, X. Chen, W. Zheng, H. Shen, X. C. Wang, B. Sun, O. M. Bakr, L. S. Liao and H. T. Sun, *J. Am. Chem. Soc.*, 2019, **141**, 15423–15432.
45 S. Cheng and H. Zhong, *J. Phys. Chem. Lett.*, 2022, **13**, 2281–2290.
46 C. Geng, S. Xu, H. Z. Zhong, A. L. Rogach and W. G. Bi, *Angew. Chem., Int. Ed.*, 2018, **57**, 9650–9654.
47 L. Liu, K. Pan, K. Xu and J. Z. Zhang, *ACS Phys. Chem. Au*, 2022, **2**, 156–170.
48 B. B. Luo, S. B. Naghadeh, A. Allen, X. M. Li and J. Z. Zhang, *Adv. Funct. Mater.*, 2017, **27**, 7.
49 J. Ye, M. M. Byranvand, C. O. Martínez, R. L. Z. Hoye, M. Saliba and L. Polavarapu, *Angew. Chem., Int. Ed.*, 2021, **60**, 21636–21660.
50 D. Yang, X. Li and H. Zeng, *Adv. Mater. Interfaces*, 2018, **5**, 1701662.
51 Y. Zhou, H. Zhong, J. Han, M. Tai, X. Yin, M. Zhang, Z. Wu and H. Lin, *J. Mater. Chem. A*, 2019, **7**, 26334–26341.
52 X. Zheng, B. Chen, J. Dai, Y. Fang, Y. Bai, Y. Lin, H. Wei, X. C. Zeng and J. Huang, *Nat. Energy*, 2017, **2**, 17102.
53 G. M. Whitesides, J. P. Mathias and C. T. Seto, *Science*, 1991, **254**, 1312–1319.
54 S. Zhang, *Biotechnol. Adv.*, 2002, **20**, 321–339.
55 S. Zhang, *Nat. Biotechnol.*, 2003, **21**, 1171–1178.
56 Z. Abdali, M. Aminzare, X. Zhu, E. DeBenedictis, O. Xie, S. Keten and N.-M. Dorval Courchesne, *ACS Synth. Biol.*, 2020, **9**, 3334–3343.
57 L. Zuo, Z. Gu, T. Ye, W. Fu, G. Wu, H. Li and H. Chen, *J. Am. Chem. Soc.*, 2015, **137**, 2674–2679.
58 Y. C. Shih, L. Y. Wang, H. C. Hsieh and K. F. Lin, *J. Mater. Chem. A*, 2015, **3**, 9133–9136.
59 B. Luo, S. B. Naghadeh, A. L. Allen, X. Li and J. Z. Zhang, *Adv. Funct. Mater.*, 2017, **27**, 1604018.
60 A. J. Prochazkova, S. Gaidies, C. Yumusak, O. Brüggemann, M. Weiter, N. S. Sariciftci, M. C. Scharber, K. Čépe, R. Zbořil, J. Krajcovic, Y. Salinas and A. Kovalenko, *Mater. Today Chem.*, 2020, **17**, 100272.
61 S. Wang, L. Zhou, F. Huang, Y. Xin, P. Jin, Q. Ma, Q. Pang, Y. Chen and J. Z. Zhang, *J. Mater. Chem. C*, 2018, **6**, 10994–11001.
62 J. Zhao, S. Cao, Z. Li and N. Ma, *Chem. Mater.*, 2018, **30**, 6737–6743.
63 A. K. Sharma, P. Bansal, G. K. Nim and P. Kar, *Part. Part. Syst. Charact.*, 2019, **36**, 1900328.

64 A. Kaiba, M. H. Geesi, P. Guionneau, T. A. Aljohani, L. Bih, H. Bih and S. Kassou, *J. Mol. Struct.*, 2020, **1204**, 129008.
65 A. Lang, I. Polishchuk, E. Seknazi, J. Feldmann, A. Katsman and B. Pokroy, *Adv. Funct. Mater.*, 2020, **30**, 2005136.
66 R. Arai, M. Yoshizawa-Fujita, Y. Takeoka and M. Rikukawa, *ACS Omega*, 2017, **2**, 2333–2336.
67 M. Ou, W. Tu, S. Yin, W. Xing, S. Wu, H. Wang, S. Wan, Q. Zhong and R. Xu, *Angew. Chem., Int. Ed.*, 2018, **57**, 13570–13574.
68 X. Li, Y. Wang, H. Sun and H. Zeng, *Adv. Mater.*, 2017, **29**, 1701185.
69 P. Li, D. Yang, Y. Tan, M. Cao, Q. Zhong, M. Chen, H. Hu, B. Sun, Y. Xu and Q. Zhang, *ACS Appl. Mater. Interfaces*, 2019, **11**, 3351–3359.
70 B. A. Koscher, J. K. Swabeck, N. D. Bronstein and A. P. Alivisatos, *J. Am. Chem. Soc.*, 2017, **139**, 6566–6569.
71 H. Bian, D. Bai, Z. Jin, K. Wang, L. Liang, H. Wang, J. Zhang, Q. Wang and S. Liu, *Joule*, 2018, **2**, 1500–1510.
72 R. K. Gautam, S. Das and A. Samanta, *ChemNanoMat*, 2022, **8**, e202200029.
73 S. Gonzalez-Carrero, R. E. Galian and J. Perez-Prieto, *J. Mater. Chem. A*, 2015, **3**, 9187–9193.
74 Z. K. Liu, Y. Bekenstein, X. C. Ye, S. C. Nguyen, J. Swabeck, D. D. Zhang, S. T. Lee, P. D. Yang, W. L. Ma and A. P. Alivisatos, *J. Am. Chem. Soc.*, 2017, **139**, 5309–5312.
75 S. K. Balakrishnan and P. V. Kamat, *Chem. Mater.*, 2018, **30**, 74–78.
76 Y.-L. Hu, Q.-L. Wen, Z.-F. Pu, A.-Y. Liu, J. Wang, J. Ling, X.-G. Xie and Q.-E. Cao, *RSC Adv.*, 2020, **10**, 34215–34224.
77 A. J. Prochazkova, S. Demchyshyn, C. Yumusak, J. Másilko, O. Brüggemann, M. Weiter, M. Kaltenbrunner, N. S. Sariciftci, J. Krajcovic, Y. Salinas and A. Kovalenko, *ACS Appl. Nano Mater.*, 2019, **2**, 4267–4274.
78 A. J. Prochazkova, Y. Salinas, C. Yumusak, M. C. Scharber, O. Brüggemann, M. Weiter, N. S. Sariciftci, J. Krajcovic and A. Kovalenko, *ACS Appl. Nano Mater.*, 2020, **3**, 1242–1249.
79 L. Liu, K. Xu, A. L. Allen, X. Li, H. Xia, L. Peng and J. Z. Zhang, *J. Phys. Chem. C*, 2021, **125**, 2793–2801.
80 S. Ghosh and P. Kar, *Inorg. Chem.*, 2022, **61**, 10079–10088.
81 J. Shi, F. Li, Y. Jin, C. Liu, B. Cohen-Kleinstein, S. Yuan, Y. Li, Z.-K. Wang, J. Yuan and W. Ma, *Angew. Chem. Int. Ed.*, 2020, **59**, 22230–22237.
82 X. Fang, J. Ye, D. Duan, X. Cai, X. Guo and K. Li, *Microchim. Acta*, 2021, **188**, 204.
83 C. G. Sanjayan, M. S. Jyothi, M. Sakar and R. G. Balakrishna, *J. Colloid Interface Sci.*, 2021, **603**, 758–770.
84 Y. Zhang, G. Li, G. Hou, J. Lin, M. Chen, S. Liu, H. Lin, J. Fang, C. Jing and J. Chu, *Chem. Eng. J.*, 2022, **438**, 135270.
85 A. Tofanello, A. L. M. Freitas, T. B. de Queiroz, A. Bonadio, H. Martinho and J. A. Souza, *J. Phys. Chem. Lett.*, 2022, **13**, 1406–1415.
86 Y. Xu, W. Zhang, K. Su, Y. X. Feng, Y. F. Mu, M. Zhang and T. B. Lu, *Chem. – Eur. J.*, 2021, **27**, 2305–2309.
87 R. Shwetharani, H. V. Vishaka, J. Kusuma and R. G. Balakrishna, *ACS Appl. Nano Mater.*, 2020, **3**, 6089–6098.
88 X. Zhang, H. Huang, Y. M. Maung, J. Yuan and W. Ma, *Chem. Commun.*, 2021, **57**, 7906–7909.
89 G. Li, J. Huang, H. Zhu, Y. Li, J.-X. Tang and Y. Jiang, *Chem. Mater.*, 2018, **30**, 6099–6107.
90 C. Tang, X. Shen, S. Yu, Y. Zhong, Z. Wang, J. Hu, M. Lu, Z. Wu, Y. Zhang, W. W. Yu and X. Bai, *Mater. Today Phys.*, 2021, **21**, 100555.
91 Z. Wang, X. Shen, C. Tang, X. Li, J. Hu, J. Zhu, W. W. Yu, H. Song and X. Bai, *ACS Appl. Mater. Interfaces*, 2022, **14**, 8235–8242.
92 Y.-L. Hu, N. Yang, R.-X. Zhao, Y.-B. Fu, J. Ling, X.-G. Xie and Q. Cao, *Dyes Pigm.*, 2022, **205**, 110537.
93 A. J. Prochazkova, Y. Salinas, C. Yumusak, O. Bruggemann, M. Weiter, N. S. Sariciftci, J. Krajcovic and A. Kovalenko, *Sci. Rep.*, 2019, **9**, 12966.
94 D. Gao, Y. Zhang, B. Lyu, X. Guo, Y. Hou, J. Ma, B. Yu and S. Chen, *Inorg. Chem.*, 2022, **61**, 6547–6554.
95 B. Lyu, X. Guo, D. Gao, M. Kou, Y. Yu, J. Ma, S. Chen, H. Wang, Y. Zhang and X. Bao, *J. Hazard. Mater.*, 2021, **403**, 123967.
96 M. Aminzare, E. Hamzehpoor, S. Mahshid and N.-M. Dorval Courchesne, *ACS Appl. Nano Mater.*, 2022, **5**, 12666–12678.
97 J.-M. Lee, J. W. Choi, I. Jeon, Y. Zhu, T. Yang, H. Chun, J. Shin, J. Park, J. Bang, K. Lim, W.-G. Kim, Y. Kim, H. Jeong, E. J. Choi, V. Devaraj, J. S. Nam, H. Ahn, Y.-C. Kang, B. Han, M. Song, J.-W. Oh and C. Mao, *Mater. Today Nano*, 2021, **13**, 100099.
98 Q. L. Li, W. X. Lu, N. Wan and S. N. Ding, *Chem. Commun.*, 2016, **52**, 12342–12345.
99 S. Huang, T. Zhang, C. Jiang, R. Qi, C. Luo, Y. Chen, H. Lin, J. Travas-sejdic and H. Peng, *ChemNanoMat*, 2019, **5**, 1311–1316.
100 F. Guo, Y.-Y. Wang, J. Zhang, X.-L. Wei and Z.-H. Mo, *New J. Chem.*, 2020, **44**, 17368–17373.
101 X. Kong, Y. Wu, F. Xu, S. Yang and B. Cao, *Phys. Status Solidi RRL*, 2021, **15**, 2100134.
102 S. Li, Y. Zhang, Y. Zu, Y. Chen, F. Luo, D. Huang, Z. Weng, B. Qiu and Z. Lin, *Sens. Actuators, B*, 2022, **355**, 131301.
103 C.-C. Hung, Y.-C. Lin, T.-H. Chuang, Y.-C. Chiang, Y.-C. Chiu, M. Mumtaz, R. Borsali and W.-C. Chen, *ACS Appl. Mater. Interfaces*, 2022, **14**, 30279–30289.
104 L. Hong, J. V. Milić, P. Ahlawat, M. Mladenović, D. J. Kubicki, F. Jahanabkhshi, D. Ren, M. C. Gélvez-Rueda, M. A. Ruiz-Preciado, A. Ummadisingu, Y. Liu, C. Tian, L. Pan, S. M. Zakeeruddin, A. Hagfeldt, F. C. Grozema, U. Rothlisberger, L. Emsley, H. Han and M. Graetzel, *Angew. Chem. Int. Ed.*, 2020, **59**, 4691–4697.
105 G. Lee, S. Y. Lee, S. Park, S. H. Jang, H.-K. Park, I. Choi, J. Park and J. Choi, *J. Mater. Res. Technol.*, 2022, **18**, 4145–4155.

106 Z. Y. Yang, J. K. Xu, S. F. Zong, S. H. Xu, D. Zhu, Y. Z. Zhang, C. Chen, C. L. Wang, Z. Y. Wang and Y. P. Cui, *ACS Appl. Mater. Interfaces*, 2019, **11**, 47671–47679.
107 M. Li, Y. J. Zeng, X. Y. Qu, M. Jalalah, S. A. Alsareii, C. Li, F. A. Harraz and G. X. Li, *Small*, 2021, **17**, 2103255.
108 F. Krieg, Q. K. Ong, M. Burian, G. Rainò, D. Naumenko, H. Amenitsch, A. Süess, M. J. Grotevent, F. Krumeich, M. I. Bodnarchuk, I. Shorubalko, F. Stellacci and M. V. Kovalenko, *J. Am. Chem. Soc.*, 2019, **141**, 19839–19849.
109 S. Karabel Ocal, N. B. Kiremitler, A. F. Yazici, N. Celik, E. Mutlugun and M. S. Onses, *ACS Appl. Nano Mater.*, 2022, **5**, 6201–6212.
110 V. G. V. Dutt, S. Akhil, R. Singh, M. Palabathuni and N. Mishra, *ACS Appl. Nano Mater.*, 2022, **5**, 5972–5982.
111 P. Bansal and P. Kar, *New J. Chem.*, 2019, **43**, 4599–4604.
112 S. C. G. J. Mannekote Shivanna, J. D. Schiffman, S. Mohan, S. Budagumpi and R. G. Balakrishna, *ACS Appl. Mater. Interfaces*, 2022, **14**, 38471–38482.
113 V. G. V. Dutt, S. Akhil, R. Singh, M. Palabathuni and N. Mishra, *J. Phys. Chem. C*, 2022, **126**, 9502–9508.
114 H. Zhu, Y. Pan, C. Peng, H. Lian and J. Lin, *Angew. Chem. Int. Ed.*, 2022, **61**, e202116702.
115 J. Zhuang, P. Mao, Y. G. Luan, X. H. Yi, Z. Y. Tu, Y. Y. Zhang, Y. P. Yi, Y. Z. Wei, N. L. Chen, T. Lin, F. Y. Wang, C. Li and J. Z. Wang, *ACS Energy Lett.*, 2019, **4**, 2913–2921.
116 C. Shen, O. Acar, W. Y. Shih and W.-H. Shih, *ACS Appl. Nano Mater.*, 2021, **4**, 10334–10343.
117 Y. Zhang, G. S. Li, C. K. She, S. H. Liu, F. Y. Yue, C. B. Jing, Y. Cheng and J. H. Chu, *Nano Res.*, 2021, **14**, 2770–2775.
118 K. Bharath Kumar Naik, B. Ananda Kumar, S. Raju and G. Nageswara Rao, *Int. J. Inorg. Chem.*, 2012, **2012**, 265249.
119 B. Liu, J. Li, G. Duan, M. Ji, Y. Lu, T. Yan, B. Cao and Z. Liu, *Opt. Express*, 2020, **28**, 10714–10724.
120 H. Huang, J. Raith, S. V. Kershaw, S. Kalytchuk, O. Tomanec, L. Jing, A. S. Susha, R. Zboril and A. L. Rogach, *Nat. Commun.*, 2017, **8**, 996.
121 V. Y. Sirenko, O. I. Kucheriv, D. D. Naumova, I. V. Fesych, R. P. Linnik, I.-A. Dascălu, S. Shova, I. O. Fritsky and I. y. A. Gural'skiy, *New J. Chem.*, 2021, **45**, 12606–12612.
122 A. Karavioti, E. Vitoratos and E. Stathatos, *J. Mater. Sci.: Mater. Electron.*, 2020, **31**, 6109–6117.
123 M. W. Heindl, T. Kodalle, N. Fehn, L. K. Reb, S. Liu, C. Harder, M. Abdelsamie, L. Eyre, I. D. Sharp, S. V. Roth, P. Müller-Buschbaum, A. Kartouzian, C. M. Sutter-Fella and F. Deschler, *Adv. Opt. Mater.*, 2022, **10**, 2200204.
124 S.-C. Yun, S. Ma, H.-C. Kwon, K. Kim, G. Jang, H. Yang and J. Moon, *Nano Energy*, 2019, **59**, 481–491.
125 M. B. AlShammari, A. Kaiba, P. Guionneau, M. H. Geesi, T. Aljohani and Y. Riadi, *Chem. Phys. Lett.*, 2018, **702**, 8–15.
126 M. Daub, D. Natalukha and H. Hillebrecht, *Eur. J. Inorg. Chem.*, 2022, **2022**, e202200136.
127 M. Ma, Q. Tang, H. Chen, B. He and P. Yang, *Sol. Energy Mater. Sol. Cells*, 2017, **160**, 67–76.
128 M. Krummer, B. Zimmermann, P. Klingenberg, M. Daub and H. Hillebrecht, *Eur. J. Inorg. Chem.*, 2020, **2020**, 4581–4592.
129 M. L. Aubrey, A. Saldivar Valdes, M. R. Filip, B. A. Connor, K. P. Lindquist, J. B. Neaton and H. I. Karunadasa, *Nature*, 2021, **597**, 355–359.
130 A. Kaiba, M. H. Geesi, P. Guionneau, Y. Riadi, T. A. Aljohani, A. Elsanousi and O. Ouerghi, *J. Mol. Struct.*, 2021, **1224**, 129008.
131 M. B. H. Salah, N. Mercier, M. Allain, N. Zouari and C. Botta, *J. Mater. Chem. C*, 2019, **7**, 4424–4433.
132 E. Shi, B. Yuan, S. B. Shiring, Y. Gao, Akriti, Y. Guo, C. Su, M. Lai, P. Yang, J. Kong, B. M. Savoie, Y. Yu and L. Dou, *Nature*, 2020, **580**, 614–620.
133 M. Yuan, L. N. Quan, R. Comin, G. Walters, R. Sabatini, O. Voznyy, S. Hoogland, Y. Zhao, E. M. Beauregard, P. Kanjanaboos, Z. Lu, D. H. Kim and E. H. Sargent, *Nat. Nanotechnol.*, 2016, **11**, 872–877.
134 Y. F. Ng, S. A. Kulkarni, S. Parida, N. F. Jamaludin, N. Yantara, A. Bruno, C. Soci, S. Mhaisalkar and N. Mathews, *Chem. Commun.*, 2017, **53**, 12004–12007.
135 L. Zhang and W. Liang, *J. Phys. Chem. Lett.*, 2017, **8**, 1517–1523.
136 L. N. Quan, Y. Zhao, F. P. García de Arquer, R. Sabatini, G. Walters, O. Voznyy, R. Comin, Y. Li, J. Z. Fan, H. Tan, J. Pan, M. Yuan, O. M. Bakr, Z. Lu, D. H. Kim and E. H. Sargent, *Nano Lett.*, 2017, **17**, 3701–3709.
137 F. Li, Y. Pei, F. Xiao, T. Zeng, Z. Yang, J. Xu, J. Sun, B. Peng and M. Liu, *Nanoscale*, 2018, **10**, 6318–6322.
138 J. Cheng, Y. Deng, X. Dong, J. Li, L. Huang, H. Zeng, G. Zou and Z. Lin, *Inorg. Chem.*, 2022, **61**, 11032–11035.
139 M. Wirkner, S. Weis, V. San Miguel, M. Alvarez, R. A. Gropeanu, M. Salierno, A. Sartoris, R. E. Unger, C. J. Kirkpatrick and A. del Campo, *ChemBioChem*, 2011, **12**, 2623–2629.
140 Y. Wu, X. Li and H. Zeng, *ACS Energy Lett.*, 2019, **4**, 673–681.
141 B. A. Krajina, A. C. Proctor, A. P. Schoen, A. J. Spakowitz and S. C. Heilshorn, *Prog. Mater. Sci.*, 2018, **91**, 1–23.
142 A. R. D. Voet and J. R. H. Tame, *Curr. Opin. Biotechnol.*, 2017, **46**, 14–19.
143 W. T. Yang, W. S. Guo, J. Chang and B. B. Zhang, *J. Mater. Chem. B*, 2017, **5**, 401–417.
144 S. L. Kuan, F. R. G. Bergamini and T. Weil, *Chem. Soc. Rev.*, 2018, **47**, 9069–9105.
145 J. Ge, J. Lei and R. N. Zare, *Nat. Nanotechnol.*, 2012, **7**, 428–432.
146 N. Song and Y.-W. Yang, *Sci. China: Chem.*, 2014, **57**, 1185–1198.
147 Z. Yang, J. Xu, S. Zong, S. Xu, D. Zhu, Y. Zhang, C. Chen, C. Wang, Z. Wang and Y. Cui, *ACS Appl. Mater. Interfaces*, 2019, **11**, 47671–47679.
148 M. Li, Y. Zeng, X. Qu, M. Jalalah, S. A. Alsareii, C. Li, F. A. Harraz and G. Li, *Small*, 2021, **17**, 2103255.

149 X. Xu, C.-C. Chueh, Z. Yang, A. Rajagopal, J. Xu, S. B. Jo and A. K. Y. Jen, *Nano Energy*, 2017, **34**, 392–398.
150 F. Cao, W. Tian, M. Wang, M. Wang and L. Li, *InfoMat*, 2020, **2**, 577–584.
151 D. Wu, J. Chi, M. Zhang, L. Cheng, X. Wang, J. Fan, Z. Huang, H. Wang, H. Xie, Q. Pan, Z. Zhang, B. Chen, M. Su, B. Xu and Y. Song, *Adv. Opt. Mater.*, 2022, **10**, 2101835.
152 W. A. Dunlap-Shohl, Y. Zhou, N. P. Padture and D. B. Mitzi, *Chem. Rev.*, 2019, **119**, 3193–3295.
153 J. Chen, Y. Zhou, Y. P. Fu, J. Pan, O. F. Mohammed and O. M. Bakr, *Chem. Rev.*, 2021, **121**, 12112–12180.
154 Y. C. Shih, Y. B. Lan, C. S. Li, H. C. Hsieh, L. Wang, C. I. Wu and K. F. Lin, *Small*, 2017, **13**, 1604305.
155 W. Zhang, X. Liu, B. He, J. Zhu, X. Li, K. Shen, H. Chen, Y. Duan and Q. Tang, *ACS Appl. Mater. Interfaces*, 2020, **12**, 36092–36101.
156 H. Yuan, Z. Zhang, T. Guo, L. Yu, Z. Deng, R. Zhao, J. Zhang and Y. Zhu, *J. Alloys Compd.*, 2021, **876**, 160140.
157 S. Yang, J. Dai, Z. Yu, Y. Shao, Y. Zhou, X. Xiao, X. C. Zeng and J. Huang, *J. Am. Chem. Soc.*, 2019, **141**, 5781–5787.
158 W. Zhang, X. Lei, J. Liu, J. Dong, X. Yan, W. Gao, H. Dong, C. Ran and Z. Wu, *Phys. Status Solidi RRL*, 2019, **13**, 1900130.
159 P. Wu, X. Ma, B. Zhao, C. Liu, Y. Chen, G. Yang and X. Li, *Sustainable Energy Fuels*, 2020, **4**, 878–883.
160 J. H. Kim, Y. R. Kim, B. Park, S. Hong, I. W. Hwang, J. Kim, S. Kwon, G. Kim, H. Kim and K. Lee, *Small*, 2021, **17**, e2005608.
161 K. Chaisan, D. Wongratanaphisan, S. Choopun, T. Sagawa and P. Ruankham, *J. Mater. Sci.: Mater. Electron.*, 2018, **30**, 939–949.
162 D. Jia, J. Chen, M. Yu, J. Liu, E. M. J. Johansson, A. Hagfeldt and X. Zhang, *Small*, 2020, **16**, e2001772.
163 X. Dong, X. Fang, M. Lv, B. Lin, S. Zhang, Y. Wang, N. Yuan and J. Ding, *Sci. Bull.*, 2016, **61**, 236–244.
164 C. Zhang, S. Zhang, X. Miao, Y. Hu, L. Staaden and G. Jia, *Part. Part. Syst. Charact.*, 2017, **34**, 1600298.
165 A. Mei, X. Li, L. Liu, Z. Ku, T. Liu, Y. Rong, M. Xu, M. Hu, J. Chen, Y. Yang, M. Gratzel and H. Han, *Science*, 2014, **345**, 295–298.
166 W. Li, D. Wang, W. Hou, R. Li, Z. Wu, W. Sun, J. Wu and Z. Lan, *Org. Electron.*, 2020, **87**, 105982.
167 L. Zhang, K. Cao, J. Qian, Y. Huang, X. Wang, M. Ge, W. Shen, F. Huang, M. Wang, W. Zhang, S. Chen and T. Qin, *J. Mater. Chem. C*, 2020, **8**, 17482–17490.
168 R. Chen, J. Cao, Y. Wu, X. Jing, B. Wu and N. Zheng, *Adv. Mater. Interfaces*, 2017, **4**, 1700897.
169 T. Zhang, L. Xie, L. Chen, N. Guo, G. Li, Z. Tian, B. Mao and Y. Zhao, *Adv. Funct. Mater.*, 2017, **27**, 1603568.
170 T. Wang, T. Zhang, Y. Chen and Y. Zhao, *Acta Phys.-Chim. Sin.*, 2020, **0**, 2007021–2007020.
171 A. Mahata, E. Mosconi, D. Meggiolaro and F. De Angelis, *Chem. Mater.*, 2019, **32**, 105–113.
172 K. Wang, Y. Hou, B. Poudel, D. Yang, Y. Jiang, M. G. Kang, K. Wang, C. Wu and S. Priya, *Adv. Energy Mater.*, 2019, **9**, 1901753.
173 K. B. Lin, J. Xing, L. N. Quan, F. P. G. de Arquer, X. W. Gong, J. X. Lu, L. Q. Xie, W. J. Zhao, D. Zhang, C. Z. Yan, W. Q. Li, X. Y. Liu, Y. Lu, J. Kirman, E. H. Sargent, Q. H. Xiong and Z. H. Wei, *Nature*, 2018, **562**, 245–248.
174 S. Das, C. Wu, Z. Song, Y. Hou, R. Koch, P. Somasundaran, S. Priya, B. Barbiellini and R. Venkatesan, *ACS Appl. Mater. Interfaces*, 2019, **11**, 30728–30734.
175 H. S. Lin, J. M. Lee, J. Han, C. Lee, S. Seo, S. Tan, H. M. Lee, E. J. Choi, M. S. Strano, Y. Yang, S. Maruyama, I. Jeon, Y. Matsuo and J. W. Oh, *Adv. Sci.*, 2020, **7**, 2000782.
176 A. R. Yusoff, J. Kim, J. Jang and M. K. Nazeeruddin, *ChemSusChem*, 2016, **9**, 1736–1742.
177 A. Peluso, T. Caruso, A. Landi and A. Capobianco, *Molecules*, 2019, **24**, 4044.
178 L. Zhang and B. Wu, *Appl. Surf. Sci.*, 2019, **483**, 1052–1057.
179 Y. Zhao, J. Zhang, J. Sun, Q. Zhou, Q. Liu, J. Chen, W. Ge, Q. Tian, B. Fan and H. Bai, *ACS Appl. Energy Mater.*, 2021, **4**, 3310–3316.
180 P. Zhang, F. Cao, W. Tian and L. Li, *Sci. China Mater.*, 2022, **65**, 321–327.
181 K. H. Wang, L. Wang, Y. Y. Liu, Y. H. Song, Y. C. Yin, J. S. Yao, J. N. Yang, J. J. Wang, L. Z. Feng, Q. Zhang, Q. Zhang and H. B. Yao, *Adv. Opt. Mater.*, 2020, **9**, 2001684.
182 N. Wang, L. Cheng, J. Si, X. Liang, Y. Jin, J. Wang and W. Huang, *Appl. Phys. Lett.*, 2016, **108**, 141102.
183 J. W. Ward, H. L. Smith, A. Zeidell, P. J. Diemer, S. R. Baker, H. Lee, M. M. Payne, J. E. Anthony, M. Guthold and O. D. Jurchescu, *ACS Appl. Mater. Interfaces*, 2017, **9**, 18120–18126.
184 Q.-B. Yan, N. Bao and S.-N. Ding, *J. Mater. Chem. B*, 2019, **7**, 4153–4160.
185 Y. Wei, X. Deng, Z. Xie, X. Cai, S. Liang, P. a. Ma, Z. Hou, Z. Cheng and J. Lin, *Adv. Funct. Mater.*, 2017, **27**, 1703535.
186 Y. Wang, L. Varadi, A. Trinchi, J. Shen, Y. Zhu, G. Wei and C. Li, *Small*, 2018, **14**, e1803156.
187 H. Zhang, X. Wang, Q. Liao, Z. Xu, H. Li, L. Zheng and H. Fu, *Adv. Funct. Mater.*, 2017, **27**, 1604382.
188 M. J. H. Tan, D. Ravichandran, H. L. Ang, E. W. Y. Ong, C. Q. X. Lim, G. M. Q. Kam, A. P. Kumar and Z.-K. Tan, *Adv. Healthc. Mater.*, 2019, **8**, 1900859.
189 Z. Yang, S. Zong, K. Yang, K. Zhu, N. Li, Z. Wang and Y. Cui, *ACS Appl. Mater. Interfaces*, 2022, **14**, 17109–17118.
190 Z. Yang, Y. Dong, S. Zong, L. Li, K. Yang, Z. Wang, H. Zeng and Y. Cui, *Nanoscale*, 2022, **14**, 6392–6401.
191 P. M. Talianov, A. A. Yakubova, A. Bukreeva, M. Masharin, I. E. Eliseev, L. Zelenkov, A. R. Muslimov, A. Bukatin, A. Gordeeva, V. Kudryavtseva, S. V. Makarov, G. B. Sukhorukov, A. S. Timin and M. V. Zyuzin, *ACS Appl. Bio Mater.*, 2022, **5**, 2411–2420.
192 S. K. Avugadda, A. Castelli, B. Dhanabalan, T. Fernandez, N. Silvestri, C. Collantes, D. Baranov, M. Imran, L. Manna,

T. Pellegrino and M. P. Arciniegas, *ACS Nano*, 2022, **16**, 13657–13666.
193 A. Pramanik, K. Gates, S. Patibandla, D. Davis, S. Begum, R. Iftekhar, S. Alamgir, S. Paige, M. M. Porter and P. C. Ray, *ACS Appl. Bio Mater.*, 2019, **2**, 5872–5879.
194 G. Getachew, W.-W. Huang, T.-H. Chou, A. S. Rasal and J.-Y. Chang, *J. Colloid Interface Sci.*, 2022, **605**, 500–512.
195 S. M. Lee, H. Jung, W. I. Park, Y. Lee, E. Koo and J. Bang, *ChemistrySelect*, 2018, **3**, 11320–11325.
196 H. Lian, Y. Li, S. Saravanakumar, H. Jiang, Z. Li, J. Wang, L. Xu, W. Zhao and G. Han, *Coord. Chem. Rev.*, 2022, **452**, 214313.
197 X. Fang, D. Duan, J. Ye and K. Li, *Anal. Chim. Acta*, 2021, **1183**, 338938.
198 M. Li, Y. Wang, H. Hu, Y. Feng, S. Zhu, C. Li and N. Feng, *Biosens. Bioelectron.*, 2022, **203**, 113979.
199 X. Jiang, H. Zeng, C. Duan, Q. Hu, Q. Wu, Y. Yu and X. Yang, *Dalton Trans.*, 2022, **51**, 3581–3589.
200 M. Li, T. Tian, Y. Zeng, S. Zhu, C. Li, Y. Yin and G. Li, *Sens. Actuators, B*, 2021, **338**, 129839.
201 C. Q. Chen, Q. Cai, F. Luo, N. Dong, L. H. Guo, B. Qiu and Z. Y. Lin, *Anal. Chem.*, 2019, **91**, 15915–15921.
202 Y. Shu, L. Sun, Y. Wang, D. Jin, Q. Xu and X. Hu, *Analyst*, 2021, **146**, 6798–6807.
203 L. Jia, Z. Xu, L. Zhang, Y. Li, T. Zhao and J. Xu, *Appl. Surf. Sci.*, 2022, **592**, 153170.
204 X. Q. Shi, M. Kralj and Y. Zhang, *J. Phys.: Condens. Matter*, 2022, **34**, 304002.
205 F. Luo, Y. Zhang, Y. Zu, S. Li, Y. Chen, Z. Chen, D. Huang, B. Qiu and Z. Lin, *Microchim. Acta*, 2022, **189**, 68.
206 F. Luo, S. Li, L. Cui, Y. Zu, Y. Chen, D. Huang, Z. Weng and Z. Lin, *Nanoscale*, 2021, **13**, 14297–14303.
207 C. Bao, W. Xu, J. Yang, S. Bai, P. Teng, Y. Yang, J. Wang, N. Zhao, W. Zhang, W. Huang and F. Gao, *Nat. Electron.*, 2020, **3**, 156–164.
208 L. Gu, S. Poddar, Y. Lin, Z. Long, D. Zhang, Q. Zhang, L. Shu, X. Qiu, M. Kam, A. Javey and Z. Fan, *Nature*, 2020, **581**, 278–282.
209 K. Xia, W. Wu, M. Zhu, X. Shen, Z. Yin, H. Wang, S. Li, M. Zhang, H. Wang, H. Lu, A. Pan, C. Pan and Y. Zhang, *Sci. Bull.*, 2020, **65**, 343–349.
210 K. Lee, H. Han, Y. Kim, J. Park, S. Jang, H. Lee, S. W. Lee, H. Kim, Y. Kim, T. Kim, D. Kim, G. Wang and C. Park, *Adv. Funct. Mater.*, 2021, **31**, 2105596.
211 X. Huang, Q. Li, W. Shi, K. Liu, Y. Zhang, Y. Liu, X. Wei, Z. Zhao, Y. Guo and Y. Liu, *Small*, 2021, **17**, 2102820.
212 J.-H. Lu, M.-T. Cheng, H.-L. Hsu, S.-W. Liu and C.-P. Chen, *Adv. Funct. Mater.*, 2020, **30**, 2002503.
213 J. Lao, W. Xu, C. Jiang, N. Zhong, B. Tian, H. Lin, C. Luo, J. Travas-Sejdic, H. Peng and C.-G. Duan, *Adv. Electron. Mater.*, 2021, **7**, 2100291.
214 Q. Shi, D. Liu, D. Hao, J. Zhang, L. Tian, L. Xiong and J. Huang, *Nano Energy*, 2021, **87**, 106197.
215 Y. Park, M.-K. Kim and J.-S. Lee, *J. Mater. Chem. C*, 2021, **9**, 1429–1436.
216 J. Lao, W. Xu, C. Jiang, N. Zhong, B. Tian, H. Lin, C. Luo, J. Travas-sejdic, H. Peng and C.-G. Duan, *J. Mater. Chem. C*, 2021, **9**, 5706–5712.
217 J. Liu, Z. Yang, Z. Gong, Z. Shen, Y. Ye, B. Yang, Y. Qiu, B. Ye, L. Xu, T. Guo and S. Xu, *ACS Appl. Mater. Interfaces*, 2021, **13**, 13362–13371.
218 A. Siddik, P. K. Haldar, T. Paul, U. Das, A. Barman, A. Roy and P. K. Sarkar, *Nanoscale*, 2021, **13**, 8864–8874.
219 L. Yang, M. Singh, S.-W. Shen, K.-Y. Chih, S.-W. Liu, C.-I. Wu, C.-W. Chu and H.-W. Lin, *Adv. Funct. Mater.*, 2021, **31**, 2008259.
220 U. Das, P. Sarkar, B. Paul and A. Roy, *Appl. Phys. Lett.*, 2021, **118**, 182103.
221 S. G. Kim, Q. Van Le, J. S. Han, H. Kim, M.-J. Choi, S. A. Lee, T. L. Kim, S. B. Kim, S. Y. Kim and H. W. Jang, *Adv. Funct. Mater.*, 2019, **29**, 1906686.
222 F. Ma, Y. Zhu, Z. Xu, Y. Liu, X. Zheng, S. Ju, Q. Li, Z. Ni, H. Hu, Y. Chai, C. Wu, T. W. Kim and F. Li, *Adv. Funct. Mater.*, 2020, **30**, 1908901.
223 F. Cao, J. Chen, D. Yu, S. Wang, X. Xu, J. Liu, Z. Han, B. Huang, Y. Gu, K. L. Choy and H. Zeng, *Adv. Mater.*, 2020, **32**, 1905362.
224 R. A. John, N. Yantara, Y. F. Ng, G. Narasimman, E. Mosconi, D. Meggiolaro, M. R. Kulkarni, P. K. Gopalakrishnan, C. A. Nguyen, F. De Angelis, S. G. Mhaisalkar, A. Basu and N. Mathews, *Adv. Mater.*, 2018, **30**, 1805454.
225 S.-I. Kim, Y. Lee, M.-H. Park, G.-T. Go, Y.-H. Kim, W. Xu, H.-D. Lee, H. Kim, D.-G. Seo, W. Lee and T.-W. Lee, *Adv. Electron. Mater.*, 2019, **5**, 1900008.
226 W. Xu, H. Cho, Y.-H. Kim, Y.-T. Kim, C. Wolf, C.-G. Park and T.-W. Lee, *Adv. Mater.*, 2016, **28**, 5916–5922.
227 J.-M. Yang, E.-S. Choi, S.-Y. Kim, J.-H. Kim, J.-H. Park and N.-G. Park, *Nanoscale*, 2019, **11**, 6453–6461.
228 H. Yu, J. Gong, H. Wei, W. Huang and W. Xu, *Mater. Chem. Front.*, 2019, **3**, 941–947.
229 X. Zhu and W. D. Lu, *ACS Nano*, 2018, **12**, 1242–1249.
230 E. Li, W. Lin, Y. Yan, H. Yang, X. Wang, Q. Chen, D. Lv, G. Chen, H. Chen and T. Guo, *ACS Appl. Mater. Interfaces*, 2019, **11**, 46008–46016.
231 L. G. Feld, Y. Shynkarenko, F. Krieg, G. Raino and M. V. Kovalenko, *Adv. Opt. Mater.*, 2021, **9**, 2100620.
232 L. Shao, D. Liu, J. Lyu, D. Zhou, N. Ding, R. Sun, W. Xu, N. Wang, S. Xu, B. Dong and H. Song, *Mater. Today Phys.*, 2021, **21**, 100495.
233 Y. W. Wang, L. Varadi, A. Trinchi, J. H. Shen, Y. H. Zhu, G. Wei and C. Z. Li, *Small*, 2018, **14**, 1803156.
234 P. M. Talianov, O. O. Peltek, M. Masharin, S. Khubezhov, M. A. Baranov, A. Drabavičius, A. S. Timin, L. E. Zelenkov, A. P. Pushkarev, S. V. Makarov and M. V. Zyuzin, *J. Phys. Chem. Lett.*, 2021, **12**, 8991–8998.
235 P. Kumar, M. Patel, C. Park, H. Han, B. Jeong, H. Kang, R. Patel, W.-G. Koh and C. Park, *J. Mater. Chem. B*, 2020, **8**, 10337–10345.
236 S. Vedi, T. Dheivasigamani, G. S. Selvam, T. Kawakami, N. Rajeswaran, S. Rajendran, A. Muthukaruppan,

S. AlFaify and M. Shkir, *Biomater. Sci.*, 2022, **10**, 5956–5967.
237 C.-Y. Zhong, L. Xiao, J. Zhou, Z. Chen, Y. Chen, Z.-Q. Liu and J. Z. Zhang, *Chem. Eng. J.*, 2022, **431**, 134110.
238 P. M. Talianov, O. O. Peltek, M. A. Masharin, S. Khubezhov, M. A. Baranov, A. Drabavičius, A. S. Timin, L. E. Zelenkov, A. P. Pushkarev, S. V. Makarov and M. V. Zyuzin, *J. Phys.: Conf. Ser.*, 2021, **2015**, 012150.
239 W. T. Song, Y. M. Wang, B. Wang, Y. F. Yao, W. G. Wang, J. H. Wu, Q. Shen, W. J. Luo and Z. G. Zou, *Nano Res.*, 2020, **7**, 795–801.
240 S. Lou, Z. Zhou, T. Xuan, H. Li, J. Jiao, H. Zhang, R. Gautier and J. Wang, *ACS Appl. Mater. Interfaces*, 2019, **11**, 24241–24246.
241 S. Ye, W. Yan, M. Zhao, X. Peng, J. Song and J. Qu, *Adv. Mater.*, 2018, **30**, e1800167.
242 Z. A. VanOrman, H. K. Drozdick, S. Wieghold and L. Nienhaus, *J. Mater. Chem. C*, 2021, **9**, 2685–2694.
243 W. J. Mir, T. Sheikh, H. Arfin, Z. Xia and A. Nag, *NPG Asia Mater.*, 2020, **12**, 9.
244 A. L. Wani, A. Ara and J. A. Usmani, *Interdiscip. Toxicol.*, 2015, **8**, 55–64.
245 G. Flora, D. Gupta and A. Tiwari, *Interdiscip. Toxicol.*, 2012, **5**, 47–58.
246 Y. Alcaraz-Contreras, L. Garza-Ocañas, K. Carcaño-Díaz and X. S. Ramírez-Gómez, *J. Toxicol.*, 2011, **2011**, 430539.
247 Y. Wu, Z. Chen, W. S. Darwish, K. Terada, H. Chiba and S.-P. Hui, *J. Agric. Food Chem.*, 2019, **67**, 7716–7725.
248 J. Shi, F. Li, J. Yuan, X. Ling, S. Zhou, Y. Qian and W. Ma, *J. Mater. Chem. A*, 2019, **7**, 20936–20944.
249 J. M. Li, H. L. Cao, W. B. Jiao, Q. Wang, M. D. Wei, I. Cantone, J. Lu and A. Abate, *Nat. Commun.*, 2020, **11**, 5.
250 I. Infante and L. Manna, *Nano Lett.*, 2021, **21**, 6–9.